30836

NATIONAL LIBRARY
OTTAWA

CANADA

BIBLIOTHÈQUE NATIONALE
OTTAWA

NAME OF AUTHOR. BRIJ BEHARI LAL SRIVASTAVA

TITLE OF THESIS. COMPUTATION OF INELASTIC
INSTABILITY IN STEEL

UNIVERSITY. UNIV. OF ALBERTA

DEGREE FOR WHICH THESIS WAS PRESENTED. M. Sc.

YEAR THIS DEGREE GRANTED. 1976

Permission is hereby granted to THE NATIONAL LIBRARY OF CANADA to microfilm this thesis and to lend or sell copies of the film.

The author reserves other publication rights, and neither the thesis nor extensive extracts from it may be printed or otherwise reproduced without the author's written permission.

(Signed) B.B.L. Srivastava

PERMANENT ADDRESS:

SHIV-SADAN
284 ALAHDAPUR
GORAKHPUR (U.P.)
INDIA.

DATED 14.7. 1976

NL-91 (10-68)

INFORMATION TO USERS

THIS DISSERTATION HAS BEEN
MICROFILMED EXACTLY AS RECEIVED

This copy was produced from a microfiche copy of the original document. The quality of the copy is heavily dependent upon the quality of the original thesis submitted for microfilming. Every effort has been made to ensure the highest quality of reproduction possible.

PLEASE NOTE: Some pages may have indistinct print. Filmed as received.

Canadian Theses Division
Cataloguing Branch
National Library of Canada
Ottawa, Canada K1A 0N4

AVIS AUX USAGERS

LA THESE A ETE MICROFILMEE
TELLE QUE NOUS L'AVONS RECUE

Cette copie a été faite à partir d'une microfiche du document original. La qualité de la copie dépend grandement de la qualité de la thèse soumise pour le microfilmage. Nous avons tout fait pour assurer une qualité supérieure de reproduction.

NOTA BENE: La qualité d'impression de certaines pages peut laisser à désirer. Microfilmee telle que nous l'avons reçue.

Division des thèses canadiennes
Direction du catalogage
Bibliothèque nationale du Canada
Ottawa, Canada K1A 0N4

THE UNIVERSITY OF ALBERTA

COMPUTATION OF INELASTIC INSTABILITY IN STEEL JOISTS

by

BRIJ BEHARI LAL SRIVASTAVA ⓒ

A THESIS
SUBMITTED TO THE FACULTY OF GRADUATE STUDIES AND RESEARCH
IN PARTIAL FULFILMENT OF THE REQUIREMENTS FOR THE
DEGREE OF MASTER OF SCIENCE
IN
CIVIL ENGINEERING

DEPARTMENT OF CIVIL ENGINEERING

EDMONTON, ALBERTA
CANADA

FALL, 1976

THE UNIVERSITY OF ALBERTA

FACULTY OF GRADUATE STUDIES AND RESEARCH

The undersigned certify that they have read, and recommend to the Faculty of Graduate Studies and Research, for acceptance, a thesis entitled, "COMPUTATION OF INELASTIC INSTABILITY IN STEEL JOISTS", submitted by BRIJ BEHARI LAL SRIVASTAVA in partial fulfilment of the requirements for the degree of Master of Science.

D W Murray
(Supervisor) D.W. Murray

J Longworth
J. Longworth

Gary Faulkner
G. Faulkner

Date: July 9, 1976

ABSTRACT

Open web steel joists are often used as simply supported flexural members in order to support roofs and lightly loaded floors. The arrangement of web members permits easy passage of heating ducts and other services through the joist. Joists also offer saving in weight over comparable members having solid webs. A common chord member is a hat shaped section.

This work is an attempt to predict, by numerical analysis, the failure of hat section top chord members of open web steel joists. A finite element formulation has been applied to study the behavior of these top chord members including non linear geometric and material effects. Critical members which failed during an experimental investigation are modelled and predicted failure loads compared with the experimental results.

The interaction curves predicted by Galambos and Ketter for symmetrical I-Sections and hat shaped sections are used to verify the finite element programs.

ACKNOWLEDGEMENTS

The author wishes to express his appreciation of his supervisor Professor D.W. Murray, who has drawn his attention to this problem and inspired him to do his work on this dissertation, providing most constructive comments and invaluable help throughout the entire program.

The author wishes to express his deep sense of gratitude to Dr. M. Epstein, for his valuable guidance and keen interest in the work.

The assistance of Dr. S.H. Simmonds and R. Matiisen is gratefully acknowledged. Appreciation is also expressed to the Canadian Steel Industries Construction Council for funding the work of R. Matiisen which provided the test data used in this thesis.

The author owes special thanks and gratitude to Mr. and Mrs. R. Zander and Dr. and Mrs. H.K. Chaurasia who helped him in many ways while the author has been working for an M.Sc. and made his stay comfortable in Edmonton. The author also wishes to express his thanks and appreciation to Mrs. Barbara Gallaiford for her expert, quick and patient typing of the manuscript. The author also thanks Mr. P.V. Joseph for his help in drafting.

TABLE OF CONTENTS

Page

Library Release Form

Title Page

Signed Approval Page

Abstract iv

Acknowledgements v

Table of Contents vi

List of Tables xi

List of Figures xiii

CHAPTER 1 INTRODUCTION 1

1.1 Introductory Remarks 1

1.2 Scope 2

CHAPTER 2 LITERATURE REVIEW 4

2.1 Elastic Beam-Columns 4

2.2 Early Work in Inelastic Behavior 7

2.3 Karman's Technique 9

2.4 Moment-Curvature Relations 13

2.5 Iterative Numerical Integration Technique 15

2.6 Interaction Equations 18

2.7 Investigation of Compression Chords of Joists 20

Page

2.7.1 Toronto Test Series 20

2.7.2 Kansas Test Series 21

2.8 Large Deformation Finite Element Solution 24

CHAPTER 3 AN INELASTIC LARGE DEFLECTION FINITE ELEMENT TECHNIQUE FOR BEAM-COLUMN TYPE PROBLEMS 25

3.1 Background To Finite Element Formulation 25

3.2 Variational Equilibrium Equations 29

3.3 Discretization 34

3.4 Computer Programs 40

3.4.1 Program ELAST 41

3.4.2 Program PLAST 41

3.4.3 Program PLAST1 42

3.5 Modifications To Program 43

3.5.1 Modification to MAIN 43

3.5.2 Modification to ABCG 44

3.5.3 Modification to FORMOM 44

CHAPTER 4 ILLUSTRATIVE APPLICATIONS OF PROGRAMS 46

4.1 Testing of Program ELAST 46

4.2 Testing of Program PLAST 47

4.3 Testing of Program PLAST1 49

4.4 Applications of NLHAT 50

Page

CHAPTER 5 A STUDY OF TOP CHORD BUCKLING OF JOISTS 53

5.1 Description Of Experimental Project 53

5.2 Description Of Models And Boundary Conditions 54

5.3 Analysis Of Member 3T For Joist AX05 56

5.3.1 Forced Boundary Condition Analysis For AX05 57

5.3.2 Displacement Boundary Condition Analysis For AX05 57

5.3.3 Spring Boundary Condition Analysis For AX05 58

5.3.4 Analysis of AX05 Including Joint Length 59

5.3.5 Review Of Analysis For AX05 60

5.4 Analysis of Member 3T For Joist AX01 60

5.4.1 Force Boundary Condition Analysis Of AX01 61

5.4.2 Spring Boundary Condition Analysis Of AX01 62

5.4.3 Analysis of AX01 Including Joint Length 62

5.4.4 Review of Analysis For AX01 63

5.5 Analysis of Member 3T For Joist AX02 63

5.5.1 Force Boundary Condition Analysis Of AX02 64

5.5.2 Analysis of AX02 Including Joint Length 64

5.5.3 Review Of Analysis Of AX02 65

		Page
5.6	Effect Of Transverse Load Position And Yield Stress	65
5.7	Summary Of Top Chord Analysis	66
CHAPTER 6	SUMMARY, CONCLUSIONS AND RECOMMENDATIONS	67
6.1	Summary	67
6.2	Conclusions	67
6.3	Recommendations and Observations	69
LIST OF REFERENCES		71
TABLES		75
FIGURES		99
APPENDIX A	ASSUMED DISTRIBUTION OF RESIDUAL STRESSES	137
APPENDIX B	DETERMINATION OF CRITICAL STRAIN LOCATIONS	143
APPENDIX C	HAND COMPUTATION OF INTERACTION CURVE	147
APPENDIX D	PROGRAM NLHAT	152
D-1	Preparation of Input Data For Program NLHAT	152
D-2	Program Listing	154
APPENDIX E	CALCULATION OF NET CHORD ROTATION	174
E-1	Calculation Of Net Chord Rotation In Joist AX05	174

Page

E-2 Calculation Of Net Chord Rotations And Spring Stiffness In Joist AX01 175

LIST OF TABLES

Table	Description	Page
1.1	Section Properties	76
4.1	Comparison Of Classical And Numerical Solutions For The "Elastica"	77
4.2	Inelastic Solution For A Beam-Column By Program PLAST	78
4.3	Moment-End Rotation For Beam-Column	79
4.4	$\frac{P}{Py}$ Results From Galambos And Ketter (6)	80
4.5	Comparison Of Compared $\frac{M}{M_p}$ Values With Interaction Curve Of Galambos And Ketter (6)	81
4.6	Moment-Curvature (M-ϕ) Relationship For Zero Slenderness Ratio And Bending Compression In Wide Flange	82
4.7	Moment Curvature (M-ϕ) Relationship For Zero Slenderness Ratio And Bending Compression In Narrow Flange	83
4.8	Finite Element Interaction Analysis For Simulated Hat Section	84
4.9	Interaction Values For Simulated Hat Section (Wide Flange In Compression σ_{rc}=o)	85
4.10	Interaction Values For Simulated Hat Section (Narrow Flange In Compression σ_{rc}=o)	86

Table	Description	Page
5.1	Design Load Results From Elastic Frame Analysis	87
5.2	Design Load Bending Moments From Elastic Frame Analysis	88
5.3	Summary Of Test Results	89
5.4	Interior And Joint Loading For Top Chord Models	90
5.5	Boundary Conditions For Top Chord Models	91
5.6	Load-Deflection Relationship Of AX05J:F	92
5.7	Load-Vertical Deflection Values At Each Node For AX05J:F	93
5.8	Load-Deflection Relationship For AX05	94
5.9	Load-Deflection Relationship For AX01	95
5.10	Load-Deflection Relationship For AX02	96
5.11	Effect Of Load Position And Yield Stress On Joist AX01	97
5.12	Summary Of Critical Load Factors Of Joists	98
C-1	Calculation Of Static Moments	148
C-2	Calculation Of Net Static Moments	149
C-3	Calculation Of Points For Interaction Curves	150

LIST OF FIGURES

Figure		Page
1.1	Typical Open Web Steel Joist	100
1.2	Type-C Shallow Hat Section	100
1.3	Equivalent Section	101
2.1	Beam-Column Model With End Moments	102
2.2	Beam-Column Model With Transverse Load	102
2.3	Bending Of Rectangular Section	102
2.4	Inelastic Stress Strain Diagram (21)	102
2.5	Stress-Strain Diagram For Structural Steel (21)	103
2.6	Effective Modulus Versus Total Strain Diagram (21)	103
2.7	M Versus Δ Curves For Rectangular Section (21)	104
2.8	Details Of Von Karman's Analysis (15)	105
2.9	Stress And Strain Distributions For Steel Section	106
2.10	Typical Progressive Yield Conditions For A Beam-Column Section (11)	106
2.11	Sample Set Of Assumed Yield Penetration Conditions For Determination Of Auxiliary Curves (11)	106
2.12	Typical Set Of Auxiliary Curves (11)	107
2.13	Moment-Curvature Relationship For P=0.2 Py (11)	107
2.14	Moment-Thrust-Curvature Relationships For 8WF31 (6)	108
2.15	Typical Numerical Integration Procedure To Obtain End Slope (6)	109

Figure Page

2.16 Typical Moment Versus End Rotation Curve (6) 110

2.17 Maximum Carrying Capacity Interaction Curves (6) 111

3.1 Geometry Of Deformation (3) 112

3.2 Basis Functions For Cubic Polynomials (3) 113

3.3 Element Node And Nodal Displacement Designation (3) 114

4.1 Comparison Of Theoretical And Numerical Solutions For The "Elastica" 115

4.2 Load-Deflection Curve Derived From Spring Stiffened Column 116

4.3 Moment-End Rotation Curve 117

4.4 Comparison Of Predicted Capacities With Interaction Curves Of Galambos And Ketter (6) 118

4.5 Moment-Curvature Relationships For Hat Section ($\frac{\ell}{r} = 4.8$) 119

4.6 Interaction Curves For Hat Section With $\frac{L}{r} = o$ 120

4.7 Interaction Curves For Hat Section ($F_y = 33$) 121

4.8 Interaction Curves For Hat Section ($F_y = 55$) 122

5.1 Member And Joint Numbering For Typical Test Joist 123

5.2 Dimensions Of Test Joists AX01 And AX02 (14) 124

5.3 Dimensions Of Test Joist AX05 (14) 125

5.4 Generalized Beam-Column Finite Element Model 126

5.5 Loading And Boundary Conditions For Models Of AX05 127

Figure		Page
5.6	Load-Deflection Curves For AX05 Models	128
5.7	Load-Deflection Curves For AX05J	129
5.8	Deflected Shapes For AX05J	130
5.9	Loading And Boundary Conditions For Models Of AX01	131
5.10	Load Deflection Curve For AX01 Models	132
5.11	Loading And Boundary Conditions For AX02 Models	133
5.12	Load-Deflection Curves For AX02 Models	134
5.13	Effect Of Load Positioning On Member Behavior	135
5.14	Effect Of Yield Stress On Member Behavior	136
A.1	Residual Stress Distribution On Symmetrical Section	142
A.2	Assumed Residual Stress Distribution On An Unsymmetrical Section	142
B.1	Residual Stress And Strain Distribution In The Web	146
B.2	Critical Strain Locations From Centroid In The Web	146
C.1	Subdivision Of Equivalent Section For Fully Plastic Computations	151

CHAPTER 1

INTRODUCTION

1.1 Introductory Remarks

Open web steel joists are often used as simply-supported flexural members. A common type of joist is shown in Figure 1.1. Details of a typical top chord section are shown in Figure 1.2. The principal axes, x and y, pass through the centroid G. The section is symmetrical about the y axis.

Matiisen (14) has recently carried out a test program in which the top chord members of joists failed due to the secondary moment resulting from joint eccentricity. The top chord members of these joists were type C sections (26) as shown in Figure 1.2.

The purpose of this work is to attempt to evaluate the maximum load carrying capacity of the chord members of these joists by modelling the critical members as inelastic beam-columns. The technique employed consists of isolating the critical top chord member, attempting to impose realistic boundary conditions upon it, and determining the peak load from a load-deformation finite element analysis. Epstein and Murray (4) developed three different finite element computer programs for the analysis of large deformations of beams on the basis of an objective non-linear formulation analogous to Budiansky's non-linear shell theory. The formulation results in a set of equilibrium equations which are solved by the Newton-Raphson procedure combined with an incremental loading technique. The virtual work form of these equations has been used to derive a finite element representation of the problem, in which cubic polynomials form the basis functions for both axial and transverse displacements. It has been demonstrated through numerical examples (4) that the resulting equations yield computationally efficient solutions to beam problems involving very large displacements and rotations. The theory is based on an objective measure of strains.

The three different programs, known as ELAST, PLAST and PLAST1 deal with linearly elastic, elasto-plastic (unsymmetrical I section), and tri-linear stress-strain relations respectively. The PLAST1 program (4) which deals with the tri-linear stress-strain case, includes initial residual stresses for a symmetrical I shape.

The author has modified program PLAST1 such than an analysis can be carried out for an unsymmetrical I shape including the effect of residual stresses with a tri-linear stress-strain curve. This program will be referred to as NLHAT.

The hat shaped sections have been converted to equivalent unsymmetrical I sections, as indicated in Figure 1.3 in order to apply the program.

1.2 Scope

Chapter 2 of this thesis deals with a review of various techniques available for analysing and computing the capacity of beam-columns. Chapter 3 describes in detail the theory for the programs of Epstein and Murray, and the author's modifications to include the effect of residual stresses for an unsymmetrical I section. The curves of Galambos and Ketter (6) are used to verify the validity of the programs PLAST1 and NLHAT. Interaction curves for different slenderness ratios having symmetric I shape are predicted by the programs and compared with those in Reference 6. Hat shaped sections are examined in Chapter 4. Chapter 5 consists of a study to simulate the failure of the critical top chord member of each of three joists in Matiisen's test series (14), under different boundary conditions. A summary of the complete work, along with conclusions is the subject matter of Chapter 6.

CHAPTER 2

LITERATURE REVIEW

2.1 Elastic Beam-Columns

Beam-columns are those members in a structure which are subjected to combined axial loads and bending moments. Bending may be caused by moments applied to the ends of the member, as shown in Figure 2.1, by transverse loads acting directly as shown in Figure 2.2, or by a combination of these effects.

The following general basic assumptions are made to solve the beam-column problems which involve inelastic bending.

1. The cross section of the beam remains plane during bending, and hence longitudinal strains are proportional to their distances from the neutral surface.

2. The relationship between stress and strain in any longitudinal fiber is given by the uniaxial stress-strain diagram of the material.

3. Curvature can be approximated by the second derivative of the transverse deflection, neglecting certain higher order terms and assuming deflections to be small.

To obtain the exact solution to a small deflection beam-column problem it is necessary to solve the basic differential equation of equilibrium. The basic differential equation for the elastic beam column problem shown in Figure 2.1 is given as (21)

$$EI \frac{d^2y}{dx^2} + Py = - M_o \left(1 + \frac{(\beta-1)x}{L}\right) \tag{2.1}$$

where EI represents the flexural rigidity, P is axial load, M_o denotes the bending moment at the left support, y is the deflection at any section x, β is ratio of end moments and L is the length. Using the following notation for simplification

$$k^2 = \frac{P}{EI} \tag{2.2}$$

equation 2.1 becomes

$$\frac{d^2y}{dx^2} + k^2y = - \frac{M_o}{EI} \left[1 + \frac{(\beta-1)x}{L}\right] \tag{2.3}$$

The general solution of this equation (21) is

$$y = A \cos kx + \beta \sin kx - \frac{M_o}{P} \left[1 + \frac{(\beta-1)x}{L}\right] \tag{2.4}$$

The constants of integration A and B are now determined from the conditions at the ends of beam-column. Since the deflections at the ends of the beam column are zero, we conclude that

$$A = \frac{M_o}{P}, \quad B = \frac{M_o}{P \sin kL} (\beta - \cos kL) \tag{2.5}$$

Substituting these values in Equation 2.4 we get

$$y = \frac{M_o}{P}\left[\frac{\sin k(L-x) + \beta \sin kx}{\sin kL} - 1 + \left(\frac{x}{L}\right)(1-\beta)\right] \tag{2.6}$$

Now from Equation 2.2

$$kL = \sqrt{\frac{P}{EI}}\,L = \pi\sqrt{\frac{PL^2}{\pi^2 EI}} = \pi\sqrt{\frac{P}{P_E}} = \alpha \tag{2.7}$$

The moment at the corresponding section is then

$$M = M_o\left[\frac{\sin \alpha(1 - \frac{x}{L}) + \beta \sin \alpha\,(\frac{x}{L})}{\sin \alpha}\right] \tag{2.8}$$

Since the maximum stress will be reached at the section of maximum moment, it is necessary to define the location of the critical section. This occurs when

$$\frac{\partial M}{\partial x} = \frac{\partial}{\partial x}\left[\sin \alpha(1 - \frac{x}{L}) + \beta \sin \alpha\,(\frac{x}{L})\right] = 0 \tag{2.9}$$

which gives

$$\beta = \frac{\cos \alpha(1 - \frac{x}{L})}{\cos \alpha(\frac{x}{L})} \tag{2.10}$$

Solving Equation 2.10 for x and substituting Equation 2.10 into Equation 2.8 gives

$$M_{max} = M_o(\text{Sec } \alpha \frac{x}{L}) \quad (2.11)$$

6 The interaction relationship to determine the conditions for first yield (for the case where no residual stress is present) is therefore

$$\frac{P}{P_y} + \frac{M_{max}}{M_y} = 1.0 \quad (2.12)$$

$$\frac{P}{P_y} + \frac{M_o}{M_y} \text{ Sec } \alpha \frac{x}{L} = 1.0 \quad (2.13)$$

$$\frac{P}{P_y} + \frac{M_o}{M_y} \tau = 1.0 \quad (2.14)$$

where $\tau = \text{Sec } \alpha \frac{x}{L}$ (2.15)

This is also known as the secant formula for beam-columns. It is an elastic limit solution to a problem where the failure load of the column is defined as the load which produces the beginning of yielding in the fibers subject to maximum compression.

2.2 Early Work in Inelastic Behavior

The use of open web steel joists has increased greatly in the recent past. However, very little research has been conducted into beam-column problems arising specifically in the top chords of joists. This chapter is concerned with a review of current techniques for solving beam-column problems and some of the investigations into the compression chords of joists. The following summary of early work in inelastic beam-column behavior is taken from Bleich (2).

Ostenfeld (2) first derived design formulas for axially and eccentrically loaded columns. His method was based upon the concept that the critical load be defined as the loading which first produces extreme fiber stresses equal to the yield strength, in a manner similar to that of Section 2.1. Karman (15) was among the first to consider the buckling of eccentrically loaded columns as a stability problem. He called attention to the high sensitivity of intermediate and short columns to eccentricity of the superimposed load, which reduces the carrying capacity of straight columns considerably.

Ros and Bruner (2) assumed the elastic curve of the column as a half sine wave and based the computation of the critical load on the actual stress-strain diagram. Westergaard and Osgood (18) assumed a cosine curve as the deflected center line of an eccentrically loaded column, thus simplifying Karman's method (see Section 2.3) without impairing the practical accuracy of results. Starting from Karman's exact concept, Chwalla (15) based all his computations on one stress-strain diagram, adopted as typical for structural steel. His laborious work brought insight into the behavior of eccentrically loaded columns and his exact results served as a basis for the approximate methods. Jezek (24) gave an analytical solution for steel columns based upon a simplified stress strain curve consisting of two straight lines and showed that the results agree rather well with the values obtained from the real stress-strain relation. Shanley (2) showed in 1946 that the double modulus theory represented a paradox and this led to the wide acceptance of the reduced (tangent) modulus concept. He said that the column begins to bend with increasing axial load and while this load is more than the tangent modulus load, i.e., the maximum load for which the column can remain straight, it is considerably less than the double modulus load.

2.3 Karman's Technique

All of the essential ideas for the computation of inelastic buckling loads are contained in the technique of analysis developed by Von-Karman (2).

Considering the rectangular section shown in Figure 2.3, let ε_1 and ε_2 be the strains in the extreme fibers on the convex and concave sides of the beam, and h_1, h_2 be the distances from the neutral axis to the convex and concave surfaces of the beam, respectively. Also let Δ be the sum of the absolute values of the maximum elongation and maximum contraction as shown in Figure 2.4, that is

$$\Delta = \varepsilon_1 - \varepsilon_2 = \frac{h_1}{\rho} + \frac{h_2}{\rho} = \frac{h}{\rho} \qquad (2.16)$$

where ρ is the radius of curvature which may be determined by this equation, if Δ is known. The position of the neutral axis is determined by the values of ε_1 and ε_2 and is, in general, shifted from its position of pure bending by an amount defined by the strain ε_0 at the centroid, caused by the centrally applied load P as shown in Figure 2.4.

The force acting at any cross section of the beam can be reduced to a compressive force P applied at the centroid of the cross section and a bending couple M. The value of P and M can be calculated in each particular case from statics by using the stress-strain diagram (Figure 2.4). If y represents the distance from the centroid to any fiber of the beam (Figure 2.3), the strain at any point is

$$\varepsilon = \varepsilon_0 + \frac{y}{\rho} \tag{2.17}$$

Rearranging Equation (2.17) $y = \rho(\varepsilon-\varepsilon_0)$ is obtained and hence $dy=\rho d\varepsilon$. Then the magnitude of the compressive force P is given by

$$P = -b \int_{-h_2}^{h_1} \sigma \, dy = - b\rho \int_{\varepsilon_2}^{\varepsilon_1} \sigma \, d\varepsilon = - \frac{bh}{\Delta} \int_{\varepsilon_2}^{\varepsilon_1} \sigma \, d\varepsilon \tag{2.18}$$

Dividing P by cross sectional area bh, average compressive stress σ_c is obtained as

$$\sigma_c = \frac{P}{bh} = - \frac{1}{\Delta} \int_{\varepsilon_2}^{\varepsilon_1} \sigma \, d\varepsilon \tag{2.19}$$

The integral in this expression represents the area under the stress-strain diagram, that is, the shaded area of Figure 2.4. The area corresponding to compression is taken negative and the area representing tension is positive. From Equation 2.19 the value of ε_2 is calculated corresponding to any assumed value of ε_1, provided the axial load P is known. Alternatively, both ε_1 and ε_2 may be assumed so that the corresponding value of P can be calculated.

The bending moment is given by the expression

$$M = b \int_{-h_2}^{h_1} \sigma\, y\, dy = b\rho^2 \int_{\varepsilon_2}^{\varepsilon_1} \sigma\, (\varepsilon-\varepsilon_0) d\varepsilon \qquad (2.20)$$

or since $\Delta = \frac{h}{\rho}$ and $I = \frac{bh^3}{12}$,

$$M = \frac{12\ I}{\rho\ \Delta^3} \int_{\varepsilon_2}^{\varepsilon_1} \sigma\, (\varepsilon-\varepsilon_0)\, d\varepsilon \qquad (2.21)$$

The integral in this expression represents the static moment of the shaded area of the stress-strain diagram (Figure 2.4), with respect to vertical axis A-A. Thus the value of M can be calculated for any assumed values of ε_1 and ε_2. Equation 2.21 can be represented in the form

$$M = \frac{E''I}{\rho} \qquad (2.22)$$

where $$E'' = \frac{12}{\Delta^3} \int_{\varepsilon_2}^{\varepsilon_1} \sigma\, (\varepsilon-\varepsilon_0)\, d\varepsilon \qquad (2.23)$$

By varying ε_1 and ε_2 in such a manner that σ_c remains constant, E" is obtained as a function of $\Delta = \varepsilon_1-\varepsilon_2 = \frac{h}{\rho}$ for any given value of σ_c. The resulting relation is expressed graphically in Figure 2.6 which was plotted for a structural steel having the stress-strain diagram of Figure 2.5 (21). When these curves are used with Equation 2.22, the bending moment M can be represented as a function of Δ for each value of σ_c as shown in Figure 2.7. The shape of the deflection curve for an eccentrically loaded bar can be obtained by using the curves of Figure 2.7 and applying either an approximate graphical method of integration, as developed by Karman, or a numerical method.

Consider the steel bar (Figure 2.8) with rectangular cross-section, as shown in Figure 2.3, symmetrical about the point 0, and having the stress-strain curve shown in Figure 2.5. Karman's graphical integration technique (15) is described as follows. Assuming definite value of ϵ_1 and ϵ_2 for the cross section, corresponding values of P and σ_c are calculated from Equations 2.18 and 2.19.Using the curves of Figure 2.7, the moment M corresponding to this value of σ_c is obtained. Thus the bending moment and the compressive force for the cross section at the center of the beam are determined, and the distance $\delta_o = \frac{M}{P}$ locates the line of action of the compressive force (Figure 2.8(b)). Next construct an element 0-1 (Figure 2.8(c)) of the deflection curve of a small length a, by using the radius $\rho = \frac{h}{\Delta}$ calculated for the middle of the bar. The deflection at the cross-section 1 is approximately the same as for a flat circular arc. Thus $\delta_1 = \frac{a^2}{2\rho}$, and the bending moment $M_1 = P(\delta_o - \delta_1)$. For the resulting M_1 we find the corresponding value of Δ, denoted by Δ_1, from Figure 2.7; and also calculate $\rho_1 = \frac{h}{\Delta_1}$. A better approximation is obtained if we repeat the calculation for the first interval by taking the radius $(\frac{\rho+\rho_1}{2})$ before going to second interval. Using the new radius, construct the second portion 1-2 of the curve and calculate the deflection δ_2, continuing these calculations to the end A of the compressed bar.

The deflection δ at the end and the eccentricity e of the load P corresponding to the assumed values of ϵ_1 and ϵ_2 are determined.

Carrying out calculations for several values of ε_1 and ε_2, and selecting these values in each case so as to make P always the same, the deflection δ is obtained as a function of the eccentricity e. Repeating this process for a range of axial loads P and bending moments M , Karman constructed equilibrium diagrams such as in Figure 2.8(d).This method forms the basis for Karman's investigation of beam-column compression members.

2.4 Moment Curvature Relations

Ketter, Kaminsky and Beedle (11) developed a "point-by-point" method for computing the moment curvature relationship for wide flange columns bent about either axis and in the presence of axial thrust. The necessity of computing M-ϕ curves arose because it was very difficult to obtain strains from the given P and M as indicated by Equations 2.18 and 2.20. These equations require an iterative solution to obtain values of strain, but it is easier to find P and M if strains are assumed.

Since strains are small in comparison to the depth h of the section, the curvature within the elastic range as shown in Figure 2.9(a) is given as

$$\phi = \frac{\varepsilon_1 - \varepsilon_2}{h} = \frac{\sigma_1 - \sigma_2}{E\ h} \qquad (2.24)$$

For an elastic perfectly plastic member loaded beyond the elastic limit, as shown in Figure 2.9(b), we have

$$\phi = \frac{\varepsilon_1 - \varepsilon_2}{h} = \frac{\varepsilon_y - \varepsilon_2}{h - t} \tag{2.25}$$

$$\phi = \frac{\sigma_y - \sigma_2}{E(h - t)} \tag{2.26}$$

It is thus possible to compute P, M and ϕ for any given stress distribution by using equations similar to Equations 2.18 and 2.20. As moment is increased under a constant axial force, successive stress distributions will be similar to those shown in Figure 2.10. Yielding first occurs at the extreme fiber on the compression side of the specimen. As the loading is increased, yielding penetrates through the web on the compression side. Eventually yielding penetrates through the tension sides and the fully plastic condition, typified in Figure 2.10 (d), may be approached.

For easy computation of the M-ϕ curve certain flexure conditions are assumed; a typical set of these is illustrated in Figure 2.11. Values of P and M are determined from the stress distribution for a number of assumed values of ϕ for each of a set of assumed values of yield penetration as shown in Figure 2.11. These values of P and M are plotted in non-dimensional form as $\frac{M}{M_y}$ vs $\frac{\phi}{\phi_y}$ and $\frac{P}{P_y}$ vs $\frac{\phi}{\phi_y}$ curves as shown in Figure 2.12. The M-ϕ curve for a particular value of $\frac{P}{P_y}$ can be determined with the help of Figure 2.12. As an example, the value $P = 0.2 P_y$ is chosen. A horizontal line is drawn for this $\frac{P}{P_y}$, cutting the various auxiliary P-ϕ curves. At these points of intersection, verticals are projected until they intersect the corresponding M-ϕ curves in the same figure. Connecting these points give the desired M-ϕ curve for $\frac{P}{P_y} = 0.2$. This is indicated separately in Figure 2.13. Similar curves may be obtained when the influence of residual stresses shown in Figure A.1 are considered. The influence of varying the axial load over a range of $\frac{P}{P_y}$ on the M-ϕ curve is shown in Figure 2.14. The dotted curves in Figure 2.14 are comparable functions considering the influence of residual stress.

2.5 Iterative Numerical Integration Technique

Ketter (10) presents the result of a continuing investigation of the ultimate carrying capacity of beam-columns. He examined two different types of loading conditions for wide flange beams and the results are presented in the form of interaction curves. The following steps were adopted for solving any problems by this technique.

1. Select a particular value of $\frac{\ell}{r}$ and P for investigation.

2. The moment-thrust curvature curve is established for the given type of material, cross-section and residual stress distribution, for the assumed value of P, as explained in Section 2.4.

3. An end moment M_1 greater than the initial yield moment is assumed.

4. A reasonable deflected shape is assumed as a first trial. The deflections defined by Equation 2.6 are assumed.

5. Using P from Step 1, M_1 from Step 3 and y from Step 4, the bending moment $[M = M_1 \frac{x}{\ell} + P_y]$ is computed at a number of equally spaced intermediate points on the span.

6. For the value of P selected in Step 1 and the bending moments computed in Step 5, corresponding curvatures are read, using either

solid or dashed lines from Figure 2.14 depending upon whether or not one wants to include residual stress effects, at the points along the span.

7. Newmark's method of numerical integration (11) is then used to determine deflections. Assuming curvatures to be constant over a half interval ($\frac{\lambda}{2}$) on either side of each intermediate point and considering all slope changes to be concentrated at these intermediate points, the angle changes are added to obtain the slope between each of the intermediate points. The deflection of each point is then estimated by a similar process of adding the slope times the distance between intermediate points. Then these deflections are corrected to satisfy the boundary conditions as explained in Step i of Figure 2.15. The final deflection is obtained as the sum of the original estimate and the correction. If there is yielding, the deflection will not agree with the elastic ones computed in Step 4.

8. Using the new deflections as a second approximation, Steps 5, 6 and 7 are repeated and this set of deflections is compared with the second one. This process of successive approximation is repeated until convergence to the derived degree of accuracy is obtained.

9. End slope θ_o is computed from the deflection of points near the support. If the deflection curve of the member within the three end intervals is assumed to be represented by a parabola, the end slope can be expressed in terms of known deflections by

$$\theta_o = \frac{4\ \delta_1 - \delta_2}{2\lambda} \qquad (2.27)$$

where δ_1 and δ_2 are the deflections at the first and second stations, and λ is the spacing of the stations.

10. For the same values of $\frac{\ell}{r}$ and P, assume a series of greater values of M_1 and repeat Step 4 through 9 for each of these.

11. From the results of the above, plot the $\frac{M_1}{M_y}$ vs θ_o. One such plot for a particular case of a beam column (when $\beta = 0$) is shown in Figure 2.16. This curve is non-linear and eventually reaches a maximum, after which it starts to descend. The member would become unstable and collapse under the combination of the assigned axial force P and M at the peak of the curve. This gives one particular point on an interaction curve.

12. Step 1 through 11 yield one critical combination of M and P for one particular slenderness ratio ($\frac{\ell}{r}$). Many such points need to be determined for a given slenderness ratio to define an interaction curve.

A series of interaction curves may then be plotted for different $\frac{\ell}{r}$ values and axial force. Galambos and Ketter (6) plotted these curves in non-dimensional form, so as to be suitable for any WF section, as shown in Figure 2.17. The effect of residual stress is included. Figure 2.17 has been obtained by solving an 8WF31 section with the numerical integration technique described above.

Mason, Fisher and Winter (13) reported an experimental investigation of eccentrically loaded hinged steel columns. Twenty four eccentrically loaded and six axially loaded columns were tested. These test results were compared with the predicted failure loads of Galambos and Ketter, and correlation was shown to be very good.

2.6 Interaction Equations

Mason, Fisher and Winter (13) compared failure loads for eccentrically loaded columns to two types of interaction formulas. The first was

$$\frac{P}{P'} + \frac{M}{M'} = 1 \qquad (2.28)$$

where P' is the axial load at failure under concentric compression,

M' is the bending moment at failure under bending only,

P is the actual load at failure under combined action,

and M is the bending moment at failure under combined action.

The second was

$$\frac{P}{P'} + \frac{M}{M'(1 - \frac{P}{P_E})} = 1 \qquad (2.29)$$

where P_E is the Euler elastic buckling load and all other terms are identical to those of Equation 2.28. Equation 2.28 overestimated the test result by 15 to 20% and more and hence it is very unconservative. On the other hand Equation 2.29 was safe in all cases in comparison to test results. Results obtained from Equation 2.14,which is a secant formula,gives very satisfactory correlation with experimental values for ultimate loads for all slenderness ratios. This formula is accurate only for bending about an axis parallel to the flanges and provided that such bending is not accompanied by torsion. Equation 2.29 is accurate for bending about either axis when torsion is prevented. The amplification factor $(1 - \frac{P}{P_E})$ is included in Equation 2.29 to account for initial imperfections.

Galambos and Ketter (6) present dimensionless interaction equations to approximate curves similar to those of Figure 2.17 in the following form

$$A \frac{M}{M_u} + B \frac{P}{P_y} + C \left(\frac{P}{P_y}\right)^2 = 1 \qquad (2.30)$$

where A, B and C are empirical coefficients that are functions of $\frac{L}{r}$ and the loading condition, P_y is the column axial load at the full yield condition, M_u is ultimate bending moment in the absence of axial load and P_u is ultimate load for a centrally loaded column with buckling in the plane of the applied moment.

Hill and Clark (7) suggested following modified formula for both elastic and inelastic range

$$\frac{P}{P_u} + \frac{M_o}{M_u(1 - \frac{P}{P_E})} \leq 1 \qquad (2.31)$$

where M_o is the maximum applied moment, not including the contribution of the axial load interacting with deflections. The possibilities of buckling in the weak plane and of lateral torsional buckling are also considered in proposing Equation 2.31. Considering unequal end moments the following interaction equation is used in modified form in place of Equation 2.31 for calculating the critical load.

$$\frac{P}{P_{cr}} + \frac{M_o C_m}{(M_o)_{cr} \left(1 - \frac{P}{P_E}\right)} = 1.0 \qquad (2.32)$$

where P_{cr} is the smallest buckling load which the member can sustain if bending is absent, $(M_o)_{cr}$ is the critical moment in the absence of axial load, and C_m is a factor used for adjusting for the different end moment ratios β. The value of C_m is recommended in CSA Standard S16-1969, "Steel Structures for Buildings" (25) for different conditions.

2.7 Investigation of Compression Chords of Joists

2.7.1 Toronto Test Series

Kennedy and Rowan (9) carried out their work to resolve conflicts existing in design requirements for the continuous compression chords of open web steel joists, their goal being to establish the proper effective length for the compression chord which is a critical factor in their design. Thus the testing was aimed at establishing the behavior of the compression chord. A total of 8 joists were tested, 6 of these were loaded at panel points of which 3 failed by in-plane buckling of the compression chord, 2 by strong axis buckling of the compression chord, due to inadequate lateral support, and one double angle joist failed by individual buckling of the angles of the compression chord. Two joists were loaded at mid points and they failed by in-plane buckling. Deflections, joint rotations and member curvatures were recorded to find the inflection points for calculating effective length factors. Stub column tests were performed on top chord sections only.

From these tests the authors arrived at the following conclusions:

1. Top chords must be adequately braced.

2. Double angles must be suitably joined to ensure composite action.

3. The column strength curve can be closely represented by a straight line.

4. The deflection of a joist can be calculated by simple truss theory and can be approximated by a 10% increase in simple beam deflections.

5. The effective length of a chord member depends upon its original shape. If all initial deflections are in the same direction, then the effective length factor K = 0.65, if the deflections are not in the same direction, then K = 0.9.

6. When the top chord is uniformly loaded, the drop in joist capacity should not be more than 10% if the panel length is 24" or less.

7. Ultimate strength,when bending is present can be conservatively predicted by $\frac{P}{P'} + \frac{M}{M_p} = 1.0$.

2.7.2 Kansas Test Series

McDonald (15) studied analytically and experimentally the top chords of open web steel joists as beam-columns loaded uniformly along their length. He did a Karman type numerical analysis, but iterated his integration to find the collapse load which fit his boundary conditions. Subsequently, he compared his results with a different interaction equation. A computer program based on the Karman technique (Sec.

2.3) was formulated, and used to evaluate the buckling strength of 51 joists. Twenty four of these joists were tested with one point mid span load, 19 were tested with uniform load applied by Ohmart's air bag method and 8 were tested in pairs by uniform dead load. The analytical study was carried out so that results of testing and analytical work could be compared. This study was mainly directed towards in-plane buckling of the compression chord on the basis of following assumptions:

1. The mechanism of failure is primary instability.
2. The Navier assumption of linear strain under bending is valid.
3. The material possesses equal stress strain properties in tension and compression.
4. The displacement boundary condition for the critical top chord member can be determined from the deflected shape of the joist by considering inelastic effects from a modified beam analysis. Inelastic effects were included by assuming a variable bending stiffness (EI) for the joist along its length.

Considering the parabolic moment distribution that results from a uniform loading of the joist, it was concluded that joists should possess their elastic EI in the outer third of their length, and the EI over the middle third should be that necessary to match the measured mid-point deflection. Thus he determined joint rotation from the gross shape of the loaded joist assuming that the rotation of joints would not be affected by the uniform load between panel points. The analytical model of a top chord member which has been investigated exhibits:

1. End conditions which change when the joist load is changed and are consistent with the assumed shape which the joist takes under load.

2. An applied load P which rotates to remain tangent to the curved form of the joist under load.

On the basis of his investigations McDonald concluded the following:

1. The analytical study agreed well with the test series and both indicated that the design formulas of the American Iron and Steel Institute (AISI), Steel Joist Institute (SJI), and the American Institute of Steel Construction (AISC) will give adequate factors of safety. However, the analytical study indicated that the factor of safety might be reduced if the ratio of uniform load to axial design load in the top chord was increased.

2. Design techniques which use only the slenderness ratio and axial load to proportion compression members are not rational.

3. The interaction formula he proposed is

$$\frac{\text{Axial Stress}}{\text{Tangent Modulus Stress}} + \frac{\text{Bending Stress}}{\text{Yield Stress}} = 0.92$$

4. Von Karman's method of analysis for beam columns may be applied to the compression chord of open web steel joists but in analytical studies an iterative process should be used to determine the indeterminate end moments which produce a deflected shape consistent with the boundary conditions.

2.8 Large Deformation Finite Element Solution

Epstein and Murray (3) presented an objective non-linear formulation of elastic in-plane beam-column problems and a corresponding set of finite element equations. A large deformation theory for in-plane beam problems was formulated on the basis of the Budiansky's non-linear shell theory. Cubic interpolating functions were used to represent finite element displacements. These displacements were introduced into a virtual work form of the equations to yield numerical solutions.

A computer program was developed to show the applicability of the theory. Programs have also been developed to solve the post buckling behavior of beam columns. The solutions for beam-column problems carried out herein have been obtained by this technique and, therefore, a detailed discussion of these programs is given in Chapter 3.

CHAPTER 3

AN INELASTIC LARGE-DEFLECTION FINITE ELEMENT TECHNIQUE FOR BEAM-COLUMN TYPE PROBLEMS

3.1 Background to Finite Element Formulation

Epstein and Murray (3) have developed a finite element formulation in order to obtain numerical solutions for non-linear inelastic in-plane beam-column problems. Reference (4) contains three programs and the theory on which these programs are based.

The methods of Chapter 2 are based upon the approximations required to derive a second order differential equation. However, Reference (4) uses an exact expression for the curvature. This theory has been developed to solve problems of very large deflections in the post-buckling region and in this sense is more elaborate than required to determine maximum load carrying capacity. Use is made of a Newton Raphson procedure combined with an incremental loading technique on a set of total Lagrangian equations in solving the problems. Since a large deformation theory should include large rigid body motions as a special case, products of small terms have been retained so that an objective set of equations is obtained. This chapter contains a summary of Epstein's formulation (3) and the resulting programs. The basic assumptions made are:

1. The x,z plane (Figure 3.1) is a plane of symmetry of the beam and of the external loads. (The z axis contains the axis of the beam before deformation.)

2. Normal sections remain plane, undistorted and normal to the axis of the beam after deformation.

Referring to Figure 3.1, the position vector of a point on the axis of the beam before deformation is given by

$$r = zk \tag{3.1}$$

and for the same point after deformation

$$\hat{r} = r + V \tag{3.2}$$

in which displacement vector V can be written in component form as

$$v = u\, i + wk \tag{3.3}$$

where i and k represent unit vectors in the coordinate directions. The natural base vector along the deformed axis is given by

$$\hat{g} = \frac{d\hat{r}}{dz} = (1 + w')k + u'i \tag{3.4}$$

where symbol ()' and (^) are used to denote z-derivatives and magnitude after deformation, respectively. The unit normal vector after deformation is

$$\hat{N} = \frac{-u'k + (1 + w')i}{\sqrt{(1+w')^2 + u'^2}} \tag{3.5}$$

The Green strain measure of the axis is given by

$$\bar{e} = \frac{1}{2} (\hat{g} \cdot \hat{g} - k \cdot k) = w' + \frac{1}{2} (w'^2 + u'^2) \qquad (3.6)$$

Substituting Equation 3.6 into Equation 3.5, $\hat{N}$ is expressed as

$$\hat{N} = \frac{-u'k + (1 + w')i}{\sqrt{2\bar{e} + 1}} \qquad (3.7)$$

Considering displacements of points not originally on the axis of beam in order to construct the two dimensional strain tensor (the third dimension, y being irrelevant), and using N to denote the unit normal vector before deformation ($N \equiv i$), the position vector of a point in the plane of symmetry x,z is given before deformation by

$$R = r + x\,N \qquad (3.8)$$

In the view of assumption 2, the same point is identified after deformation by the position vector

$$\hat{R} = \hat{r} + x\,\hat{N} \qquad (3.9)$$

The components of Green's strain tensor are given by the matrix equation

$$[\varepsilon] = \frac{1}{2}\left(\begin{bmatrix} \frac{d\hat{R}}{dZ}\cdot\frac{d\hat{R}}{dZ} & \frac{d\hat{R}}{dZ}\cdot\frac{d\hat{R}}{dx} \\ \frac{d\hat{R}}{dx}\cdot\frac{d\hat{R}}{dZ} & \frac{d\hat{R}}{dx}\cdot\frac{d\hat{R}}{dx} \end{bmatrix} - \begin{bmatrix} 1 & 0 \\ 0 & 1 \end{bmatrix}\right) \qquad (3.10)$$

The vector derivatives appearing in Equation 3.10 are evaluated as

$$\frac{d\hat{R}}{dx} = \hat{N} \qquad (3.11)$$

$$\frac{d\hat{R}}{dz} = \frac{d\hat{r}}{dz} + x\,\frac{d\hat{N}}{dz} = \hat{g} + x\,\frac{d\hat{N}}{dz} \qquad (3.12)$$

where $\hat{g}$ is given by Equation 3.4 and $\frac{d\hat{N}}{dz}$ is a vector tangent to the axis after deformation and expressible, therefore, as

$$\frac{d\hat{N}}{dz} = -\,\phi\,\hat{g} \qquad (3.13)$$

The scalar ϕ is a measure of the curvature of the deformed axis and it identifies with the "physical" curvature (i.e. $|\phi| = |\frac{d\hat{N}}{ds}|$, where s measures length along the curve).

Substituting Equation 3.13 into Equation 3.12

$$\frac{d\hat{R}}{dz} = (1 - \phi\,x)\,\hat{g} \qquad (3.14)$$

Using Equations 3.11 and 3.14 yields Green's strain tensor as defined in Equation 3.10

$$[\varepsilon] = \begin{bmatrix} \{(1-\phi x)^2(\bar{e} + \frac{1}{2}) - \frac{1}{2}\} & 0 \\ 0 & 0 \end{bmatrix} \qquad (3.15)$$

Since all but the first component of the strain tensor vanish, as a direct consequence of the above hypotheses, $\bar{\varepsilon}$ is used to denote non vanishing component of $[\varepsilon]$.

3.2 Variational Equilibrium Equations

The internal virtual work (IVW) is obtained by integrating the following integral extended over the volume of the beam after deformation.

$$\mathrm{IVW} = \int_{\hat{\ell}} \int_{A} \sigma \, \delta \, \bar{\varepsilon} \, dA \, d\hat{\ell} \qquad (3.16)$$

Here σ is the stress component corresponding to $\bar{\varepsilon}$, $\hat{\ell}$ is the length of the axis after deformation and A is the area of the cross section of the beam.

Since $\bar{e}$ and ϕ are independent, the variation $\delta\bar{\varepsilon}$ is obtained from Equation 3.15 as

$$\delta \, \bar{\varepsilon} = (1-\phi x)^2 \, \delta \, \bar{e} - 2(1-\phi x)x \, (\bar{e} + \frac{1}{2}) \, \delta\phi \qquad (3.17)$$

Defining a modified curvature as

$$\bar{\phi} = (2\bar{e} + 1)\,\phi \tag{3.18}$$

it can be seen that for small strains $\bar{\phi}$ reduces to ϕ. Substituting the variation $\delta\phi$ from Equation 3.18 into Equation 3.17,

$$\delta\,\bar{\varepsilon} = ((1-\phi x) + \phi x(1-\phi x))\;\delta\,\bar{e} - x(1-\phi x)\;\delta\bar{\phi} \tag{3.19}$$

Substituting Equation 3.19 into Equation 3.16 and defining stress resultants as

$$N^* = \int_A \sigma(1-\phi x)\,dA \tag{3.20}$$

$$M^* = -\int_A \sigma(1-\phi x)\,x\,dA \tag{3.21}$$

Equation 3.16 can be written as

$$IVW = \int_{\hat{\ell}} \{N^*\delta\bar{e} + M^*(\delta\bar{\phi} - \phi\delta\bar{e})\}\,d\hat{\ell} \tag{3.22}$$

Introduce modified variables, defined as

$$\tilde{N} = \;2\bar{e}+1\;\; N^* \tag{3.23}$$

$$\tilde{\phi} = \sqrt{2\bar{e}+1}\;\;\bar{\phi}\;, \tag{3.24}$$

into Equation 3.22 to avoid the following two inconveniences,

1. Integration extends over the deformed axis, and
2. ϕ and $\bar{\phi}$ are not rational functions of displacements.

Again, for small strains $\tilde{N}$ and $\tilde{\phi}$ reduce to N^* and $\bar{\phi}$ respectively. Define another variable

$$\tilde{\tilde{N}} = \tilde{N} - 2\,\phi^*\,M^* \tag{3.25}$$

where

$$\phi^* = \frac{\tilde{\phi}}{2\bar{e}+1} = \sqrt{2\bar{e}+1}\;\phi \tag{3.26}$$

Introducing these modified variables expressed by Equation 3.23 to Equation 3.25, Equation 3.22 can be written as

$$IVW = \int_{\ell} (\tilde{\tilde{N}}\,\delta\bar{e} + M^*\,\delta\tilde{\phi})dz \tag{3.27}$$

We can note the following about Equation 3.27:

1. It is exact, in the sense that it contains no approximations whatsoever concerning the magnitude of displacements or strains. It is equivalent to the exact three dimensional internal virtual work expression, provided the two basic assumptions of the beam theory are valid.

2. Integration extends over the original configuration of the beam axis.

3. All the strain variables appearing explicitly in Equation 3.26 are rational expressions in the displacements u and w and their derivatives.

Two types of loads are considered:

1. A force per unit undeformed length of axis.

$$f = f_s k + f_n i \qquad (3.28)$$

2. A force per unit deformed length and acting normally to the axis after deformation

$$P = p \hat{N} \qquad (3.29)$$

where P is an external force and p is its magnitude. The total force per unit undeformed length is then

$$q = \sqrt{(2\bar{e}+1)}\, p \hat{N} + f_s k + f_n i \qquad (3.30)$$

or, according to Equations 3.5 and 3.7, Equation 3.30 can be written as

$$q = (f_s - pu')k + (f_n + p(1+w'))i \qquad (3.31)$$

The external virtual work (EVW), corresponding to the two types of external loads discussed above, is given by

$$\begin{aligned} \text{EVW} &= \int_{\ell} q\ \delta\ v dz \\ &= \int_{\ell} \{(f_s - pu')\delta w + (f_n + p(1+w'))\delta u\} dz \qquad (3.32) \end{aligned}$$

The total variational equilibrium equation is obtained upon excluding the end forces, by equating the right hand sides of Equations 3.27 and 3.32, so that

$$\int_{\ell} \{\tilde{\tilde{N}}\ \delta\bar{e} + M^*\delta\tilde{\phi} - (f_s - pu')\delta w - (f_n - p(1+w'))\delta u\} dz = 0 \qquad (3.33)$$

Substituting

$$\bar{e} = w' + \frac{1}{2}(w'^2 + u'^2) \qquad (3.34)$$

and

$$\tilde{\phi} = u''(1+w') - u'w'' \qquad (3.35)$$

into Equation 3.33 and integrating by parts, we obtain the Euler equations corresponding to Equation 3.33 as well as the natural boundary conditions. The resulting differential equations of equilibrium are

$$[\tilde{\tilde{N}}\,(1+w')]' + [M^*u'']' + [M^*u']'' + f_s - pu' = 0 \qquad (3.36)$$

$$-[\tilde{\tilde{N}}\,u']' + [M^*(1+w')]'' + [M^*w'']' - f_n + p(1+w') = 0 \qquad (3.37)$$

3.3 Discretization

A set of algebraic equations is obtained by dividing the beam axis into elements and allowing the displacements in each element to belong to a finite parameter family of functions.

Third degree polynomials are used to define the displacement functions for the given degrees of freedom as shown in Figure 3.2. The basis functions are expressed as

$$f_1 = 2\zeta^3 - 3\zeta^2 + 1 \qquad (3.38)$$

$$f_2 = (\zeta^3 - 2\zeta^2 + \zeta)\,h_I \qquad (3.39)$$

$$f_3 = -2\zeta^3 + 3\zeta^2 \qquad (3.40)$$

$$f_4 = (\zeta^3 - \zeta^2)\,h_I \qquad (3.41)$$

in which ζ is a non-dimensional coordinate which varies from zero at the left end to 1 at the right end of each element, and where h_I is the length of the element number I. The coefficients of these functions in the linear combination are the displacements and their first derivatives at the ends of the element. The nodal displacements U_I and W_I and their derivatives U'_I and W'_I are shown in Figure 3.3.

There are four degrees of freedom at each node in the element denoted by U, W, U' and W'. Making use of Equations 3.38 to 3.41, the following expressions are obtained for the displacements within the Ith element and for their first and second derivatives in terms of the notation shown in Figure 3.3

$$
\begin{aligned}
u &= U_{2(I-1)+j}\, f_j & w &= W_{2(I-1)+j}\, f_j \\
u' &= U_{2(I-1)+j}\, f'_j & w' &= W_{2(I-1)+j}\, f'_j \qquad (3.42) \\
u'' &= U_{2(I-1)+j}\, f''_j & w'' &= W_{2(I-1)+j}\, f''_j
\end{aligned}
$$

Here j is a summation index having the range 1 to 4. The strain variation $\bar{e}$ and $\tilde{\phi}$ and their first variations then become

$$
\begin{aligned}
\bar{e} = {} & W_{2(I-1)+j} f'_j + \frac{1}{2} (W_{2(I-1)+j} W_{2(I-1)+k} \\
& + U_{2(I-1)+j}\, U_{2(I-1)+k})\, f'_j f'_k \qquad (3.43)
\end{aligned}
$$

$$\tilde{\phi} = U_{2(I-1)+j}(1 + W_{2(I-1)+k}f'_k)f''_j - U_{2(I-1)+j}W_{2(I-1)+k}$$

$$f'_jf''_k \qquad (3.44)$$

$$\delta\bar{e} = \delta W_{2(I-1)+j}f'_j + (W_{2(I-1)+j}\delta W_{2(I-1)+k} + U_{2(I-1)+j}$$

$$\delta U_{2(I-1)+k})f'_jf'_k \qquad (3.45)$$

$$\delta\tilde{\phi} = (1 + W_{2(I-1)+k}f'_k \quad \delta U_{2(I-1)+j}f''_j$$

$$+ U_{2(I-1)+j}\,\delta W_{2(I-1)+k}f''_jf'_k$$

$$- (U_{2(I-1)+j}\,\delta W_{2(I-1)+k}\,\delta U_{2(I-1)-j})f'_jf''_k \qquad (3.46)$$

and the internal virtual work is evaluated as

$$IVW = \int_0^{\ell}(\tilde{N}\,\delta\bar{e} + M^*\delta\tilde{\phi})dz = \sum_{I=1}^{N} h_I \int_0^{\ell}(\tilde{\tilde{N}}\,\delta\bar{e}$$

$$+ M^*\delta\tilde{\phi})_I\,d\zeta = \sum_{I=1}^{N} h_I\{N^{**}_j\delta W_{2(I-1)+j}$$

$$+N^{***}_{jk}(W_{2(I-1)+j}\,\delta W_{2(I-1)+k} + U_{2(I-1)+j}\,\delta U_{2(I-1)+k})$$

$$+ M^{**}_j\,\delta U_{2(I-1)+j}$$

$$+ \left(W_{2(I-1)+k}\,\delta U_{2(I-1)+j} + U_{2(I-1)+j}\,\delta W_{2(I-1)+k}\right)$$

$$\times \left(M^{***}_{jk} - M^{***}_{kj}\right)\} \qquad (3.47)$$

in which the following notation is introduced,

$$N^{**}_{j} = \int_{o}^{\ell} \overset{\approx}{N}\, f'_{j}\, d\zeta \qquad (3.48)$$

$$N^{***}_{jk} = \int_{o}^{\ell} \overset{\approx}{N}\, f'_{j} f'_{k} d\zeta \qquad (3.49)$$

$$M^{**}_{j} = \int_{o}^{\ell} M^{*} f''_{j} d\zeta \qquad (3.50)$$

$$M^{***}_{jk} = \int_{o}^{\ell} M^{*} f''_{j} f'_{k} d\zeta \qquad (3.51)$$

dependence on I being understood.

The external virtual work (assuming dead load forces and moments are concentrated at the nodes only), is given by

$$EVW = \sum_{J=o}^{N} \{Z_{J}\delta W_{2J+1} + X_{J}\delta U_{2J+1} + M_{J}[(1 + W_{2J+2})\,\delta U_{2J+2}$$

$$- U_{2J+2}\,\delta W_{2J+2}]\} \qquad (3.52)$$

in which X_J, Z_J and M_J are transverse force, axial force and moment at node J.

The equilibrium equations associated with Equations 3.48 to

3.52 are obtained by assuming sequentially that all but one of the variations vanish. Thus, for instance, assume that the only non-vanishing variation is $\delta u_L = \delta U_{2L+1}$. In Equation 3.47 all the indices affecting δU are of the form $2(I-1)+j$, the only possibility for a term containing $\delta U_{2(I-1)+j}$ not to vanish is that

$$2(I-1)+j = 2L + 1 \tag{3.53}$$

or, solving for I,

$$I = L - \frac{j-3}{2} \tag{3.54}$$

Since j is a positive integer not greater than 4, it must necessarily be either 1 or 3, resulting respectively in $I = L + 1$ and $I = L$. Therefore, for each non-vanishing variation considered, there are in general only two surviving contributors to the overall summation of Equation 3.47, namely those corresponding to the elements adjacent to the node considered. Only one element contributes to the summation when first and last nodes are considered. The equilibrium equations are

$$\sum_{K=1}^{2} h_{J-K+2}[M^{**}_{2K-1} + N^{***}_{j(2K-1)} U_{2(J-K+1)+j} + W_{2(J-K+1)+j}(M^{**}_{(2K-1)j} - M^{***}_{j(2K-1)})] = X_J \tag{3.55}$$

$$\sum_{K=1}^{2} h_{J-K+2}[M^{**}_{2K} + N^{***}_{j(2K)} U_{2(J-K+1)+j} + W_{2(J-K+1)+j}(M^{***}_{(2K)j} - M^{***}_{j(2K)})] = M_J(1 + W_{2J+2}) \tag{3.56}$$

$$\sum_{K=1}^{2} h_{j-K+2}[N^{**}_{2K-1} + N^{***}_{j(2K-1)} W_{2(J-K+1)+j} + U_{2(J-K+1)+j}(M^{***}_{j(2K-1)} - M^{***}_{(2K-1)j})] = Z_j \tag{3.57}$$

$$\sum_{K=1}^{2} h_{J-K+2}[N^{**}_{2K} + N^{***}_{j(2K)} W_{2(J-K+1)} + U_{2(J-K+1)+j}(M^{***}_{j(2K)} - M^{***}_{(2K)j})] = - M_J U_{2J+2} \tag{3.58}$$

where $J = 0,1,2,\ldots N$.

A boundary condition of displacement results in the impossibility of assuming a non-vanishing variation for the particular displacement prescribed. The corresponding equilibrium equation must therefore be dropped and substituted by the specified value of the unknown. These conditions do not necessarily have to be imposed at the ends. They can be specified at any nodal point, allowing the solution of a continuous beam.

Due to the particular choice of stress and strain measures in the analytical formulation, the resulting discrete equilibrium equations (for the case of a linearly elastic material) are cubic polynomials in the nodal displacements and their first z-derivatives. The Newton-Raphson procedure is adopted to solve the set of equations (Equations 3.55 to 3.58). The Jacobian matrix is calculated in which the elements are derivatives of the equilibrium equations with respect to the unknowns. This matrix results in a band matrix of width 12. It is partitioned into submatrices of 4x4 which are arranged in a tri-diagonal manner. Potter's technique (20) is used at each step to solve the set of linear equations.

3.4 Computer Programs

Three different computer programs have been developed on the basis of the theory explained above. They are referred to as ELAST, PLAST and PLAST1 and their scope is as follows:

(a) ELAST deals with the linearly elastic case.

(b) PLAST deals with an ideally elasto-plastic-material. Plasticity effects as such, however, are not accounted for. The cross sectional shape may be a combination of three arbitrary rectangles, that is, an unsymmetrical I.

(c) PLAST1 deals with a tri-linear 'elastic' material. Initial (residual) stresses are included but the shape has to be a symmetric I.

Double precision is used and all the programs include an automatic recording of the present step and the last converged solution for added flexibility in restarting the iterative process. A more detailed description follows.

3.4.1 Program ELAST

The program ELAST has the following limitations.

1. A constant element length is assumed.
2. Constraints on degrees of freedom may be imposed at any node, but elastic supports are ruled out.
3. Loads (forces and moments) are assumed concentrated at the nodes.

For details of data preparation, Reference (4) should be consulted. Two types of output are generated by the program, viz., printed and permanent disk files. The printed output consists of intermediate results (with no explanatory headings) and final results (displacements, forces and co-ordinates). The output on disk is intended to allow for the restarting of the iteration process. The last trial vector is always stored in file 15 (erasing the previous vector). It is also convenient to have at hand the last converged solution. This may be accomplished by specifying NF1=1 (see a description of data preparation in Appendix D) which will cause the program to write the solution on file 16 only if convergence is achieved.

3.4.2 Program PLAST

The equations of equilibrium are the same as for ELAST, but yielding effects imply the existence of an upper bound. For the external load, an augmented structure technique (23) on this load carrying capacity is used. For post-buckling behavior, the augmentation has been realized only by means of linear horizontal, vertical and angular springs at the last node (right end) of the beam. The limitations on other procedures, including output are the same as for ELAST except that only the degree of freedom associated with the last node can be elastically supported.

3.4.3 Program PLAST1

PLAST1 is a generalisation of PLAST in two respects:

(a) It considers a trilinear constitutive equation, and

(b) It allows for the inclusion of initial stresses (linearly distributed along the flanges and constant on the web).

It is assumed that the walls are thin enough so that stresses can be considered constant through the thickness and the integration of stresses over the cross section is not complicated. Analysis of symmetric I sections only is allowed. The limitations are the same as in PLAST but final results in the output will include positions where changes in modulus of elasticity occur (in several sections along each element).

The integrals appearing in the equilibrium equations are evaluated numerically with the use of Simpson's rule over the length of element. Elements of the Jacobian matrix are evaluated by numerical differentiation.

3.5 Modifications to Programs

To achieve a generalisation to other shapes with consideration of a trilinear constitutive equation and inclusion of initial stresses, the program PLAST1 has been modified by the author. The flow chart is essentially the same as that in Epstein and Murray's report (4).

Modification has been made to the following subroutines.

1. MAIN
2. ABCG
3. FORMOM

3.5.1 Modification to MAIN

MAIN has been modified such that:

(a) Combinations of linear horizontal, vertical and angular springs can be used at any node in the entire beam.

(b) A residual (initial) stress pattern for unsymmetric I section has been calculated from the equilibrium considerations. The stress on the top and bottom of the web and in the narrow flange are determined from the given initial compressive stress at the top of the wide flange. Initial stresses are assumed constant on the narrow flange and linearly varying along web and the wide flange as shown in Figure A.2. The detailed calculation of the stress distribution is indicated in Appendix A. This pattern of residual stresses is intended to simulate those arising in a hat section.

The centre of gravity of an equivalent unsymmetrical I-section used to simulate a hat shaped section, is also calculated by the program. The program reads all data; including the initial trial vector of displacement which is given either on file 15 or file 16. Output has been modified so that the program prints all initial and final yielding values for both of the flanges and the web.

3.5.2 Modifications to ABCG

Subroutine ABCG evaluates the non-vanishing band (width = 12) of the Jacobian matrix, by means of DNMP, as well as the right hand side, by means of NMP, for use in the Newton-Raphson procedure. Thus subroutine ABCG formulates equilibrium equations and its derivatives. It has been modified such that augmenting springs can be applied at any nodes to get the descending part of load-deflection curve without altering the band character of Jacobian matrix. The band of the Jacobian matrix is subdivided into a tridiagonal partition of 4x4 submatrices for use in POTRS. Force and moment vectors are also modified since spring stiffnesses have been applied.

3.5.3 Modifications to FORMOM

Subroutine FORMOM has the function of calculating the axial force and bending moment stress resultants from the given two measures of strain ($\bar{e}$ and ϕ) for the given symmetric I-section and for a given trilinear constitutive equation. It is modified such that it calculates the axial force and bending moment stress resultants for a given equivalent unsymmetric I-section.

The stress and strain diagram and the system of coordinates are exactly the same as indicated in Reference 4. The technique of computing distances to the initiation of yielding in the web (y values) has been changed because the residual stress is no longer constant in the web but varies from compression at the top to tension at bottom. Derivations are shown in Appendix B. With these modified values of y, values of axial force and moment stress resultant are computed. Once this subroutine was tested and modified it was attached to the main program. MAIN with all its subroutines is stored in object form in a permanent file called NLHAT. The function of each subroutine is described in Reference 4.

CHAPTER 4

ILLUSTRATIVE APPLICATIONS OF PROGRAMS

4.1 Testing of Program ELAST

In order to verify the capabilities of the programs developed by Epstein and Murray (4) to predict the behavior of beam-columns, the programs have been used to solve problems whose solutions are already known.

The first problem chosen to verify the programs is the elastica (21), shown in Figure 4.1, which involves the elastic post-buckling behavior of a simply supported beam-column. A small transverse load was added in addition to the axial compressive force P to act as an initial imperfection. Results so obtained are tabulated in Table 4.1, where they are compared with the elastica solution (22). The plot of Figure 4.1 shows good agreement between these two sets of results in the post-buckling region. The number of elements used was four for one half of the column taking account of symmetry. The method of data preparation is described in Reference 4.

The solution to this problem by program ELAST was obtained by Epstein and Murray in Reference 4. It is repeated here to demonstrate the capability of the program to handle very large geometric non-linearities. Since the geometric formulation is identical for all programs contained in Reference 4, the capabilities of the programs PLAST and PLAST1 to represent similar types of deformation have been established.

4.2 Testing of Program PLAST

Use of program PLAST is made herein to analyse for plastic post buckling behavior. The solution for a W·8x31 simply supported beam of 210" span, subjected to the action of a constant transverse load Q at mid span, and to a varying uniform compressive force P, is shown in Figure 4.2. A sketch of the model, taking account of symmetry, is also shown in this figure. The points plotted are tabulated in Table 4.2. The transverse load Q was taken as 3413 lbs, so as to simulate an initial imperfection of 0.2". The boundary conditions at the left end are u=w=o, and at the right end u'=o. u and w are the vertical and horizontal deflections in the beam, respectively and u' is the slope at the end of the beam.

The half beam was divided into four finite elements. The yield strain was assumed to be 0.12% and the modulus of elasticity to be 30 x10^6 psi.

For the first trial an initial vector of zero is assumed with a compressive load of 200,000 lbs. It can be seen from Figure 4.2 that this load is quite close to the carrying capacity of the member. Since no plastic penetration is present, convergence was achieved very rapidly. Since yielding effects imply the existence of an upper bound for the external load, an augmented structure technique (23) is used. Augmentation is realized by means of an application of springs in the beam-column. Hence for the second load step a horizontal spring with a stiffness of 5 x 10^6 lb/in was added, which corresponds to roughly double the stiffness of the beam in that direction. The spring stiffness is doubled to achieve more rapid convergence and a smooth load deflection curve. This means that the total stiffness is approximately three times the stiffness of the member and a force of 600,000 lbs should be applied to maintain the augmented structure in its equilibrium configuration. As the load is increased, more and more of the increment goes into the spring until net force in the original structure diminishes. The total load and net load are shown in Table 4.2 as well as in Figure 4.2. If a very high load is adopted, the computer time limit may be exceeded, with the intermediate results showing a divergent behavior. This indicates that the load step is too large, and a smaller step has to be adopted.

Since the contents of file 15 represent the last trial vector, NF = 2 is specified for the subsequent run. This will cause the program to take the last converged solution as the first trial vector. Convergence may then be achieved at a smaller load step. The logical thing in using this program is to give a very small increase in load steps when plastic effects are about to begin in the section.

The computer time for convergence is relatively high when the load is either at the maximum of the load deflection curve or when the structure has passed its maximum carrying capacity. This occurs because it requires a greater number of cycles for convergence. The plastic penetration is very deep and is a maximum at the last equilibrium position of this example,affecting more than 70% of the beam depth as shown in Table 4.2.

This example problem for program PLAST is that used by Epstein in Reference 4. It illustrates the technique of applying springs to augment the stiffness of the structure in the descending region of the load deflection curve, in order to maintain a positive stiffness of the augmented structure. The presence of initial stresses smoothes the peak of the moment rotation curve. Also, the strain-hardening phenomenon has its effect on slowing down deformations past the maximum load.

4.3 Testing of Program PLAST1

The end rotation for the solution of a beam-column problem with constant axial load and increasing end moment is tabulated in Table 4.3 and plotted in Figure 4.3. The residual stress patterns that of Figure A.1 with σ_{rc} of 9900 psi ($\cdot 3\sigma_y$). The geometric and loading conditions are illustrated in the sketch in Figure 4.3. In this problem σ_y = 33 ksi and it is assumed that at a strain of 0.24% the strain hardening process begins with a modulus of 6 x 10^6 psi. Ordinates of points where changes in elasticity occur are also obtained in the computer output. The maximum point on this curve corresponds to the highest end moment which this column can support, thus giving the point on the interaction curve of Figure 4.4 with $\frac{P}{P_y} = 0.8$ and $\frac{\ell}{r} = 40$. Twelve such points, that define the maximum strength for various values of $\frac{\ell}{r}$ and $\frac{P}{P_y}$ have been obtained and are plotted in Figure 4.4. Points so obtained have been compared with the curves of Galambos and Ketter (6), shown by the solid lines in Figure

4.4, which include the effect of residual stresses. The points used for Galambos and Ketter's curves are tabulated in Table 4.4 and a numerical comparison is given in Table 4.5. These results differ by from 0 to 8% from those of Galambos and Ketter and indicate that PLAST1 gives reliable results for beam columns.

4.4 Applications of NLHAT

PLAST1 was modified, as explained in Section 3.5, to obtain the program NLHAT. It is difficult to obtain solutions in the literature for the verification of NLHAT since little attention has been devoted to the inelastic instability analysis of unsymmetric sections. However, the modifications are essentially concerned with the pattern of residual stress and the support conditions and therefore the fundamental capabilities of PLAST1 have been retained. The ability of NLHAT to predict the behavior of an unsymmetric section can be verified by testing for the plastification of the cross-section under the action of combined axial load and moment, since the conditions for complete plastification can be predicted by hand computation. Therefore, moment curvature curves were obtained from the program for a very short segment of the section and the fully plastic conditions from these results were compared with those obtained by hand computation.

The moment-curvature response for a segment of a C type chord section, with $F_y = 33000$ psi and $\sigma_{rc} = 9900$ psi, is shown in Figure 4.5 for various ratios of $\frac{P}{P_y}$. In order to simulate this section, the unsymmetric I - section shown in Figure 1.3 was used. Section properties of the simulated section and the chord section are given in Table 1.1. In deriving the dimensions of the simulated section the objective was to approximate the area and the moment of inertia as closely as possible. The length of the segment used in the computer analysis was 2 inches and therefore the plots in Figure 4.5 actually apply to a hat section column with $\frac{L}{r} = 4.8$. Note that two moment curvature curves are obtained for each fixed value of P, one for moment subjecting the wide flange to compressive stress (Table 4.6) and the other for moment subjecting the narrow flange to compressive stress (Table 4.7). The fully plastic moments, for the various values of $\frac{P}{P_y}$, obtained from the maximum moments on the moment-curvature curves of Figure 4.5, are tabulated (for $\frac{\ell}{r} = 0$) in Table 4.8 and plotted as the two solid interaction curves in Figure 4.6. (Moments producing compression on the narrow flange are considered positive and those producing compression on the wide flange are considered negative.) Hand computations for the fully plastic interaction curves of this section are carried out in Appendix C and plotted as the two dashed interaction curves in Figure 4.6. A comparison of these curves indicates that the finite element program underestimates the stress resultants required to produce fully plastic conditions for both signs of moment, the maximum error in $\frac{M}{M_p}$ being about 10%. This indicates that instability loads predicted by the finite element technique may be considered conservative.

For another comparison of the fully plastic interaction curves, the curve for a symmetric 8WF31 section, as plotted by Galambos and Ketter (6), is also shown in Figure 4.6. It should be noted that both the finite element and hand computed interaction curves for the hat section straddle that for the symmetric section. Since Galambos and Ketter's curves (6) are based on the behavior of an 8WF31, this indicates that their curves are not conservative for unsymmetric sections, if the applied loads produce compression on the narrow flange. This is demonstrated below for two different $\frac{\ell}{r}$ ratios.

Stability analysis, as described in Section 4.3, were carried out for the simulated hat section for $\frac{\ell}{r}$ ratios of 40 and 120. The results of these analyses are tabulated in Table 4.8 and plotted as the solid lines in Figure 4.7.

Galambos and Ketter's curves (6) are also plotted in Figure 4.7 for the same slenderness ratios. These results indicate that the moment capacity of this hat section may be over estimated by as much as 35%, for $\frac{\ell}{r} = 40$, by the curves based on symmetric sections.

Interaction curves for unsymmetric sections may be conveniently displayed as shown in Figure 4.8, where the lack of symmetry due to the sign of the moment is apparent. The values plotted in Figure 4.8 come from a series of analyses which are tabulated in Tables 4.9 and 4.10.

CHAPTER 5

A STUDY OF TOP CHORD BUCKLING OF JOISTS

5.1 Description of Experimental Project

Matiisen (14) has investigated the effect of joist eccentricity on the behavior of joints by performing tests on a series of joists. He derived the following conclusions:

1. The primary effect of joint eccentricity is to induce moment in the chord.
2. These moments, in the elastic range, can be predicted with good accuracy by modelling the joist as a frame.

In his test series five of the seven joists failed due to top chord instability. Two of these five had a type of joint which transferred little moment into the chord. The remaining three had a type of rigid welded connection which was capable of transferring substantial moments into the chords. In these three joists, designated as AX01, AX02 and AX05, failure was induced in a top chord member which did not have the maximum axial force. Thus, it is apparent that the moments in the critical members had a significant influence on the behavior of these members and contributed to their collapse. This chapter is concerned with an attempt to model the critical member in these joists as a beam-column, to predict the failure load of this member on the basis of an analysis of the model, and to compare the predicted capacity with the failure load observed in the tests.

The top chord member of joists AX01, AX02 and AX05, which failed due to inelastic instability, is shown as member 3T in Figure 5.1. The measured dimensions of these joists are shown in Figures 5.2 and 5.3. Concentrated loads were placed between top chord panel points to simulate uniform loading in joists AX01 and AX02, whereas in joist AX05 loads were applied at the centre of each of the top chord joints. In addition to testing the joists, material testing and elastic plane frame stress analyses, which computed joint rotations, displacements, axial forces and moments at the ends of each member, were carried out by Matiisen (14). The pertinent results which effect member 3T are tabulated in Tables 5.1 and 5.2. The member and joint numbering corresponds to that in Figure 5.1.

In joists AX01 and AX02 there are large moments generated in member 3T due to top chord loading, chord continuity and joint eccentricity. However, the moments in member 3T of joist AX05 are due primarily to joint eccentricity and continuity effects. A summary of the failure conditions for these joists is given in Table 5.3. All joists had C-section top chords.

The present study attempts to predict the load at which instability failure occurs by modelling the critical members as beam-columns with approximate boundary conditions, and compares predicted failure loads with those shown in Table 5.3.

5.2 Description of Models and Boundary Conditions

Member 3T was, at various times, analysed with three different kinds of boundary conditions, namely, force, spring and displacement boundary conditions. AX05 was analysed under all three boundary conditions, while AX01 was analysed under spring and force boundary conditions, and AX02 was analysed under only the force boundary condition. Force boundary conditions were also applied to models that included the joint as a part of the member, for all the joists. The program used for the analysis was NLHAT, described in Chapter 3. The method of data preparation and a listing of the program are given in Appendix D.

A typical finite element model of a top chord member with n elements, as idealized herein, is shown in Figure 5.4. The length of the member between panel point joints is denoted by ℓ. If a joint is included in the model, the length of this joint is denoted by ℓ_j. Loads on the model may consist of the axial force (shown as P), loads applied at the panel point joint (shown as Xj, Zj and Mj), and sets of interior loads (shown as Xi, Zi and Mi).

A summary of the geometric dimensions, the joint loads, and the interior loads, which are applicable to the six models used herein, is given in Table 5.4. Unfortunately, the program required a model with elements of equal length. The number of elements was chosen to obtain the joint loads as close as possible to a nodal point. For those models which include the joist joint, a J has been appended to the joist designation. For interior loads, the loads were replaced by statically equivalent forces at the two joints which straddled the actual point of application of the load on the joist. These statically equivalent loads are also shown in Table 5.4. The technique of obtaining joint loads will be more fully discussed in subsequent sections.

The joint boundary condition may, in general, be represented by a combination of an external moment, an angular spring and an imposed angular rotation, as shown at end A of Figure 5.4. A force boundary condition may be represented by $k_A = 0$ and specifying a non zero value for M_A. A displacement boundary condition may be represented by setting $k_A = \infty$ and specifying θ_A. A spring boundary condition may be represented by setting $\theta_A = 0$, and specifying the appropriate values of k_A and M_A. The boundary conditions at end B are similar, except that displacement in the axial direction is not restrained and the axial load P is applied at this joint. When necessary for numerical purposes, a linear horizontal spring is attached to joint B and the net axial force applied to the member is then P minus the spring force as explained in Section 4.2.

A summary of the boundary conditions for the analyses to be presented subsequently is contained in Table 5.5. The symbol F, S or D has been appended to the model designation of Table 5.4 to indicate force, spring or displacement boundary conditions, respectively. The material for all models is assumed to be elastic-perfectly plastic.

5.3 Analysis of Member 3T for Joist AX05

The center line geometry of this joist is shown in Figure 5.3. The length of member 3T is seen to be 22.96 inches and the length of the joint member (between joints 4 and 5) is seen to be 2.36 inches. The axial force and joint displacements arising from a plane frame analysis of this joist, subjected to design loads, are shown in Table 5.1. The load displacement plots for the analysis which were run on this member are shown in Figure 5.6. Each of these is described below.

5.3.1 Force Boundary Condition Analysis for AX05

The model of AX05 is detailed in Table 5.4. At design load the axial force in the member is 14730 lbs (Table 5.1). Table 5.2 indicates that under design conditions the moments M_A and M_B acting on the member are -2.56 and -.116 in kips. The boundary conditions for the member are then those summarised in Table 5.5 for model AX05:F and a sketch of the loading condition is shown in Figure 5.5(a). Applying these boundary forces in direct proportion to the axial load, a non-linear load deformation analysis may be carried out. The result is shown as curve AX05:F in Figure 5.6. The maximum carrying capacity of the member is 1.75 times the design load. The test value for this member, indicated in Table 5.3 and Figure 5.6, was 1.77. Thus, good correlation exists between the analysis with force boundary conditions, and the test value for this joist.

5.3.2 Displacement Boundary Condition Analysis for AX05

It can be argued that a force boundary condition on an isolated member will underestimate the collapse condition for the member as a part of a frame. The bases for this argument are: (a) the assumption that the moments applied to the member increase in proportion to the load overestimates these moments if yielding occurs around the ends of the member, and (b) when the initial member becomes unstable, the end conditions tend to restrain deformations rather than allow free rotation. To determine the influence of these effects, the member may be analysed by assuming the rotations at the ends of the member increase proportionately with load. This may be expected to produce an upper bound on the capacity of a member, whereas the force boundary condition may be considered to produce a lower bound.

The member end displacements may be computed from the output of the elastic frame analysis of Table 5.1 and a sketch of deformations shown in Figure 5.5(b). The rotation of the member from the chord is obtained by substracting the chord rotation, obtained by dividing the relative vertical displacement of joints 6 and 5 by the member length, from the absolute rotations of Table 5.1. Detailed calculations are contained in Appendix E. The resulting rotations, at design load, are shown as the displacement boundary conditions for model AX05:D in Table 5.5. These rotations may now be increased in proportion to the axial load, and the resulting behavior of the member is shown as curve AX05:D in Figure 5.6. The member has a considerably higher failure load under these conditions.

5.3.3 Spring Boundary Condition Analysis for AX05

It can also be argued that the web members framing into a joint act as restraining angular springs on the rotation of the chord and a better model would be obtained by considering the top chord member to be elastically restrained at the ends. Analysis of this type was carried out by obtaining the stiffness of the angular spring in the following manner.

The elastic moments in members 4, 34 and 5 framing into joint 5 are shown in Table 5.2. If member 34 is considered to act as an angular spring restraining joint rotation, the spring stiffness may be obtained by dividing the moment of 2.205 in-kips in this member by the net rotation at the end of member 3T (6.058 radians as shown in Table 5.5), resulting in a spring stiffness of 367900 in-kips/radian. The external moment to be applied to this joint is then the moment arising in member 4, namely 4.789 in-kips. These values are shown as the spring boundary condition for AX05:S in Table 5.5. The conditions at end B are determined in a similar manner. A sketch of the model is shown in Figure 5.5(c).

Increasing the forces in a proportional manner on the spring boundary condition model of member 3T of AX05 results in the load deflection curve denoted as AX05:S in Figure 5.6. The behavior falls between that for force and displacement boundary conditions.

5.3.4 Analysis of AX05 Including Joint Length

A final model of member 3T in joist AX05 was developed by including the length of the joint with the member. End A of the member was considered to be joint 4 of Figure 5.1, and was subjected to the force boundary condition arising from the sum of the moments in members 3 and 33. The boundary conditions are shown as those for AX05J in Table 5.5. Joint 5 then became node 2 of the finite element model and the loads applied at this point, shown in Table 5.4, represent the summation of the components of forces in member 34 and one-half the external panel point load. A sketch of the model is shown in Figure 5.5(d). The load deflection analysis for this model is shown as line AX05J:F in Figure 5.6. The critical load obtained from this model is at a load factor of 1.63 which is 7.9% less than the test value of 1.77.

Some difficulty was encountered in this model in obtaining the unloading part of the load deflection curve. The curve is plotted in more detail in Figure 5.7. The reason for this behavior is shown in Figure 5.8 where it is apparent that once the critical load has been reached the deflections at the centre of the member begin to decrease because of large curvatures developed in the joint region. The load-deflection curve for horizontal displacement of end B is also shown in Figure 5.6 which indicates an increasing displacement as the load decreases in the post-buckling region.

5.3.5 Review of Analysis for AX05

The numerical values from which Figures 5.6 and 5.7 have been plotted are given in Tables 5.6, 5.7 and 5.8. The maximum load factors for each of the four analyses are underlined in Table 5.8. It is apparent that analysis AX05:F gives the best results for this member.

5.4 Analysis of Member 3T for Joist AX01

The primary difference in loading conditions between joist AX05 and joist AX01 is that the external loads were applied directly to the top chord in joist AX01 rather than at the joints. The joist geometry is detailed in Figure 5.2 and the elastic results of the plane frame stress analysis, for loads applied 2.915 and 4 inches from the centers of joints 5 and 6, respectively, are summarized in Tables 5.1 and 5.2.

The loads acting on the model are shown in Table 5.4. Since the load adjacent to end B did not fall on a nodal point, the actual design load of 843 lbs was replaced by two statically equivalent nodal loads determined by the inverse lever rule as indicated in Table 5.4. Boundary conditions were handled in the same way as for member AX05 as described in Section 5.3. However, since the displacement boundary conditions give an unrealistically high collapse load, only force and spring boundary conditions have been considered.

5.4.1 Force Boundary Condition Analysis of AX01

The model of AX01 is detailed in Table 5.4. At design load the axial force in the member is 14660 lbs (Table 5.1). Table 5.2 indicates that under design conditions the moments, M_A and M_B acting on the member are -.400 and -2.79 in-kips. The design load boundary conditions for the member are then those summarised in Table 5.5 for model AX01:F and a sketch of the loading condition is shown in Figure 5.9(a). Multiplying these by a common load factor a non-linear load deformation analysis may be carried out. The result is shown as curve AX01:F in Figure 5.10. This result predicts about 11% higher capacity than the test result indicated in Table 5.3 and Figure 5.6.

5.4.2 Spring Boundary Condition Analysis of AX01

The spring stiffness at joints 5 and 6 are obtained in a similar manner to those for AX05. The external moments to be applied to these joints are then the moments arising in members 4 and 6, namely 2.604 and 2.973 in-kips. These values are shown as the spring boundary conditions for AX01:S in Table 5.5. A sketch of the model is shown in Figure 5.9(b).

Increasing the forces in a proportional manner on the spring boundary condition model results in the load deflection curve denoted as AX01:S in Figure 5.10. As expected, this behavior predicts a higher capacity than the force boundary condition.

5.4.3 Analysis of AX01 Including Joint Length

Since both of the above models overestimate the strength of the member, a model including the length of joint with the member, similar to AX05J, was analyzed. The boundary conditions are shown as those for AX01J in Table 5.5. Joint 5 became node 2 of the finite element model and the loads applied at this point, shown in Table 5.4, represent the summation of the components of forces in member 34 and one half the external panel point load. A sketch of the model is shown in Figure 5.9(c). The load deflection analysis for this model is shown as curve AX01J:F in Figure 5.10. The maximum carrying capacity of the member is 1.76 times the design load. The test value for this member, indicated in Table 5.3 and Figure 5.10, was 1.64. Thus, this model overestimates the capacity of the member to be 7.3%.

5.4.4 Review of Analysis for AX01

The numerical values from which Figure 5.10 have been plotted are given in Table 5.9. The maximum load factors from the three analyses are underlined in Table 5.9. It is apparent that none of these analyses give very good results. All analyses predict a higher capacity than the test value. However, in contrast to AX05, the analysis including the joint yields a better value than that excluding the joint.

5.5 Analysis of Member 3T for Joist AX02

There is practically no difference between joist AX01 and AX02 except that joist AX02 was fabricated with larger joint eccentricities. External loads were directly applied on the top chord. The joist geometry is detailed in Figure 5.2 and the elastic results of the plane frame stress analysis, for loads applied 2.515 and 4 inches from the centres of joints 5 and 6 on member 3T, are summarised in Tables 5.1 and 5.2.

The loads acting on the model are shown in Table 5.4. Since the interior loads did not fall on nodal points, the actual design load of 843 lbs was replaced by two statically equivalent nodal loads as indicated in Table 5.4. Boundary conditions were handled in the same way as described in Section 5.3. However, since displacement and spring boundary conditions overestimate the collapse load, only analyses for force boundary conditions, with and without the inclusion of the joint length, have been considered.

5.5.1 Force Boundary Condition Analysis of AX02

The model of AX02 is detailed in Table 5.4. At design load the axial force in the member is 14670 lb(Table 5.1). Table 5.2 indicates that under design conditions the moments M_A and M_B acting on the member are -1.784 and -2.969 in-kips. The boundary conditions for the member are then those summarized in Table 5.5 as model AX02:F, and a sketch of the loading condition, at design load, is shown in Figure 5.11(a). Multiplying these by a common load factor a nonlinear load deformation analyses may be carried out. The result is shown as curve AX02:F in Figure 5.12. The maximum carrying capacity of member is 1.69 times the design load. The test value for this member, was 1.55. Thus, this analysis overestimates the member capacity.

5.5.2 Analysis of AX02 Including Joint Length

The joint model was developed similar to joist AX01. The boundary conditions are shown as those for AX02J in Table 5.5. The joint length is 2.97 inches and the length of each element is assumed as 1.5 inches. Hence the joint length is approximately two element lengths, so joint 5 becomes node 3 of finite element model. The loads applied at this point, shown in Table 5.4, represent the summation of the components of forces in member 34 and one half the external panel point load. A sketch of the model is shown in Figure 5.11 (b). The load deflection analysis for this model is shown as curve AX02J:F in Figure 5.12. The maximum carrying capacity of the member is 1.56 times the design load. The test value for this member, indicated in

Table 5.3 and Figure 5.12, was 1.55. Thus, very good correlation exists between this analysis, with the effect of joint length, and the test value for this joist.

5.5.3 Review of Analysis of AX02

The numerical values from which Figure 5.12 has been plotted, and the load factors for these analyses, are given in Table 5.10. It is apparent that analysis AX02J:F gives the best result for this member.

5.6 Effect of Transverse Load Position and Yield Stress

The influence of the location of the transverse loads on the member is illustrated for joist AX01 in Figure 5.13. Two solutions were obtained:

(a) With the transverse loads placed 6" from either end.

(b) With the transverse loads placed 3" from either end.

Force boundary conditions were used (AX01:F of Table 5.5). The numerical values for the analyses are shown in Table 5.11 and the ultimate load factors are 1.84 and 1.35 for cases (a) and (b), respectively.

It is apparent that the positioning of the transverse loads on the span has a dramatic effect on the carrying capacity of the member.

The influence of yield stress on the ultimate load factor is illustrated for joist AX01 in Figure 5.14. The numerical values for the analyses are tabulated in Table 5.11. The analyses were carried out for loads positioned as in case (b) above, and result in ultimate load factors of 1.35 and 1.42 for F_y = 60.3 ksi and F_y = 65 ksi, respectively. This result indicates that the ultimate load is also sensitive to the yield stress.

5.7 Summary of Top Chord Analyses

A summary of critical load factors for the different models that have been analyzed in this chapter is given in Table 5.12, where they are compared with the test results.

CHAPTER 6

SUMMARY, CONCLUSIONS AND RECOMMENDATIONS

6.1 Summary

The application of a set computer program for the large deformation analysis of inelastic beams has been investigated for a variety of problems. The programs were used to obtain maximum loading conditions for W8x31 sections which compare favorably with the interaction curve of Galambos and Ketter. The inelastic program with initial stresses (PLAST1) has been modified (to NLHAT) so that it is applicable to unsymmetric I sections with a residual stress pattern simulating that which could occur in a hat section. The hat section has been simulated as an unsymmetric I section and interaction curves have been generated for this type of section.

The program NLHAT was then applied to models of the critical member in the top chord of three of the joists in Matiisen's test series in an attempt to determine if such a model can properly predict the failure conditions of the member when it is a part of a joist framework. The models considered the effect of boundary conditions and the effect of including the joint length as a part of the member.

6.2 Conclusions

The following conclusions may be drawn from the investigation.

1. The finite element program used herein can properly account for the effect of large in-plane deformations.

2. When used with the augmented stiffness technique the programs can be applied to predict ultimate carrying capacities of members.

3. The programs predict ultimate strength conditions for symmetric sections which are in good agreement with the beam-column interaction curves of Galambos and Ketter.

4. The program NLHAT underestimates the fully plastic interaction conditions for unsymmetric sections and is, therefore, conservative.

5. The interaction curve for a beam-column with an unsymmetric section is considerably lower than that for a symmetric section when bending produces compression on the narrow flange. Thus, design rules formulated for symmetric sections may be inadequate when applied to unsymmetric sections.

6. Models of top chord members which have either spring or displacement boundary conditions consistently overestimate the capacity of the member in a joist framework.

7. The ratios of test to predicted load factors are 1.01, 0.89 and 0.91,for force boundary conditions, for joists AX05, AX01 and AX02, respectively.

8. The ratios of test to predicted load factors are 1.09, 0.93 and 0.99, for force boundary conditions applied to members augmented by the joint lengths, for joists AX05, AX01 and AX02, respectively.

9. The load factors for the members augmented with the joint lengths are consistently lower than those without, and this type of model gives the best correlation with the test values for the three joists examined.

10. The number of joists for which test values were available is insufficient to draw any firm conclusions about the reliability of the modeling techniques described herein.

6.3 Recommendations and Observations

The following recommendations and observations are made for future work.

1. It is recommended that predictions of top chord capacities be carried out for other joists, associated with the Canadian Steel Industries Construction Council Research Project No. 744, as test results become available. In this way the reliability of the predictive capacity of the program can be established.

2. In view of the sensitivity of the predicted failure load to the location of transverse loads it is recommended that an experimental study of this effect be carried out.

3. In view of the sensitivity of the predicted failure load to yield stress it is recommended that improved techniques be developed for measuring the mechanical properties of hat-shaped sections.

4. It is observed that the models of the members with force boundary conditions, but without joint lengths, considerably overestimated the capacity of two of the three joists available for study. This may be a result of the inadequacy of the boundary conditions imposed on the model. However, test observations indicate that there is considerable deformation of the cross-section prior to failure, which cannot be predicted with the present programs. It is possible, therefore, that

the discrepancy between predicted and observed collapse conditions results from the fact that distortion of the cross-section produces a decrease in carrying capacity of the section, and it is recommended that programs be developed which can adequately account for this effect.

LIST OF REFERENCES

1. Austin, W.J., "Strength and Design of Metal Beam-Columns",Journal of Structural Division, ASCE vol. 87, St4, April 1961 pp. 1-32.
2. Bleich, F., "Buckling Strength of Metal Structures", McGraw Hill Book Company, N.Y., 1952.
3. Epstein, M., and Murray, D.W., "Large Deformation In-Plane Analysis of Elastic Beams", Computers and Structures, vol. 6, Jan. 1975, pp. 1-9.
4. Epstein, M., and Murray, D.W., "A System of Computer Programs for the Large Deformation In-Plane Analysis of Beams", Structural Engineering Report No. 57, Civil Engineering Department, University of Alberta, May 1976.
5. Galambos, T.V., "Structural Members and Frames", Prentice-Hall, Inc., Englewood Cliffs, N.J., 1968.
6. Galambos, T.V., and Ketter, R.L., "Columns Under Combined Bending and Thrust", Trans. ASCE, vol. 126, 1961, pp. 1-23.
7. Hill, H.N., and Clark, J.W., "Lateral Buckling of Eccentrically Loaded I and H-Section Columns", Proceeding of the First National Congress of Applied Mechanics, (ASME) 1951, p. 407.
8. Jhonston, B.G., "Guide to Design Criteria for Metal Compression Members",Column Research Council, John Wiley and Sons Inc., New York, N.Y., 1966.

9. Kennedy, D.J.L., and Rowan, W.H.D., "Behavior of Compression Chords of Open Web Steel Joists", M.Sc. thesis, University of Toronto, 1963.

10. Ketter, R.L., "Further Studies of the Strength of Beam-Columns", Journal of Struct. Dn, ASCE, vol. 87, St6, Aug. 1961, pp. 135.

11. Ketter, R.L., Kaminsky, E.L., and Beedle, L.S., "Plastic Deformation of Wide Flange Beam-Columns", Trans. ASCE, vol. 120, 1955, pp. 1028 - 1095.

12. Mansell, D.C., and Neal, B.G., "The effects of restraint upon the collapse loads of mild steel trusses", International Journal of Mechanical Sciences, vol. 5, Feb. 1963, pp. 87-97.

13. Mason, R.E., Fisher, and Winter George,"Eccentrically loaded hinged steel columns", Journal of Engineering Mechanics Division, ASCE, vol. 84, No. EM4, Oct. 1958, paper 1732 pp. 1-19.

14. Matiisen, R., "Effect of Joint Eccentricity on Open Web Steel Joists", A thesis to be submitted to the Faculty of Graduate Studies of the University of Alberta in partial fulfillment for the degree of M.Sc. in Civil Engineering, Fall 1976.

15. McDonald, W.S., "Inelastic Behavior of Compression Chords of Open Web Steel Joists", Ph.D. thesis, University of Kansas, 1966.

16. McGuire, W., "Steel Structures", Prentice Hall, Inc. Englewood Cliffs, N.J. 1968.

17. Murray, D.W. and Simmonds, S.H., "Second, Third and Fourth Progress reports to Canadian Steel Industries Construction Council", Research Project No. 744, University of Alberta.

18. Osgood, W.R., and Westergaard, "Strength of Steel Columns', Trans. ASME, vols. 49, 50, APM-50-9, 1928, p. 65.

19. Salvadari, M., "Lateral Buckling of I-beams", Trans. ASCE vol. 120, 1955, pp. 1165-1182.

20. Tene, Y., Epstein, M., and Sheinman, I., "A generalisation of Potter's method", Computers and Structures, vol. 4, 1974, pp. 1099-1103.

21. Timoshenko, S.P., and Gere, J.M., "Theory of Elastic Stability", McGraw Hill Book Company, Inc., N.Y., 1961.

22. Wang Chi-Teh, "Applied Elasticity", McGraw Hill Book Company Inc., N.Y., 1953.

23. Wright, E., Whitman, and Gaylord, Edwin H., "Analysis of Unbraced Multistory Steel Rigid Frames", Journal of the Structural Division, ASCE, vol. 44, No. ST5, May 1966, pp. 1143-1163.

24. ASCE-Manuals and Reports on Engineering Practice No. 41, "Plastic design in steel - A guide and commentary", 1971.

25. Handbook of Steel Construction-Canadian Institute of Steel Construction 1973.

26. Great West Steel, "Open Web Steel Joists:Western (W) 1973 Series", Great West Industries Limited.

27. Specification for the Design, Fabrication and Erection of Structural Steel for Building, American Institute of Steel Construction (1963).

TABLES

Table 1.1 Section Properties

Type-C Shallow hat section (Figure 1.2)		Equivalent I-section (Figure 1.3)	
Area	.638	Area	.6378
W	3.25		
y	.685	y	.6805
I_{xx}	.109	I_{xx}	.1147
r_{xx}	.422	r_{xx}	.424
F	1.0	A1	.134
H	1.134	A2	.866
c	.111	A3	.134
T	.134	B1	1.1
S_{xx}	.16	B2	.229
r_{yy}	.838	B3	2.18

Note: Units are in inches

Table 4.1 Comparison of Classical and Numerical Solutions for the "Elastica"

LOAD(lbs)	DEFLECTION (inches)	
	ELAST	Wang's Result(22) (Theoretical Solution)
3	0.2966	
5	0.41458	
6	0.51656	
7	0.68122	
8	0.97628	
9	1.52914	0.9127
9.8	2.14979	0.9939
10	2.30522	1.015
12	3.4	3.4
15	3.944	4.01
17	4.01	4.01
20	3.97754	3.98
24	3.8249	3.83

Table 4.2 Inelastic Solution for a Beam-Column by Program PLAST

Total Load in lbs.	Net Load in lbs.	Vertical Deflection in inch	% Plastic Penetration at x = 1/2 *
200,000	200,000	0.2739	Nil
747,200	253,115	0.3436	30
747,500	253,104	0.3461	31
748,000	253,068	0.3506	33
749,000	252,927	0.3611	36
749,500	252,811	0.3672	37
750,000	252,655	0.3742	39
750,500	252,448	0.3822	41
751,000	252,184	0.3913	43
755,000	245,673	0.5447	62
760,000	236,000	0.7434	71

* % Plastic Penetration = $[d - y_2 - y_3]$x100/d (see Figure B.2)

Table 4.3 Moment-End Rotation for Beam Column*

M (lbs-in)	θ
120,000	0.445
128,400	0.508
134,176	0.602
129,703	0.795
134,163	0.706
134,867	0.665
134,621	0.685
134,836	0.669
134,906	0.657
134,912	0.653
134,907	0.849

*Example of Section 4.3: ℓ=138.8", $\frac{\ell}{r}$ = 40, $\frac{P}{P_y}$ = 0.8, F_y = 33 ksi

Table 4.4 $\frac{P}{P_y}$ Results from Galombos and Ketter (6)

$\frac{M}{M_y}$ \ $\frac{\ell}{r}$	0	40	60	80	100	120
0	1.0	0.92	0.88	0.83	0.76	0.62
0.1	0.92	0.83	0.77	0.69	0.58	0.45
0.2	0.84	0.74	0.67	0.57	0.47	0.35
0.3	0.75	0.65	0.56	0.47	0.38	0.29
0.4	0.67	0.55	0.47	0.39	0.32	0.23
0.5	0.58	0.46	0.39	0.32	0.26	0.19
0.6	0.49	0.37	0.31	0.25	0.20	0.15
0.7	0.40	0.28	0.23	0.19	0.15	0.11
0.8	0.30	0.20	0.15	0.13	0.10	0.08
0.9	0.20	0.11	0.08	0.07	0.05	0.04

Table 4.5 Comparison of Compared $\frac{M}{M_p}$ Values with Interaction Curve of Galambos and Ketter (6)

$\frac{P_o}{P_y}$ \ $\frac{\ell}{r}$	40	60	80	100	120
0.2	(0.80) 0.783 [0.796]				
0.4	(0.57) 0.54 [0.556]	(0.49) 0.447	(0.385) 0.351	(0.27) 0.248	(0.14) 0.139
0.6	(0.35) 0.32 [0.348]				
0.8	(0.14) 0.13 [0.161]				

[] - without residual stress obtained from PLAST1

() - Galambos and Ketter with residual stress

Unbracketted Quantity - without residual stress obtained from PLAST1

Table 4.6 Moment-Curvature (M-ϕ) Relationship for Zero Slenderness Ratio and Bending Compression in Wide Flange

$\frac{P}{P_y} = 0$		$\frac{P}{P_y} = 0.2$		$\frac{P}{P_y} = 0.4$		$\frac{P}{P_y} = 0.6$		$\frac{P}{P_y} = 0.8$	
$M_{k\text{-}in}$	ϕ	$M_{k\text{-}in}$	ϕ	$M_{k\text{-}in}$	ϕ	$M_{k\text{-}in}$	ϕ	$M_{k\text{-}in}$	ϕ
5	.14	5	.14	4	.12	3	.095	2	.0911
6	.175	6	.177	4.5	.154	4	.154	2.1	.102
6.5	.197	6.5	.194	6	.216	4.5	.232	2.2	.118
7.0	.246	7	.213	6.5	.282	4.8	.361	2.3	.142
7.5	.351	7.5	.241	7	.418	4.9	.47	2.4	.189
7.7	.444	7.8	.317	7.1	.488	4.946	.58	2.43	.214
7.8	.524	7.9	.366	7.11	.519	4.96	.674	2.437	.222
7.9	.885	8	.456	7.113	.531	4.9518	.77	2.481	.3
7.91	.972	8.05	.543	7.124	.574			2.491	.383
7.915	1.023	8.1	.745	7.1352	.646			2.478	.468
7.92	1.08	8.11	.852	7.135	.719				
7.95	1.54	8.111	.87						
		8.1138	.974						
		8.117	1.08						

Table 4.7 Moment-Curvature (M-ϕ) Relationship for Zero Slenderness Ratio and Bending Compression in Narrow Flange

$\frac{P}{P_y} = 0$		$\frac{P}{P_y} = .2$		$\frac{P}{P_y} = 0.4$		$\frac{P}{P_y} = 0.6$		$\frac{P}{P_y} = 0.8$	
Min K in	ϕ	M k-in	ϕ	M k-in	ϕ	M k-in	ϕ	M k-in	ϕ
5	.14	5	.163	4	.156	2	.0585	.5	.0144
6	.18	5.5	.226	4.5	.295	2.5	.089	.6	.174
6.5	.225	6.0	.373	4.6	.365	2.8	.139	.7	.02
7	.3	6.3	.704	4.65	.419	3.0	.216	.8	.023
7.5	.459	6.35	.924	4.68	.464	3.1	.312	.9	.026
7.7	.611	6.353	.964	4.709	.524	3.115	.338	1.0	.029
7.8	.76	6.354	1.11	4.738	.62	3.132	.376	1.2	.048
7.803	.77	6.333	1.258	4.753	.717	3.15	.434	1.5	.142
7.812	.79			4.756	.816	3.162	.533	1.562	.243
7.83	.84			4.748	.916	3.159	.633	1.573	.342
7.848	.91							1.565	.943
7.843	.88								
7.85	.957								
7.87	1.645								

Table 4.8 Finite Element Interaction Analysis for Simulated Hat Section* (Figures 4.6 and 4.7)

$\frac{P}{P_y}$ \ $\frac{\ell}{r}$	0		40		120	
	+ve	-ve	+ve	-ve	+ve	-ve
0	1	1				
.2	.807	1.021	.703	.934	.392	.576
.4	.604	.897	.744	.477	.134	.187
.6	.402	.624	.252	.453	.0044	.0074
.8	.200	.313	.124	.200		
.975			0	0		
.992	0	0				

* $\sigma_{rc}=0$, σ_y = 33 ksi

Table 4.9 Interaction Values for Simulated Hat Section

(Wide Flange in Compression: $\sigma_{rc}=o$)

$\frac{\ell}{r} = o$		$\frac{\ell}{r} = 40$		$\frac{\ell}{r} = 80$		$\frac{\ell}{r} = 120$	
$\frac{P}{P_y}$	$\frac{M}{M_p}$	$\frac{P}{P_y}$	$\frac{M}{M_p}$	$\frac{P}{P_y}$	$\frac{M}{M_p}$	$\frac{P}{P_y}$	$\frac{M}{M_p}$
0	1	0	1	0	1	0	1
.09	1.026	.05	.965	.15	.74	.05	.7539
.18	1.03	.15	.927	.295	.519	.15	.49
.25	1.02	.40	.68	.39	.353	.19	.393
.36	.95	.58	.431	.52	.185	.21	.343
.45	.86	.76	.222	.60	.1099	.25	.242
.54	.75	.90	.084	.68	.054	.36	.01
.77	.385						

Table 4.10 Interaction Values for Simulated Hat Section

(Narrow Flange in Compression : $\sigma_{rc} = o$)

$\frac{\ell}{r} = o$		$\frac{\ell}{r} = 40$		$\frac{\ell}{r} = 80$		$\frac{\ell}{r} = 120$	
$\frac{P}{P_y}$	$\frac{M}{M_p}$	$\frac{P}{P_y}$	$\frac{M}{M_p}$	$\frac{P}{P_y}$	$\frac{M}{M_p}$	$\frac{P}{P_y}$	$\frac{M}{M_p}$
0	1	0	1	0	1	0	1
.09	.935	.05	.89	.025	.87	.01	.893
		.15	.74	.15	.56	.1	.5
				.295	.33	.19	.27
.313	.74	.4	.44				
				.39	.23	.25	.16
.54	.51	.58	.28				
				.52	.12	.325	.05
.77	.27	.76	.14			.36	.01
				.7	.03		
1	0	.9	.05				
		1	0				

Table 5.1 Design Load Results from Elastic Frame Analysis

Joist	Yield Stress (ksi)	Axial Force in 3T(lbs)	Joint	Rotation	Vertical Deflection (inches)
AX01	65	14660	5	-0.0110928	-0.4091547
			6	-0.0017483	-0.5159207
AX02	65	14670	5	-0.0135107	-0.4730675
			6	-0.00142	-0.5840069
AX05	57.5	14730	5	-0.0109852	-0.4625646
			6	-0.0021092	-0.5756908

Table 5.2 Design Load Bending Moments from Elastic Frame Analysis

Member	Node	AX01	AX02	AX05
3	3	3.356	3.693	0.754
	4	-3.065	-2.839	-0.755
4 (Joint)	4	8.801	11.111	7.658
	5	2.604	4.79	4.789
5 (3T)	5	-0.40	-1.784	-2.56
	6	-2.79	-2.969	-0.116
6	6	2.973	3.228	0.339
	7	-2.459	-2.304	-0.136
33	4	-5.736	-8.271	-6.903
	20	-8.348	-12.103	-10.322
34	5	-2.205	-3.006	-2.229
	21	-2.057	-2.773	-2.19
35	6	-0.185	-0.26	-0.222
	22	-0.418	-0.589	-0.482

Note: Moments are in Kips - inch

Table 5.3 Summary of Test Results

No.	Joist Factors	AX01	AX02	AX05
1	Design Load (lbs)	1686	1686	1686
2	Total Ultimate Load (lbs)	2759	2769	2984
3	Load Factor ($\frac{\text{2nd Row}}{\text{1st Row}}$)	1.64	1.55	1.77
4	Amount of Eccentricity	Medium	Large	Medium
5	Type of Loading	Top Chord	Top Chord	Panel Point
6	Mode of Failure	Buckling 3T	Buckling 3T	Buckling 3T

Table 5.4 Interior and Joint Loading for Top Chord Models

Model	No. of Elements	ℓ_j (in)	ℓ (in)	Joint Loads				Interior Loading					
								On Joist		On Model			
				Node	X_j	Z_j	M_j	x	X	Node	X_j	Node	X_j
AX01	8	0	23.17					2.915	-843	2	-843		
								19.17	-843	7	-321	8	-522
AX01J	12	2.17	23.17	2	-4565	2824	2204	5.085	-843	3	-520	4	-323
								21.34	-843	11	-754	12	-89
AX02	15	0	22.57					2.515	-843	4	-295	5	-548
								18.57	-843	15	-559	16	-284
AX02J	17	2.97	22.57	3	-4666	2907	3006	5.485	-843	4	-295	5	-548
								21.54	-843	15	-559	16	-284
AX05	8	0	22.96										
AX05J	11	2.36	22.96	2	-5446	2805	2229						

Note: Units are inches and pounds

Table 5.5 Boundary Conditions for Top Chord Models

Model	B.C	M_A	$\theta_A \times 10^{-3}$	$k_A \times 10^3$	M_B	$\theta_B \times 10^{-3}$	$k_B \times 10^3$
AX01:F	Force	-4.00	-	0	-2790	-	0
AX01:S	Spring	+2604	0	339.6	+2973	0	64.9
AX01J:F	Force	8800	-	0	-2790	-	0
AX02:F	Force	-1784	-	0	-2969	-	0
AX02J:F	Force	11100	-	0	-2969	-	0
AX05:F	Force	-2560	-	0	-116	-	0
AX05:S	Spring	+4789	0	367.9	-339	0	78.8
AX05:D	Disp.	0	-6.058	∞	0	-2.818	∞
AX05J:F	Force	+7658	-	0	-116	-	0

Note: Units are K-inches

Table 5.6 Load Deflection Relationship of AX05J:F

Load Factor	U(10^{-1} inches)	W(10^{-1} inches)
1	.410	.196
1.4	.679	.281
1.6	.86	.36
1.626	.872	.42
1.6	.6688	.62
1.53	.481	.83

Table 5.7 Load-Vertical Deflection (10^{-1}) Values at Each Node for AX05J:F

Load Factor / Node No.	1	1.63	1.53	1.60
1	0	0	0	0
2	.148	.226	-.229	-.12
3	.271	.506	.49	.267
4	.355	.707	.259	.474
5	.401	.828	.403	.607
6	.412	.872	.481	.669
7	.393	.844	.5	.666
8	.346	.754	.466	.605
9	.278	.611	.388	.496
10	.194	.429	.277	.351
11	.992	.22	.143	.181
12	0	0	0	.481

Note: All deflections are in inches

Table 5.8 Load-Deflection Relationships for AX05

AX05:F		AX05J:F		AX05:S		AX05:D	
Load Factor	$U(10^{-1})$ inches	Load Factor	$U(10^{-1})$ inches	Load Factor	$U(10^{-1})$ inches	Load Factor	$U(10^{-1})$ inches
1	.31	1	.41	1	.26	.954	.25
1.5	.56	1.4	.68	1.72	.52	1.43	.39
1.7	.73	1.6	.86	1.8	.56	1.64	.45
						1.81	.51
1.745	.92	1.63	.872	1.99	1.02	2.1	.63
1.64	1.72			1.9	1.27	2.14	.66
						2.17	.83
						2.22	1.07
						2.16	1.45

Table 5.9 Load-Deflection Relationship for AX01

AX01:S		AX01J:F		AX01:F	
Load Factor	U(10^{-1}) inches	Load Factor	U(10^{-1}) inches	Load Factor	U(10^{-1}) inches
1	.36	1	.50	1	.42
1.4	.55	1.6	1.025	1.5	.74
		1.7	1.14	1.7	.91
1.5	.60				
		1.757	1.207	1.813	1.09
1.6	.66				
1.8	.781	1.763	1.382	1.835	1.170
1.9	.87	1.74	1.91	1.824	1.277
2	1.125				
2.03	1.492				
2.026	1.62				

Table 5.10 Load-Deflection Relationships for AX02

AX02J:F		AX02:F	
Load Factor	$U(10^{-1})$ inches	Load Factor	$U(10^{-1})$ inches
1	.7439	1	.506
1.4	1.2037	1.4	.801
1.483	1.344	1.55	.935
1.535	1.4636	1.695	1.16
1.559	1.5255		
1.564	1.672		
1.565	1.777		
1.5615	1.919		

Table 5.11 Effect of Load Position and Yield Stress on Joist AX01

Deflection at mid span for AX01:F					
Load at 3" from joints $F_y = 60.3$		Load at 6" from Joints			
		$F_y = 60.3$		$F_y = 65$	
Load Factor	$U(10^{-1})$ inches	Load Factor	$U(10^{-1})$ inches	Load Factor	$U(10^{-1})$ inches
1	.4165	1	.9857	1	.9857
1.5	.7412	1.3	1.552	1.3	1.347
1.7	.9133	1.35	1.911	1.4	1.659
1.813	1.0916	1.327	2.289	1.42	2.013
1.835	1.17			1.42	2.078
1.824	1.277			1.4	2.6086

Table 5.12 Summary of Critical Load Factors of Joists

Joist	Load Factor From Analysis	Load Factor From Test	Test Factor / Predicted Factor
AX05:F	1.75	1.77	1.01
AX05J:F	1.63		1.09
AX05:S	1.99		0.89
AX05:D	2.22		0.80
AX01:S	2.03	1.64	0.81
AX01:F	1.84		0.89
AX01J:F	1.76		0.93
AX02:F	1.70	1.55	0.91
AX02J:F	1.57		0.99

FIGURES

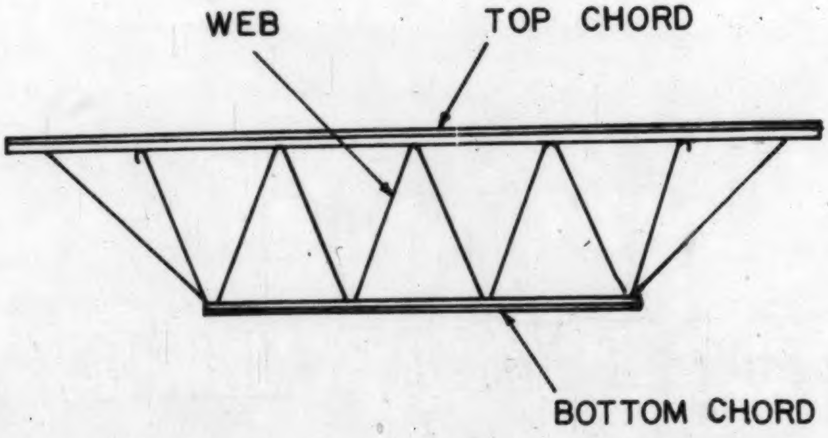
WEB
TOP CHORD
BOTTOM CHORD

FIG. 1·1 TYPICAL OPEN WEB STEEL JOIST

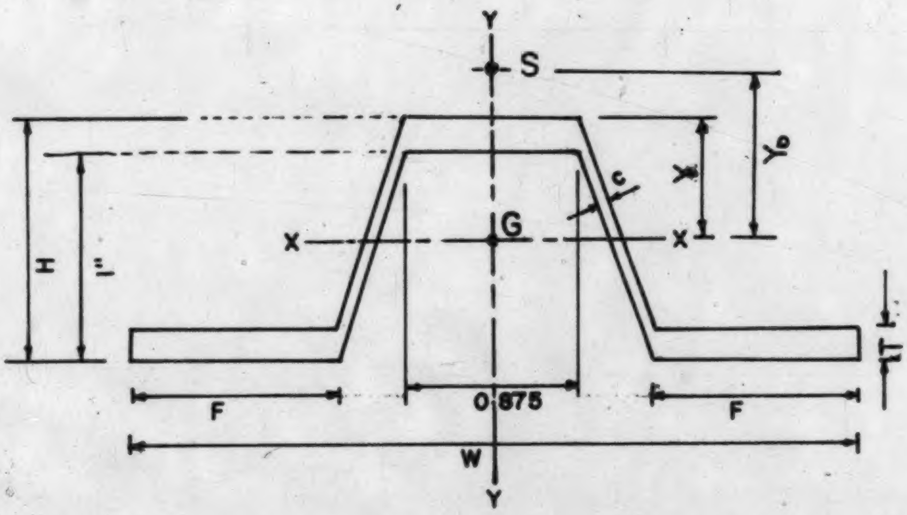
Y
S
Y_0
$\bar{Y}$
c
G
X
X
H
H'
T
F
0.875
F
W
Y

FIG. 1.2. TYPE C - SHALLOW HAT SECTION

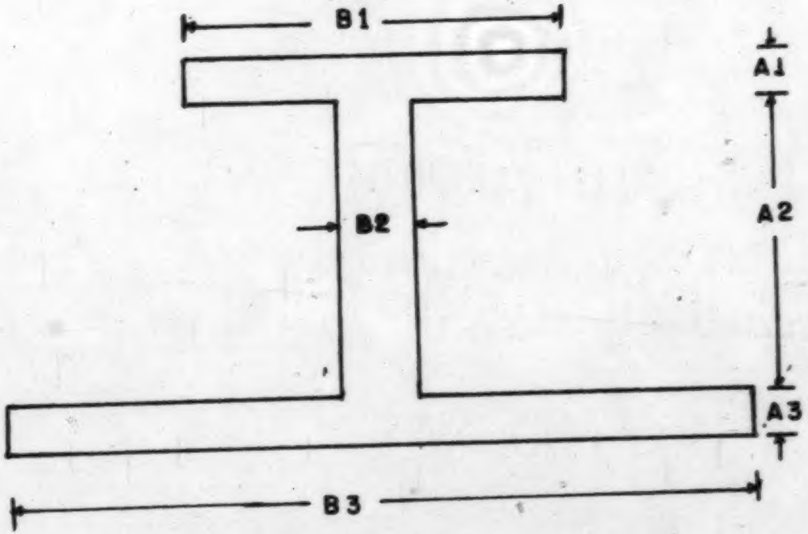
B1
A1
A2
B2
A3
B3

FIG.1. 3. Equivalent Section.

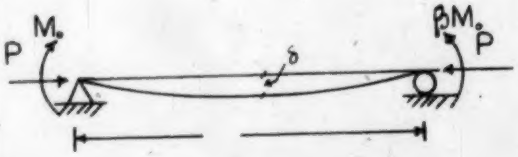

Fig. 2.1. Beam- Column Model with End Moments.

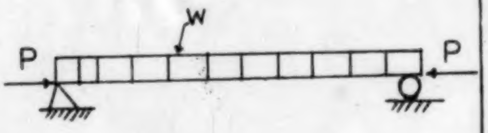

Fig. 2.2. Beam- Column Model with Transverse Loads.

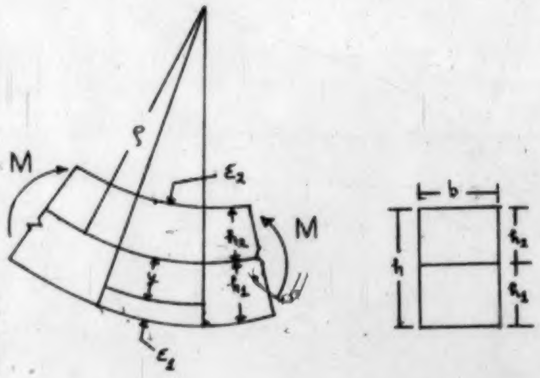
ρ
M
ε$_2$
h$_2$
y
h$_1$
M
ε$_1$
b
h
h$_2$
h$_1$

Fig. 2.3. Bending of Rectangular Section.

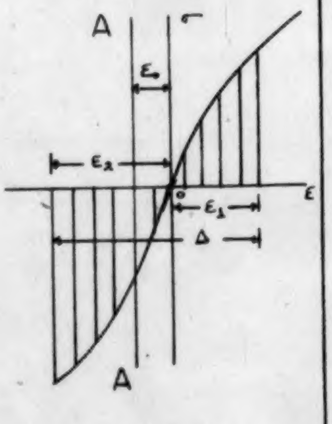
A
σ
ε$_o$
ε$_2$
0
ε$_1$
ε
Δ
A

Fig. 2.4. Inelastic Stress- Strain Diagram (21)

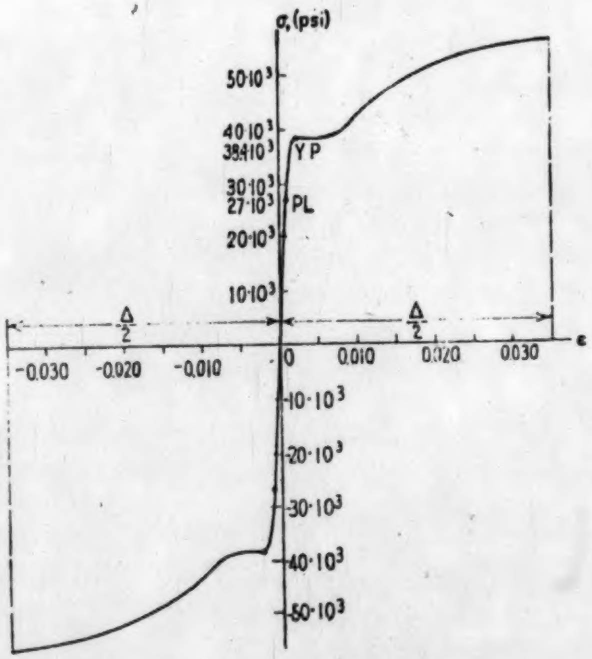

Fig. 2.5. Stress - Strain diagram for Structural Steel (21)

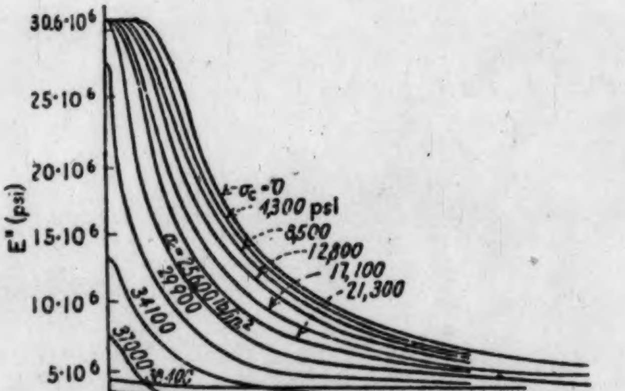

Fig. 2.6. Effective Modulus versus Total Strain diagram (21)

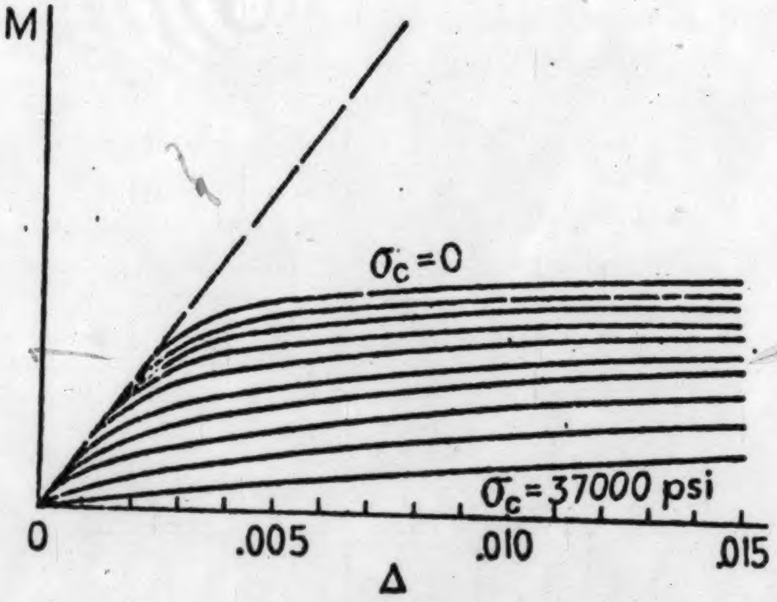

Fig. 2.7. Moment versus Total Strain Curves for Rectangular Section (21)

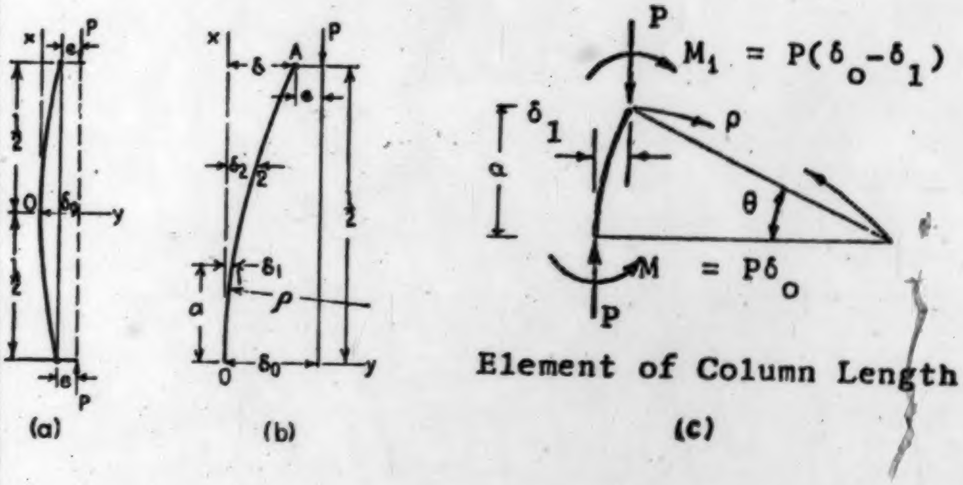
x
e
P
l/2
O
δ_0
y
l/2
e
P
x
P
A
δ
e
δ_2
l/2
l
δ_1
a
ρ
0
δ_0
y
P
$M_1 = P(\delta_o - \delta_1)$
δ_1
a
ρ
θ
$M = P\delta_o$
P

(a) (b)

Element of Column Length

(c)

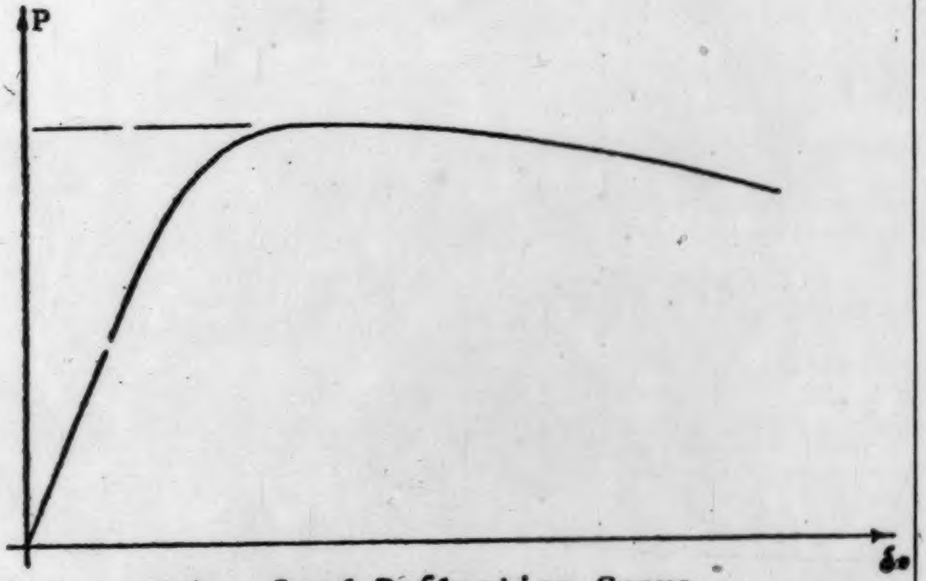

(d) Load Deflection Curve

Fig. 2.8. Details of Von-Karman's Analysis (15)

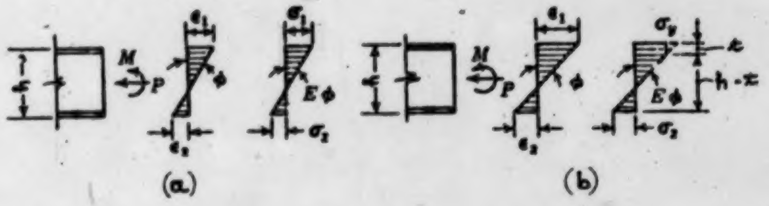
M
P
e₁
e₂
σ₁
σ₂
φ
Eφ
σy
x
h-x
(a)
(b)

Fig. 2.9. Stress-Strain Distributions for a Steel Section.

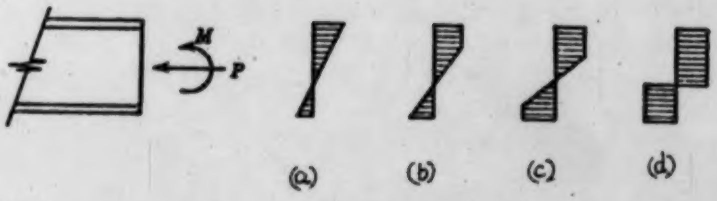

Fig. 2.10. Typical Progressive Yield Conditions for a Beam-Column Section (11)

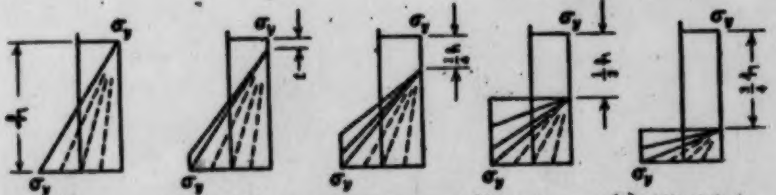
σy
σy
σy
σy
σy
σy
σy
σy
σy
σy

(a) Elastic Limit (b) Yielded Through Flange (c) Yielded $\frac{1}{4}$ h (d) Yielded $\frac{1}{2}$ h (e) Yielded $\frac{3}{4}$ h

Fig. 2.11 Sample Set of Assumed Yield Penetration conditions for Determination of Auxilliary Curves (11)

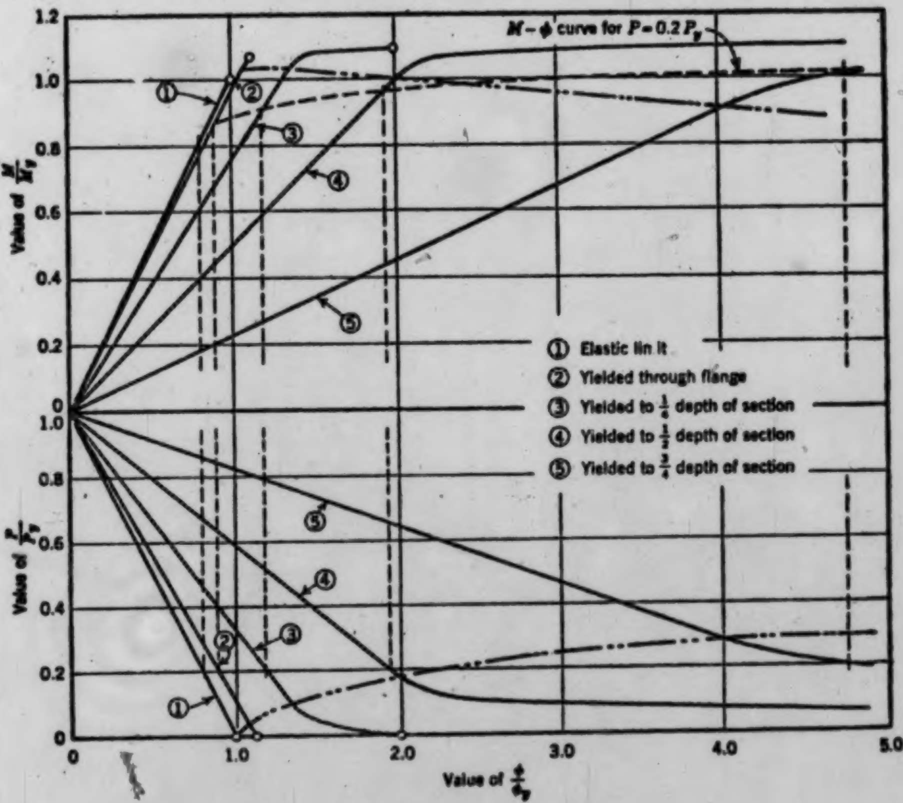

Fig. 2.12. Typical Set of Auxilliary Curves (11)

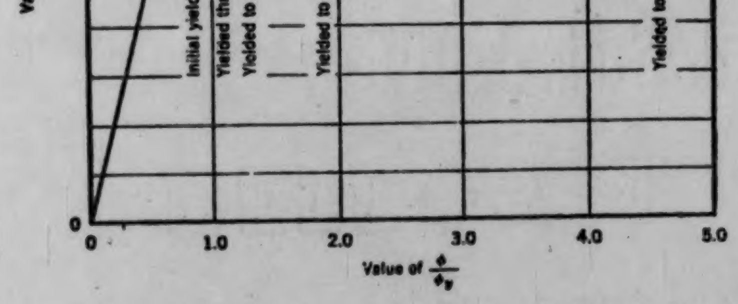

Fig. 2.13. Moment - Curvature relationships for P=0.2 Py (11)

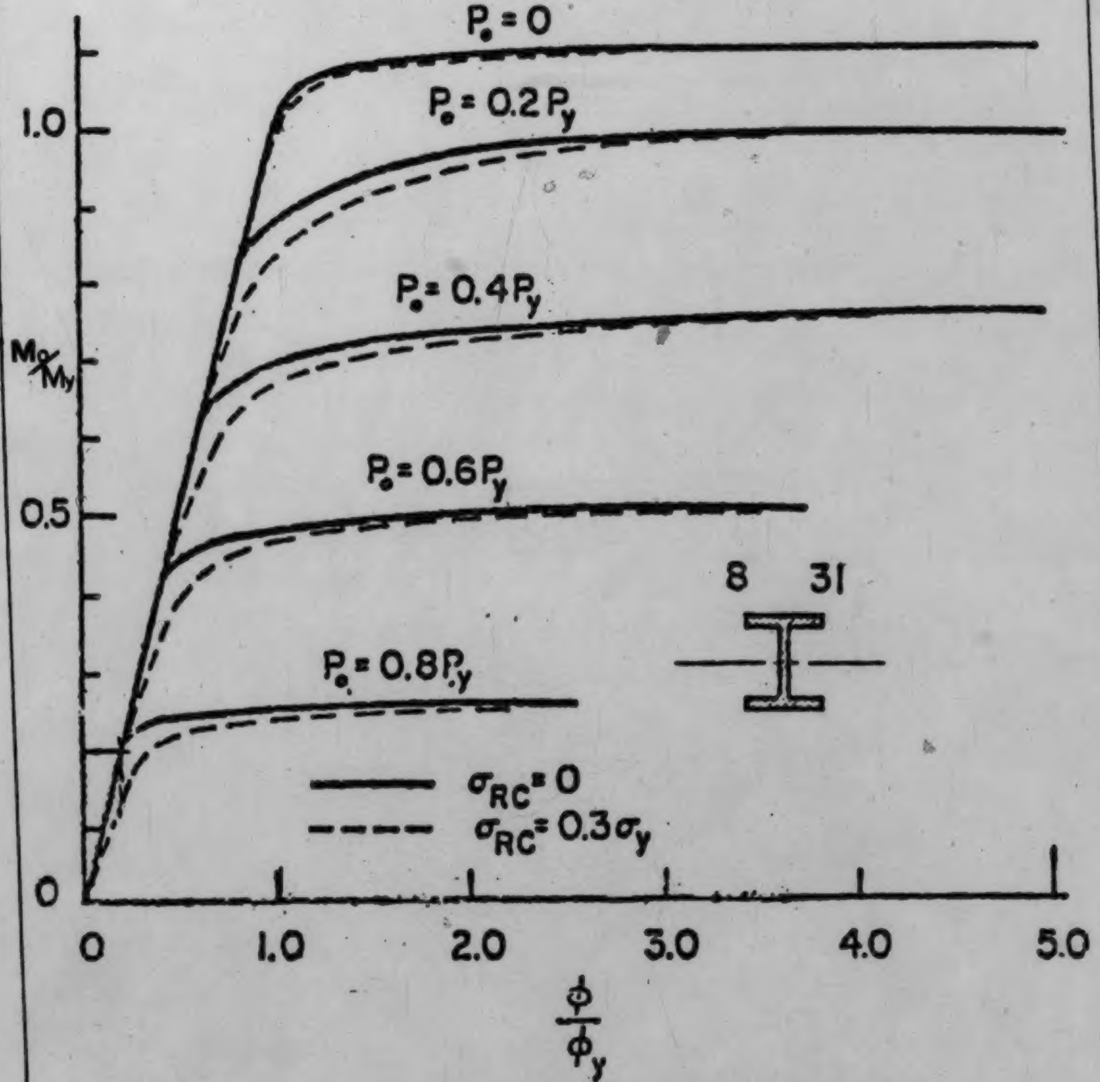

Fig. 2.14. Moment- Thrust Curvature Relationships for 8WF31 (6)

Given: $\frac{L}{r_x} = 40$; $\frac{P_o}{P_y} = 0.8$; 8WF31 Section; $L = 138.8''$; $\lambda = 17.35''$

Assumed: $\frac{M_o}{M_y} = 0.2$

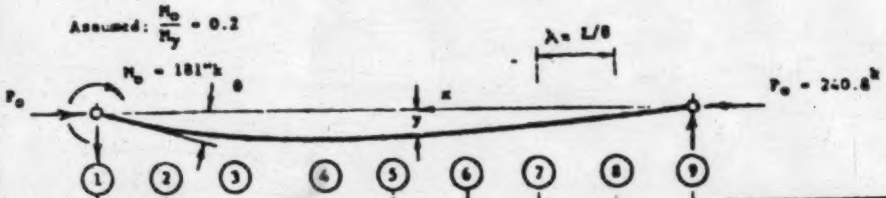

First Trial

	1	2	3	4	5	6	7	8	9	MF*	Notation
a	181	158	136	113	90	68	45	23	0		Moment due to M_o
b	0	0.026	0.049	0.068	0.047	0.044	0.032	0.008	0		Assumed Deflection
c	0	5	10	14	10	9	7	2	0		Moment due to P_o
d	181	163	146	127	100	77	52	25	0		Total Moment (a + c)
e	0.200	0.180	0.161	0.140	0.111	0.085	0.058	0.028	0		M_x/M_y
f	0.350	0.290	0.250	0.210	0.151	0.119	0.083	0.045	0	$\lambda\phi_y$	Concentrated Angle Changes **
g	0.350	0.640	0.890	1.100	1.251	1.370	1.453	1.498		$\lambda\phi_y$	Slope
h	0	0.350	0.990	1.880	7.980	4.231	5.601	7.045	8.552	$\lambda^2\phi_y$	Deflection
i	0	1.069	2.138	3.207	4.276	5.345	6.141	7.483	8.552	$\lambda^2\phi_y$	Correction to Deflection
j	0	0.719	1.143	1.327	1.296	1.114	0.540	0.429	0	$\lambda^2\phi_y$	Final Deflection
k	0	0.060	0.095	0.110	0.107	0.092	0.045	0.036	0		Final Deflection in Inches

Fourth Trial

	1	2	3	4	5	6	7	8	9		
a'	0	0.069	0.112	0.131	0.129	0.112	0.081	0.043	0		Assumed Deflection***
k'	0	0.070	0.113	0.132	0.130	0.112	0.082	0.043	0		Final Deflection

* Multiplication Factor

** From Fig. 3, corresponding to $\frac{M_x}{M_y}$

*** Line k from third trial = line a' of fourth trial

The corresponding endslope $\theta = \frac{4 \times 0.070 - 0.113}{2 \times 17.35} = 0.00481$

Fig.2.15 —TYPICAL NUMERICAL INTEGRATION PROCEDURE TO OBTAIN END SLOPE (6)

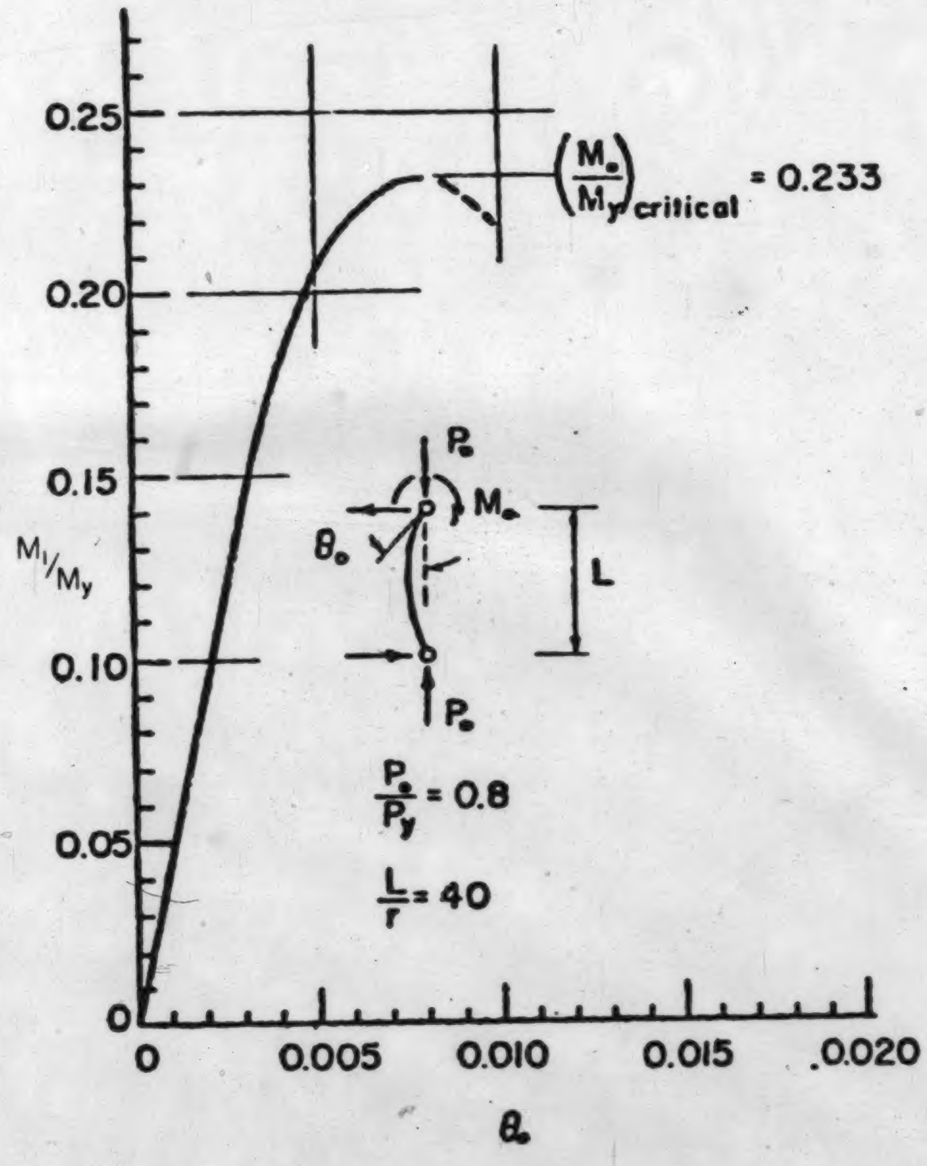

Fig. 2.16 —TYPICAL MOMENT VERSUS END ROTATION CURVE (6)

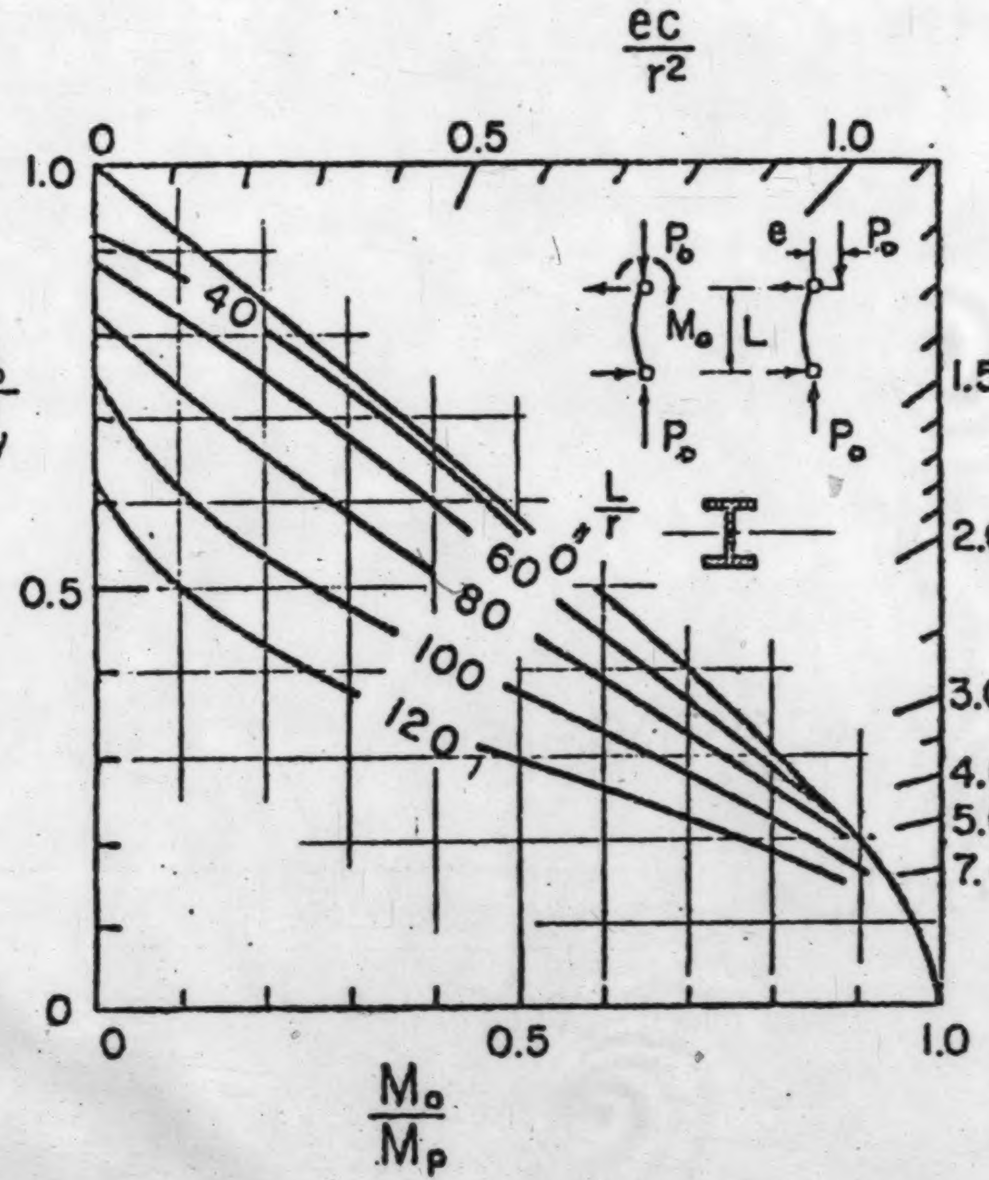

Fig. 2.17. Maximum Carrying capacity Interaction Curves (6)

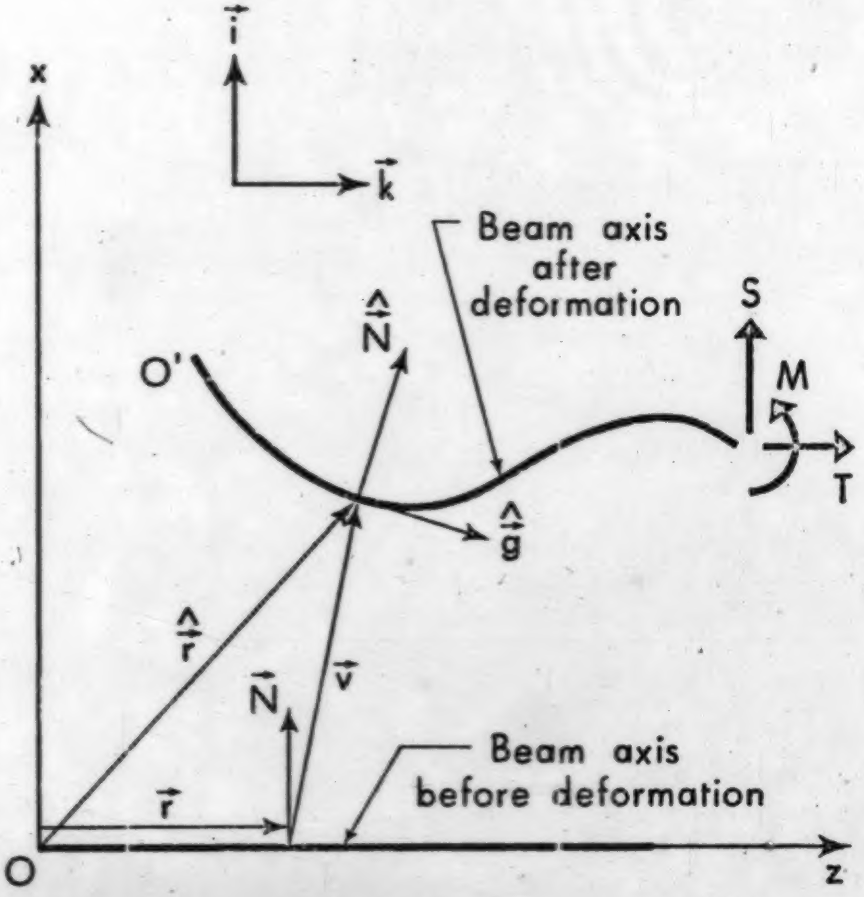
$\vec{i}$
$\vec{k}$
x
Beam axis after deformation
$\hat{N}$
S
O'
M
T
$\hat{g}$
$\hat{\vec{r}}$
$\vec{v}$
$\vec{N}$
Beam axis before deformation
$\vec{r}$
O
z

Fig.3.1 Geometry of Deformation

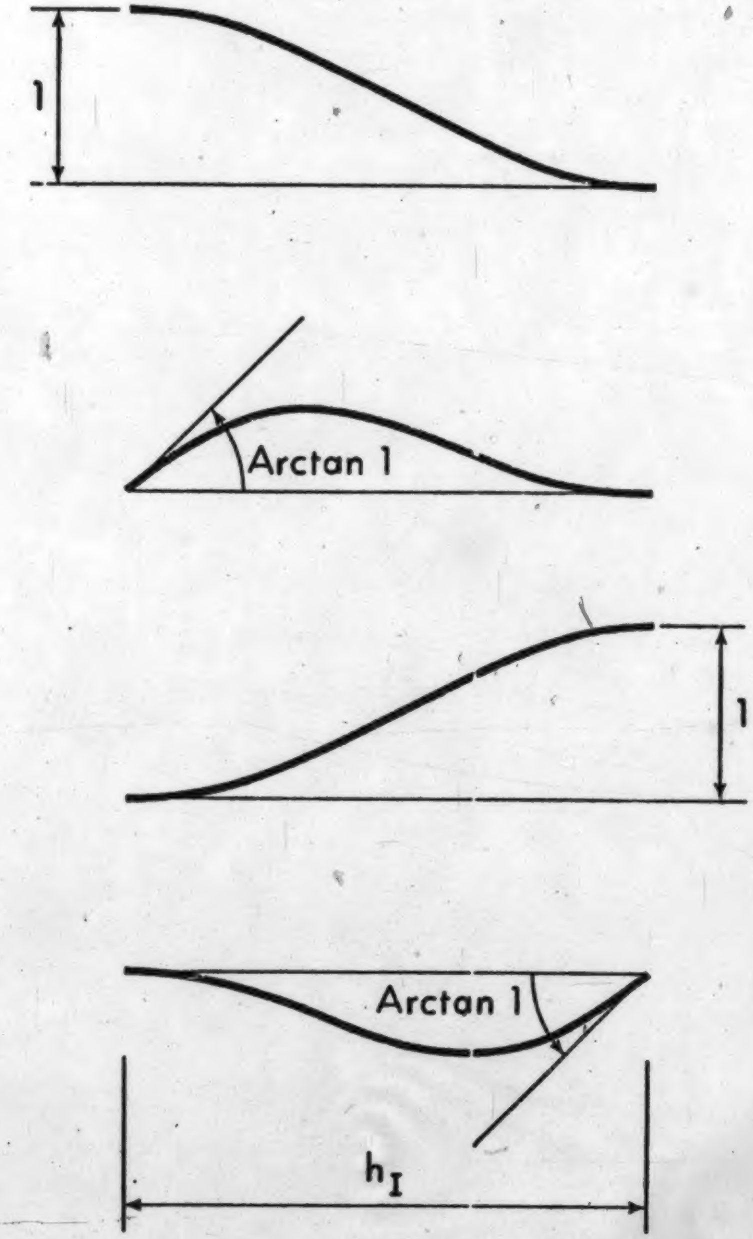
1
Arctan 1
1
Arctan 1
h_I

Fig.3:2 Basis Functions for Cubic Polynomial

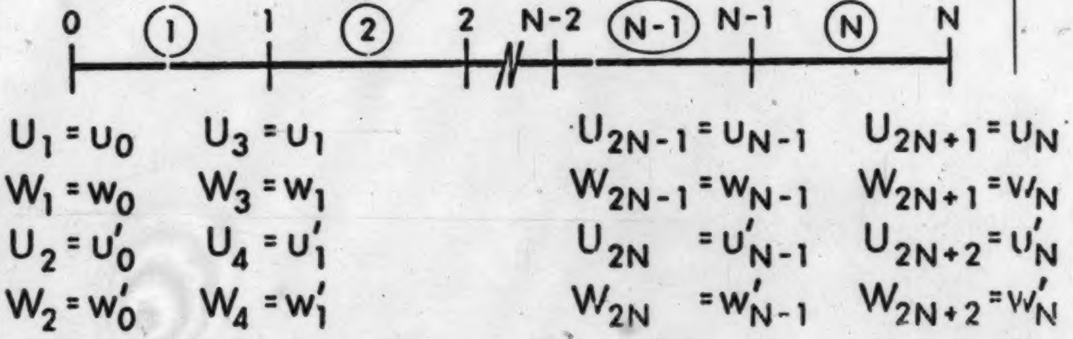
0
①
1
②
2
N-2
(N-1)
N-1
Ⓝ
N
$U_1 = u_0$
$W_1 = w_0$
$U_2 = u'_0$
$W_2 = w'_0$
$U_3 = u_1$
$W_3 = w_1$
$U_4 = u'_1$
$W_4 = w'_1$
$U_{2N-1} = u_{N-1}$
$W_{2N-1} = w_{N-1}$
$U_{2N} = u'_{N-1}$
$W_{2N} = w'_{N-1}$
$U_{2N+1} = u_N$
$W_{2N+1} = w_N$
$U_{2N+2} = u'_N$
$W_{2N+2} = w'_N$

Fig.3.3 Element, Node, and Nodal Displacement Designation

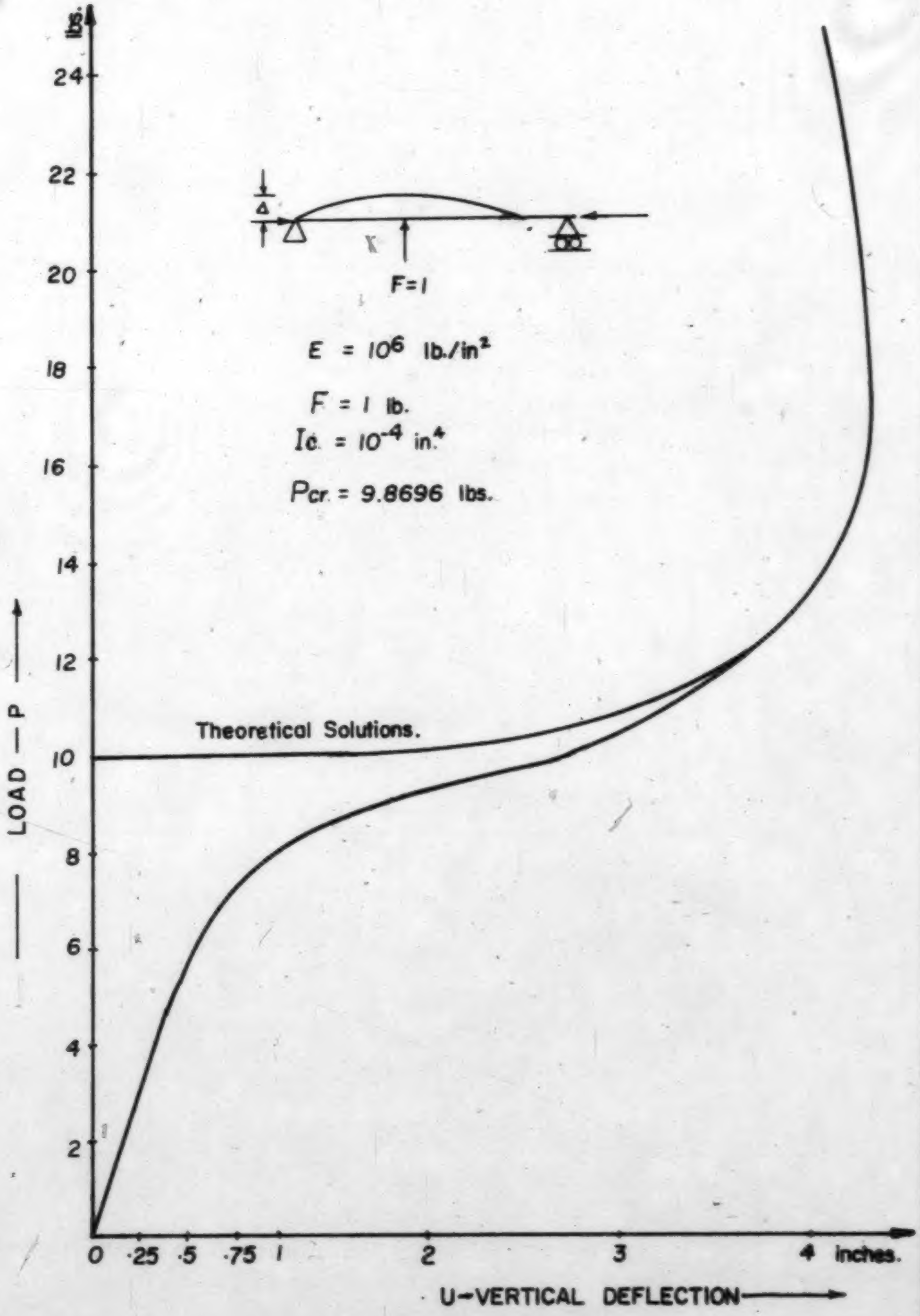

Fig. 4.1. COMPARISON OF THEORETICAL AND NUMERICAL SOLUTIONS FOR THE "ELASTICA"

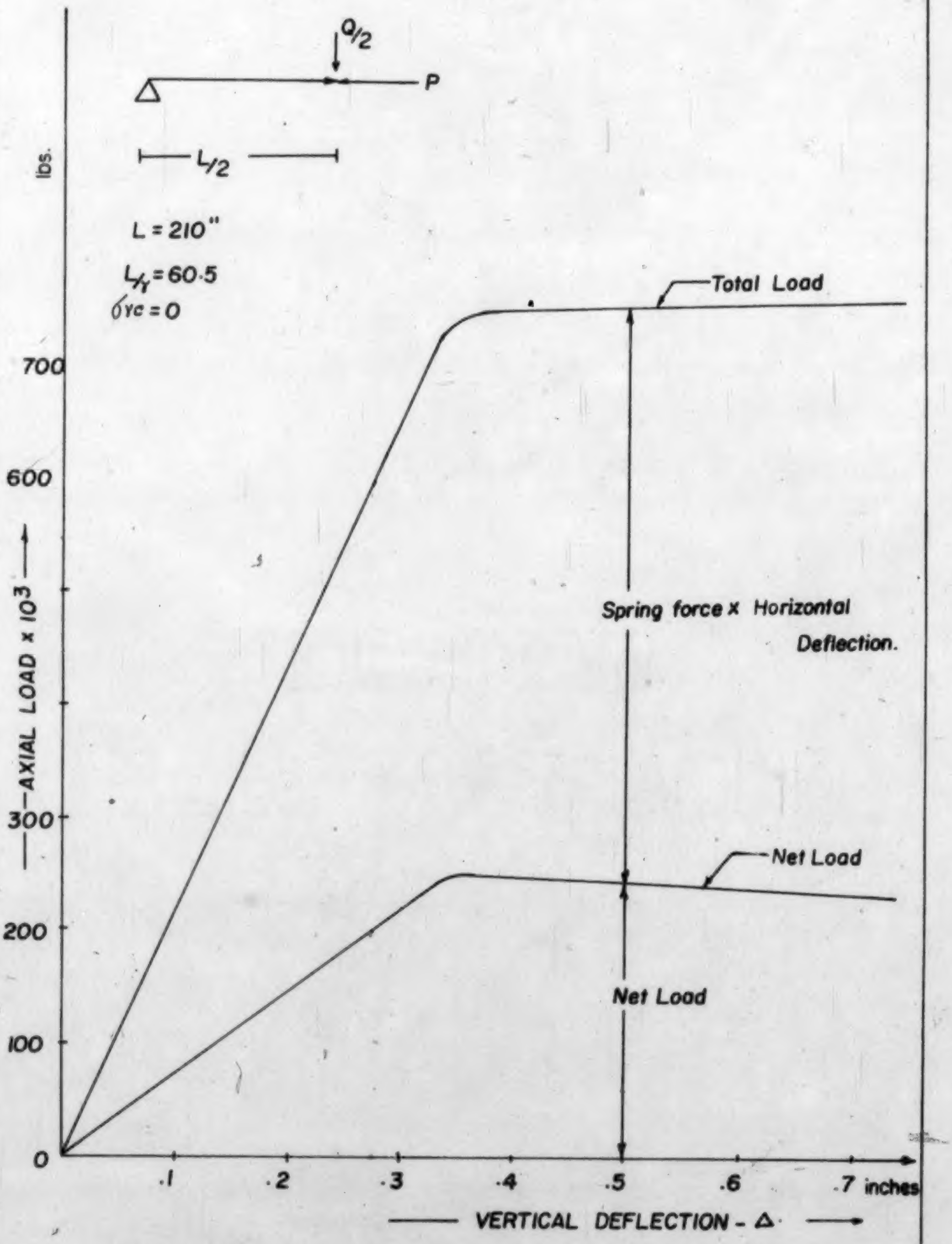

FIG. 4.2. Load-Deflection Curve Derived from STIFFENED COLUMN.

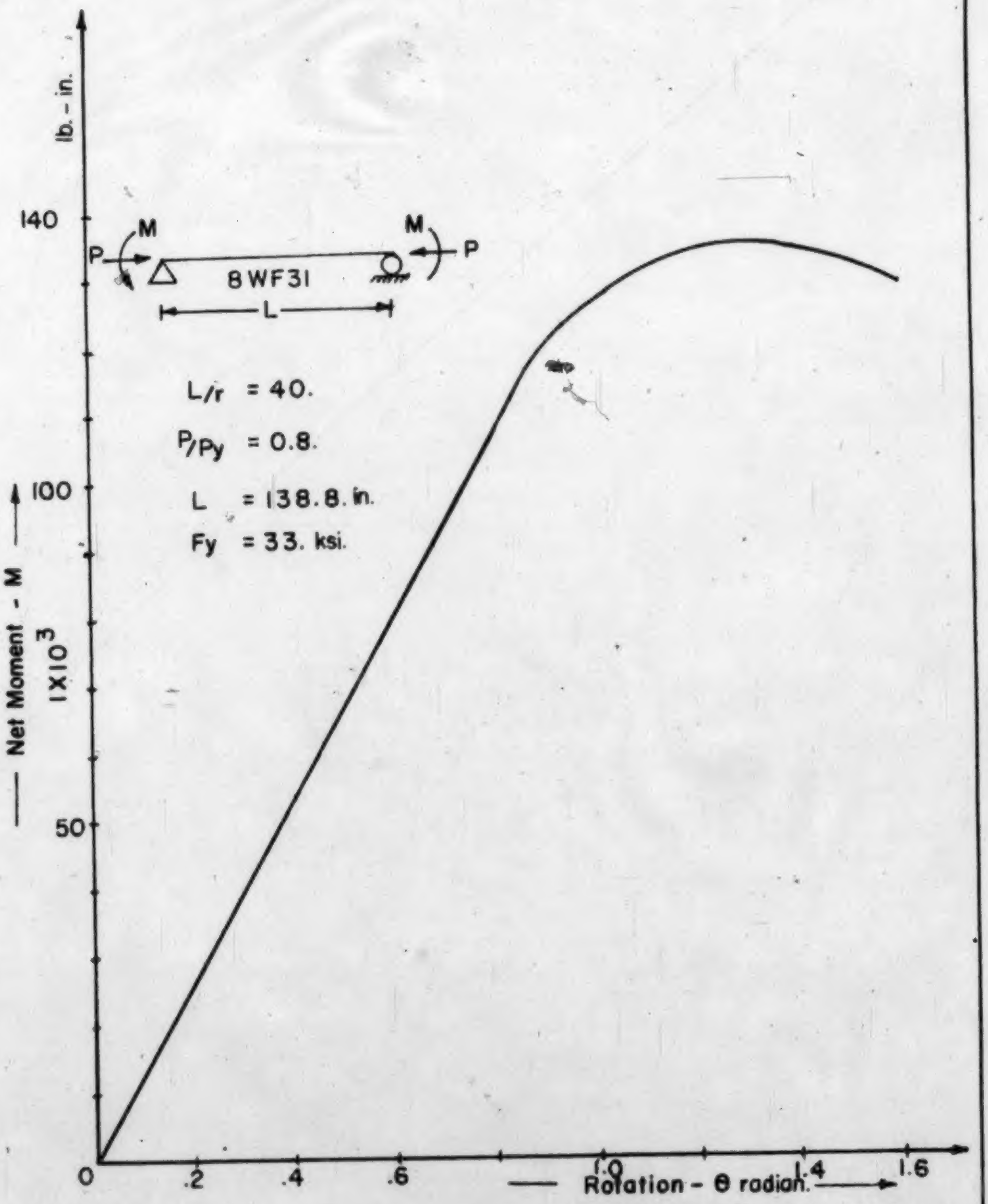

Fig. 4.3. MOMENT-END ROTATION CURVE

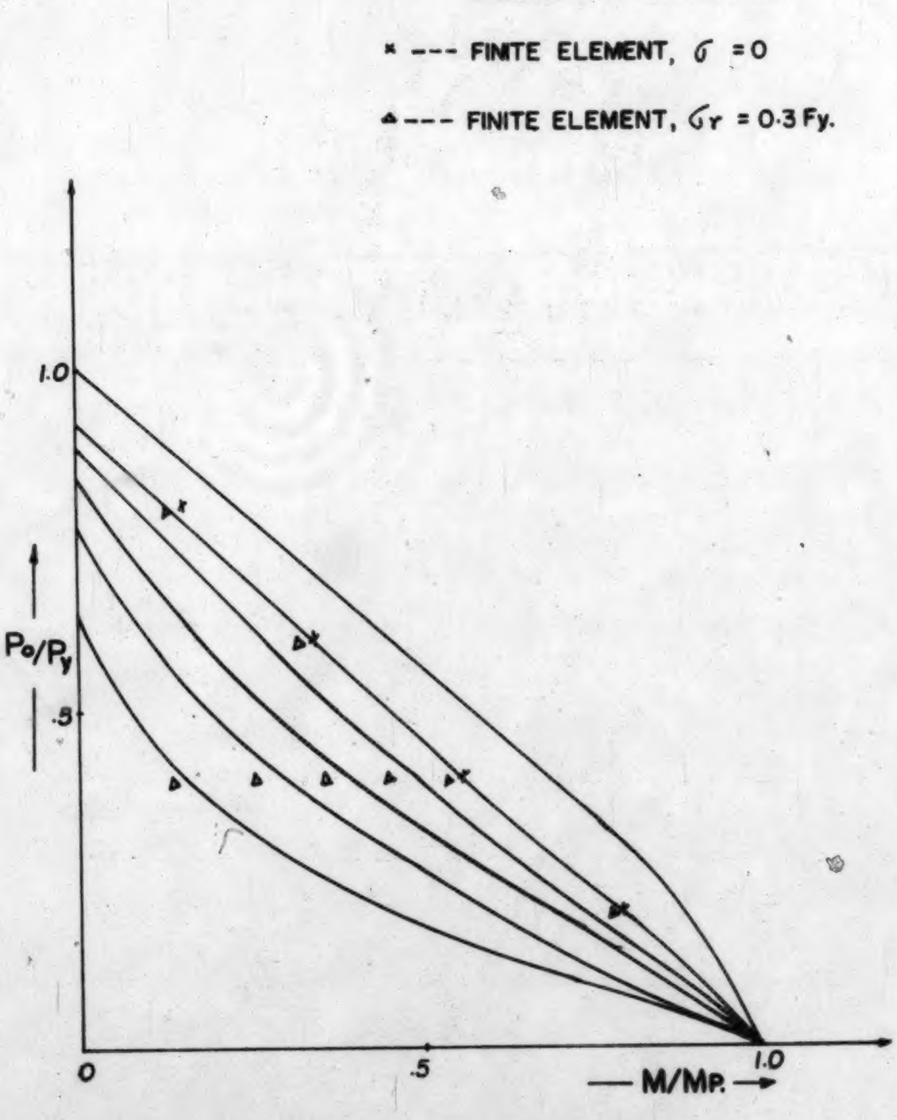

Fig. 4.4. COMPARISON OF PREDICTED CAPACITIES WITH Interaction Curves of GALAMBOS and KETTER (6)

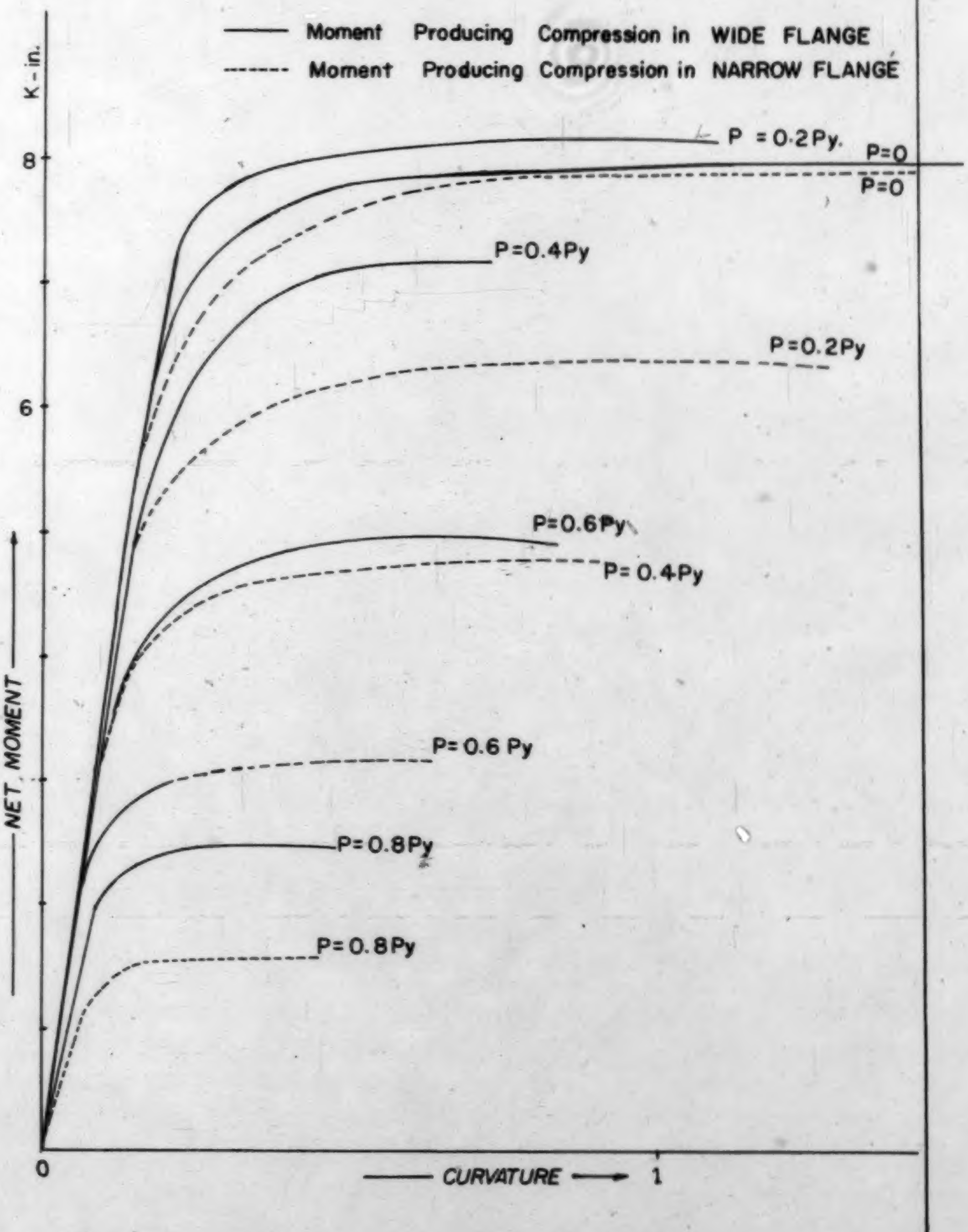

Fig. 4.5 Moment - Curvature Relationship (Fy = 33)

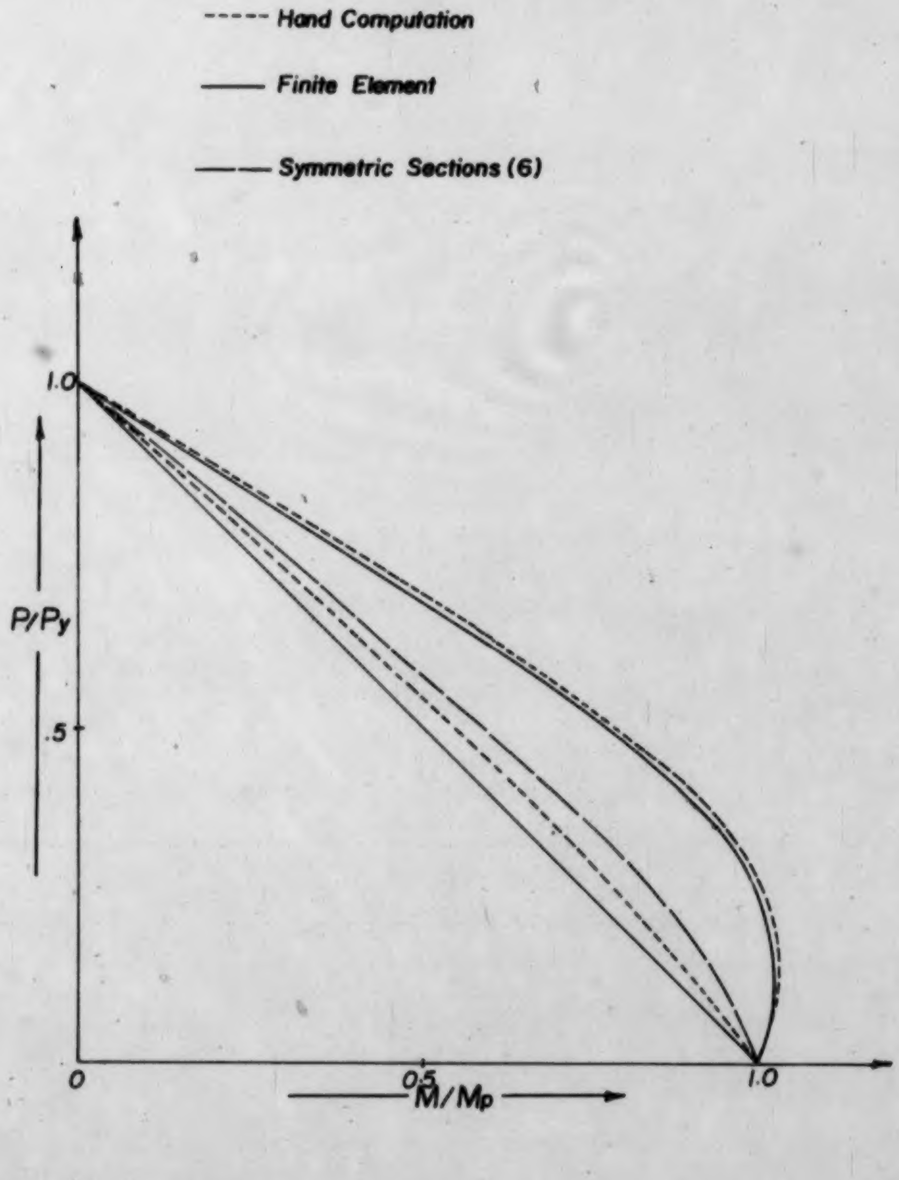

FIG. 4.6. Interaction Curve for Hat Section with $L/r = 0$

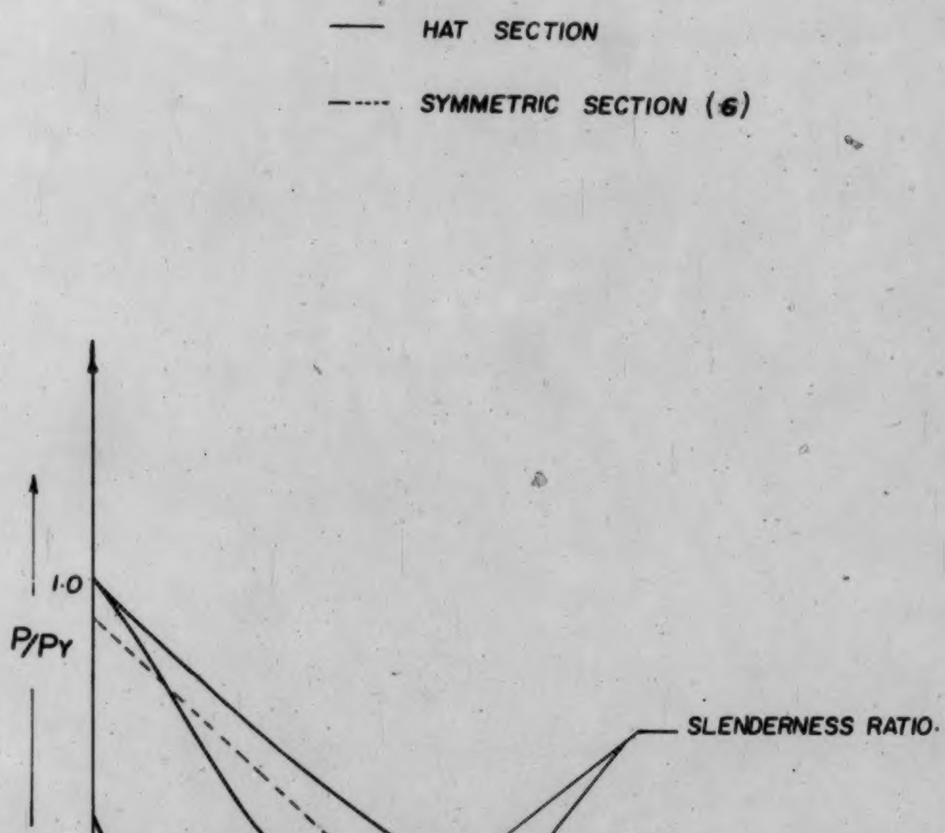

FIG. 4.7. Interaction Curves for HAT SECTION ($F_Y = 33$)

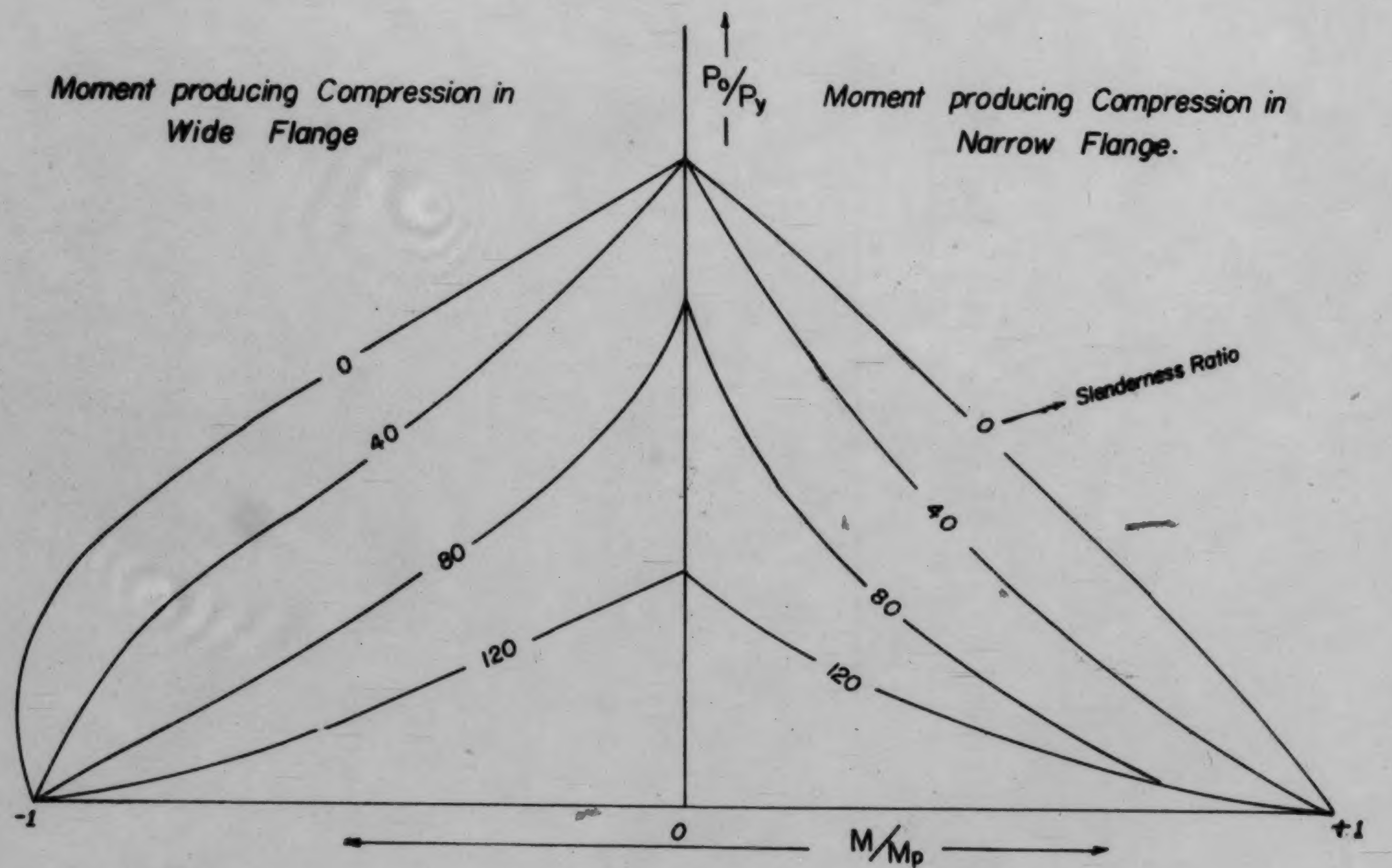

Fig. 4·8· Interaction Curves for Hat Section ($F_y = 55$, $\sigma_r = 0$)

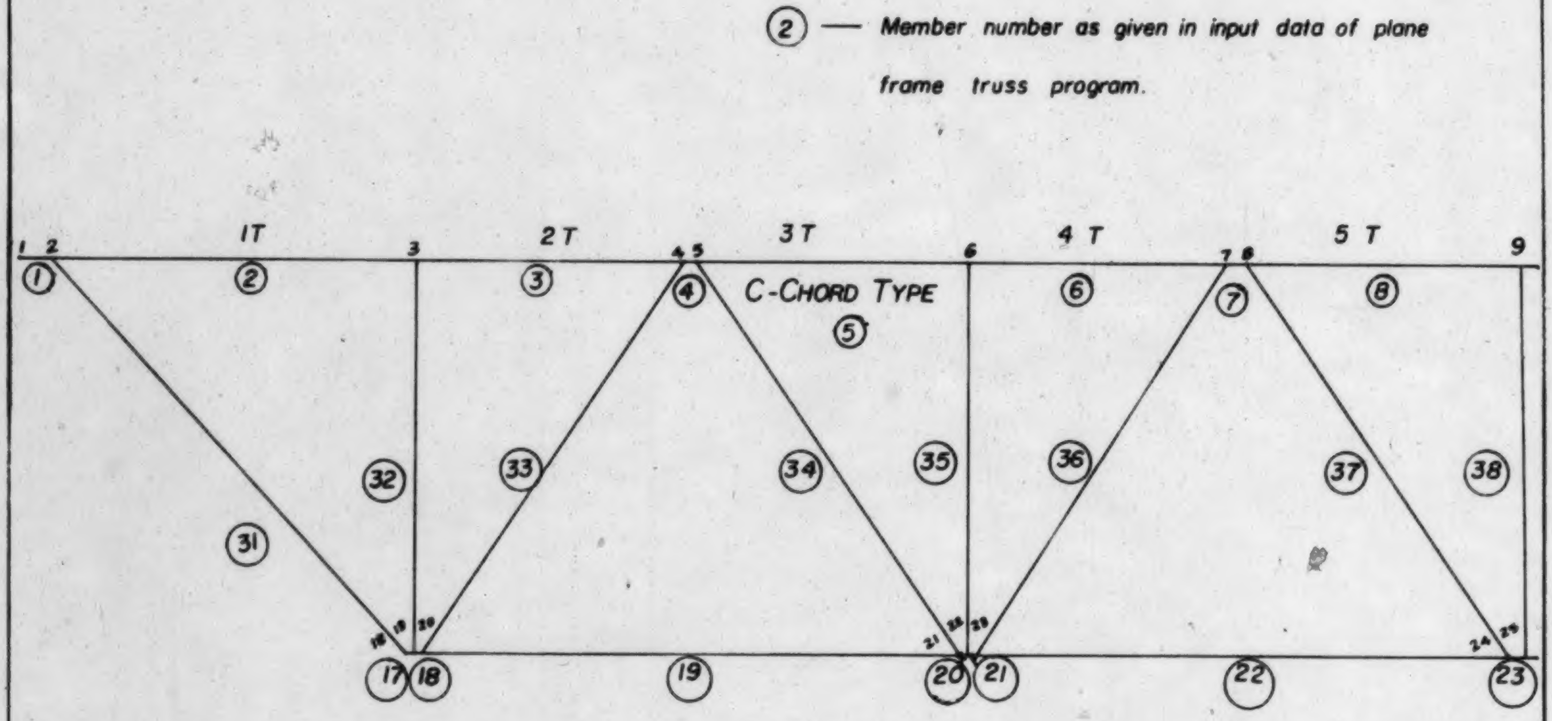
② — Member number as given in input data of plane frame truss program.
1
2
1T
3
2T
4
5
3T
6
4T
7
8
5T
9
C-CHORD TYPE
①
②
③
④
⑤
⑥
⑦
⑧
31
32
33
34
35
36
37
38
16
19
20
21
22
23
24
25
17
18
19
20
21
22
23

FIG. 5.1. Member and Joint Numbering for Typical Test Joist.

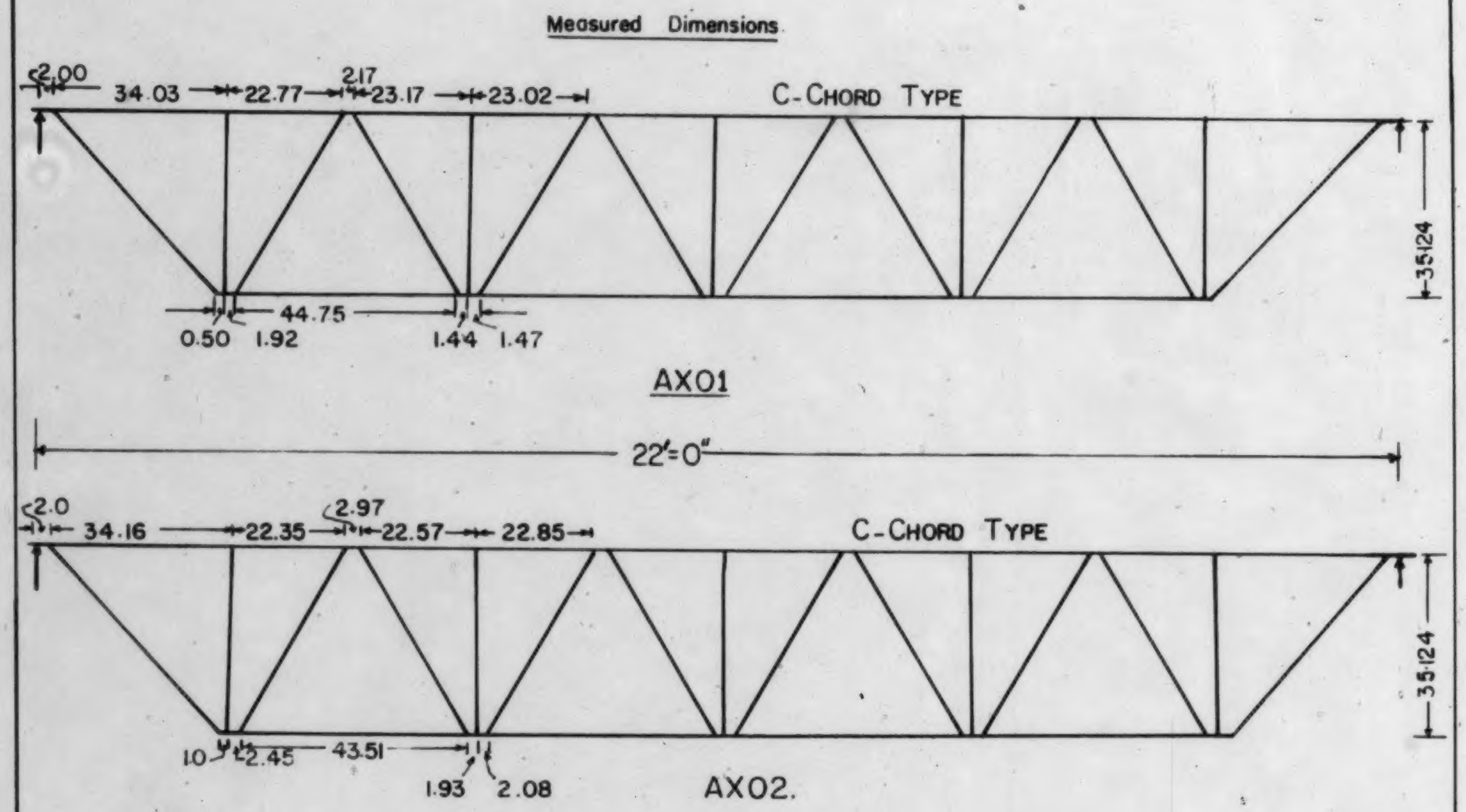
Measured Dimensions.
2.00
34.03
22.77
2.17
23.17
23.02
C-CHORD TYPE
35.124
0.50
1.92
44.75
1.44
1.47
AX01
22'=0"
2.0
34.16
22.35
2.97
22.57
22.85
C-CHORD TYPE
35.124
1.0
2.45
43.51
1.93
2.08
AX02.

FIG. 5.2. Dimensions of Test joists, AX01 and AX02 (14) in inches.

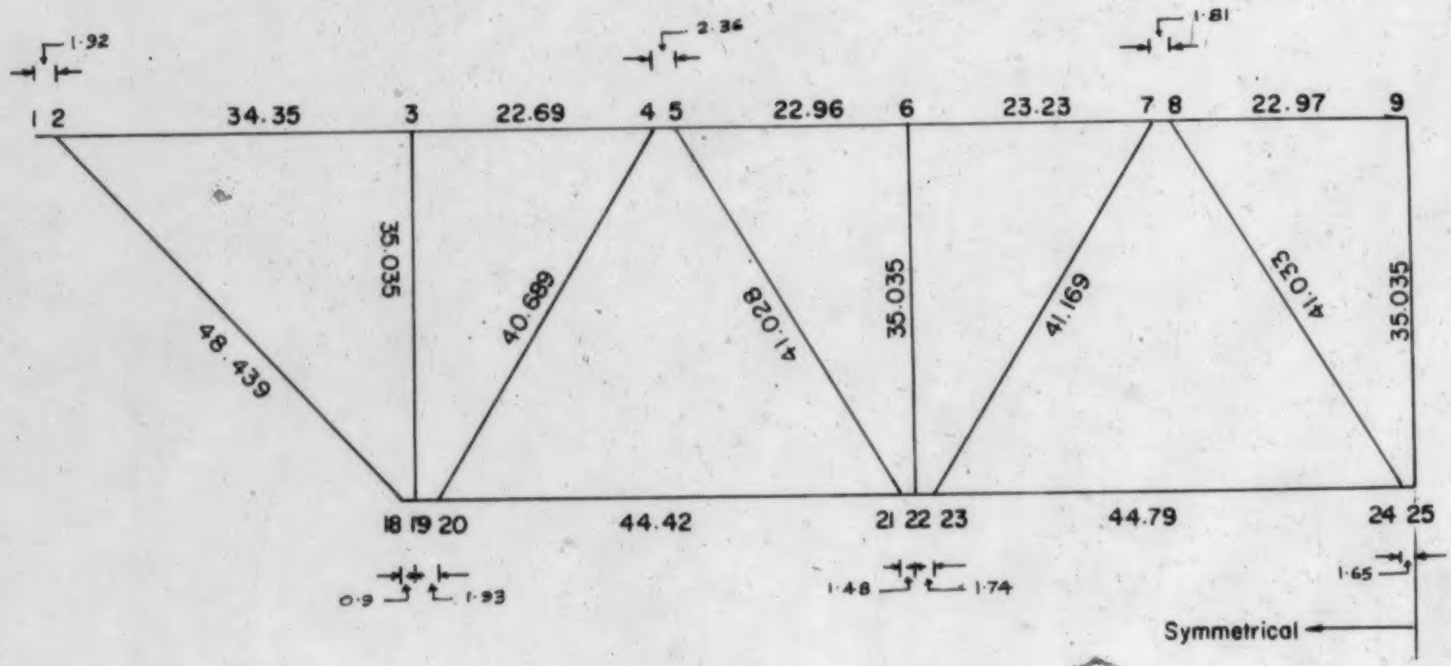
1.92
2.36
1.81
1 2
34.35
3
22.69
4 5
22.96
6
23.23
7 8
22.97
9
48.439
35.035
40.689
41.028
35.035
41.169
41.033
35.035
18 19 20
44.42
21 22 23
44.79
24 25
0.9
1.93
1.48
1.74
1.65
Symmetrical

FIG. 5.3. Dimensions of Test Joist AX05 (14) in inches.

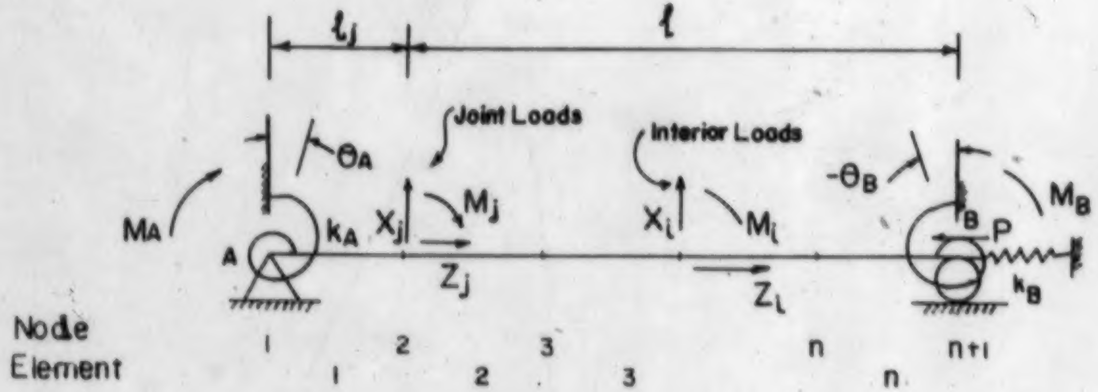
ℓ_j
ℓ
Joint Loads
Interior Loads
θ_A
$-\theta_B$
M_A
k_A
A
X_j
M_j
Z_j
X_i
M_i
Z_i
B
P
M_B
k_B
Node
Element
1
2
3
n
n+1
1
2
3
n

Fig. 5.4. Generalized Beam- Column Finite Element Model.

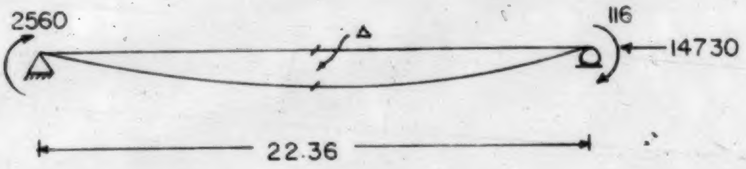
2560
Δ
116
14730
22.36

(a) AXO5 : F

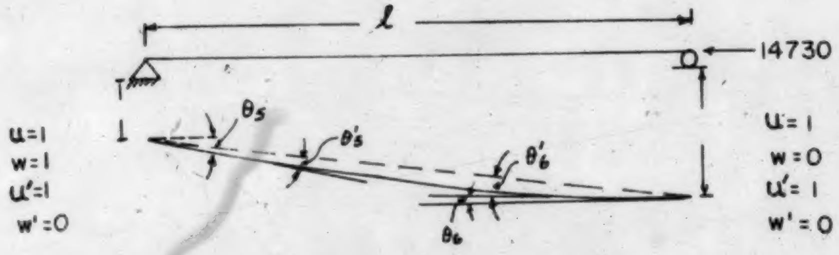
ℓ
14730
θ_5
θ'_5
θ'_6
θ_6
u=1
w=1
u'=1
w'=0
u=1
w=0
u'=1
w'=0

(b) AXO5 : D

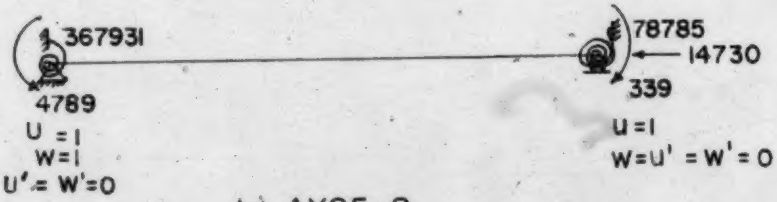
367931
4789
U =1
W=1
U'= W'=0
78785
14730
339
u=1
W=u' = W' = 0

(c) AXO5 : S

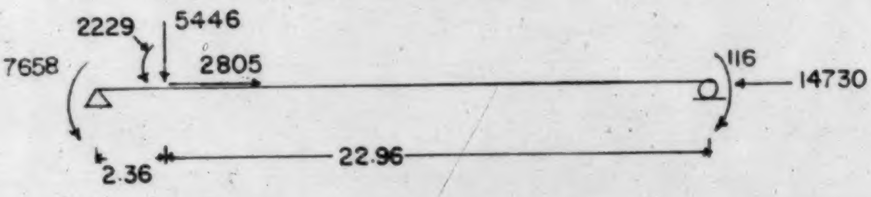
2229
5446
7658
2805
116
14730
2.36
22.96

(d) AXO5J : F

Note: **Units are in inches and pounds.**

FIG. 5.5. Loading and Boundary Conditions for AXO5 Models.

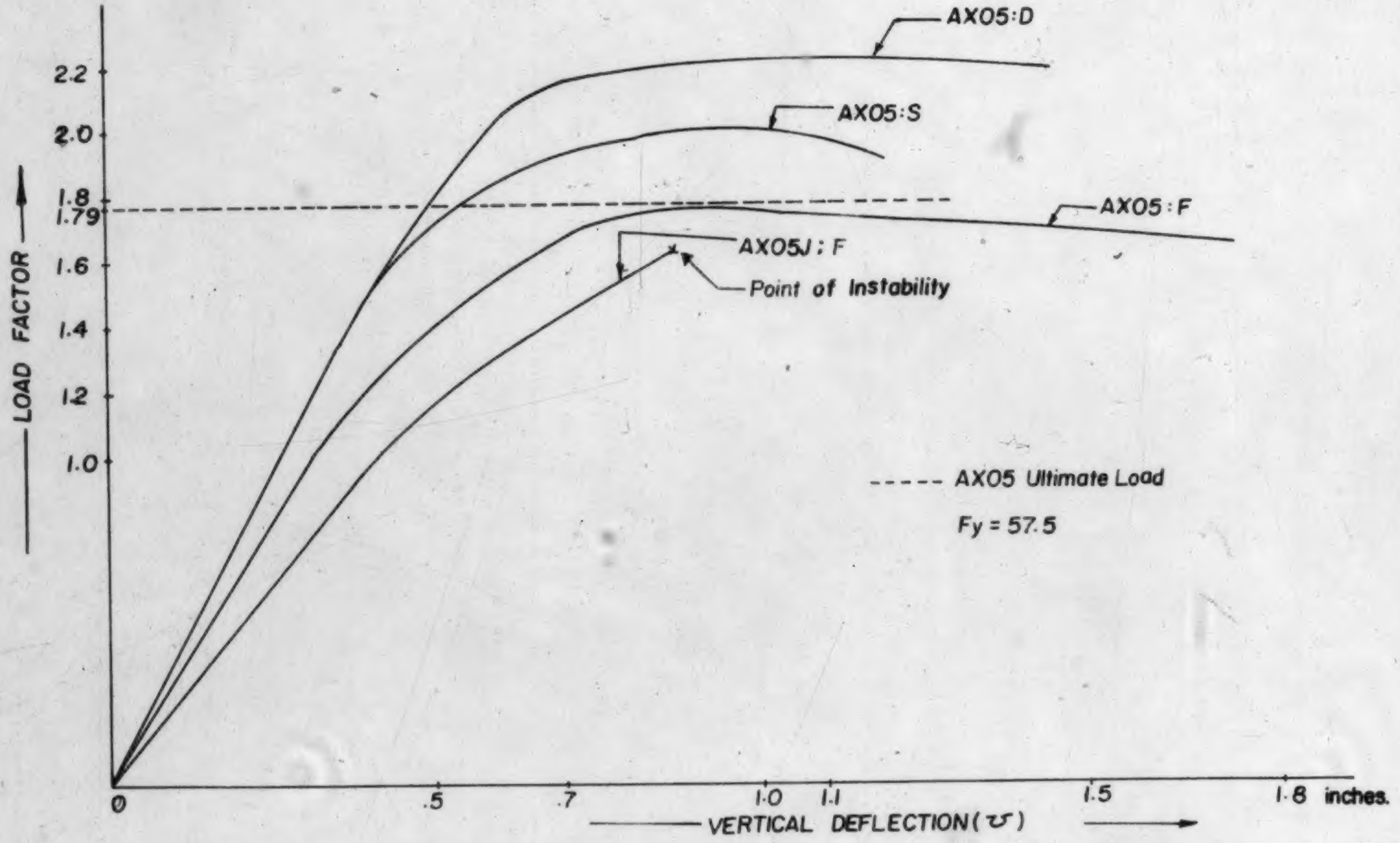

Fig. 5.6 LOAD-DEFLECTION CURVES FOR AX05 MODELS

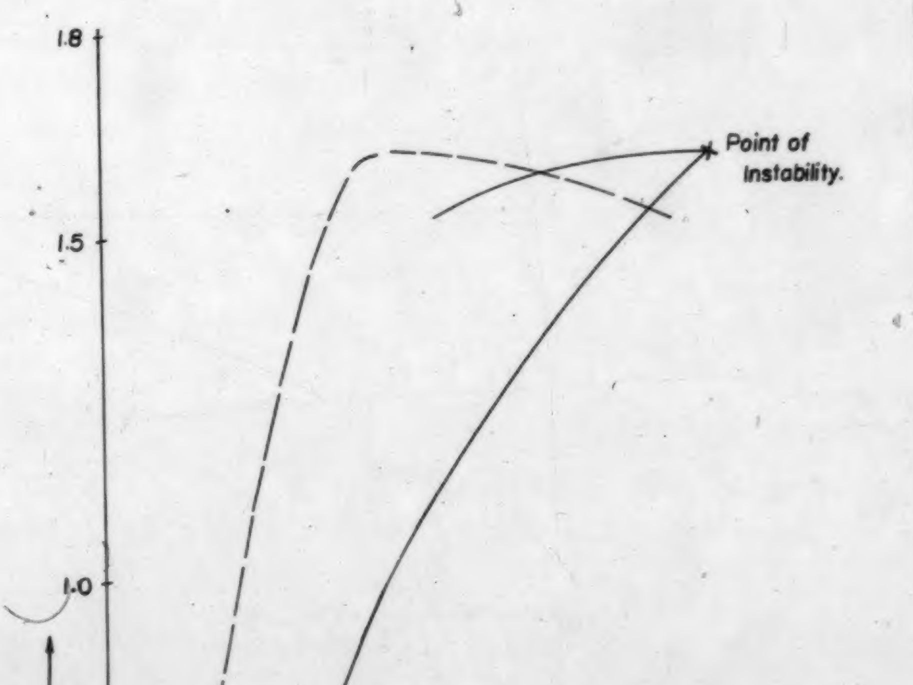

FIG. 5.7. Load-Deflection Curve for AX05J.

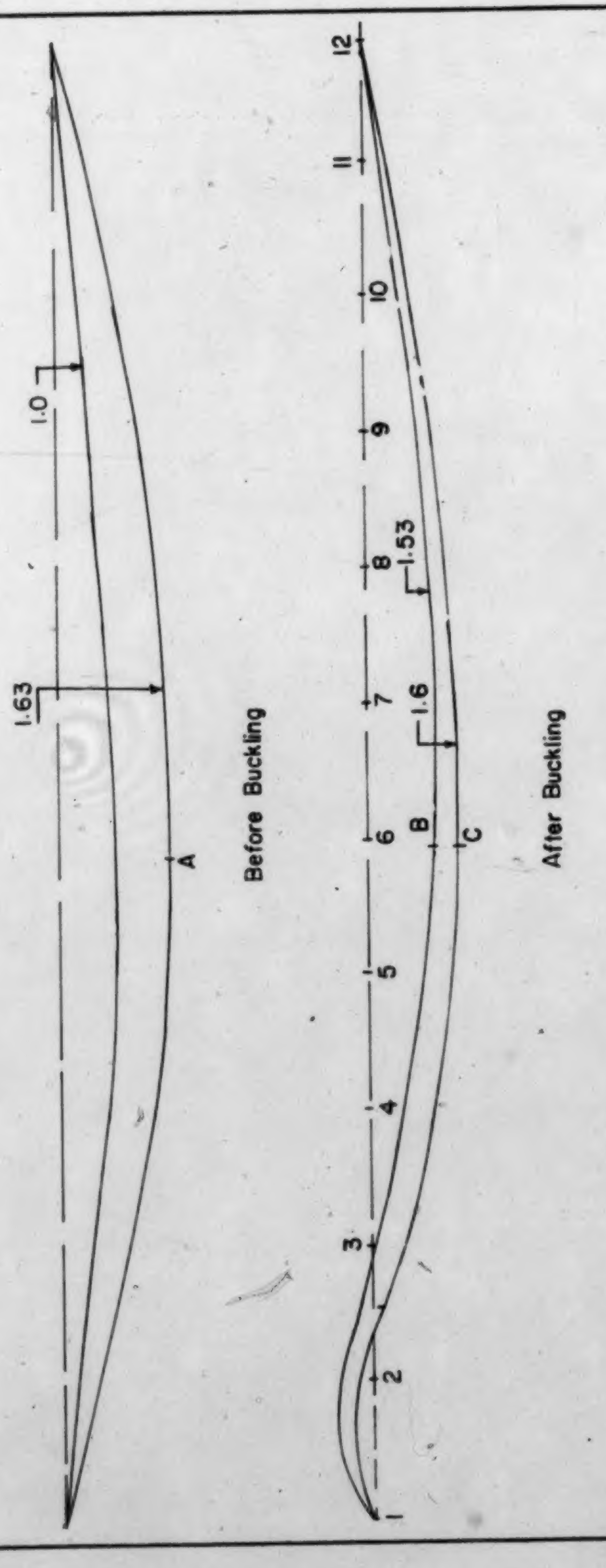
1.0
1.63
A
Before Buckling
1
2
3
4
5
6
7
8
9
10
11
12
1.53
1.6
B
C
After Buckling

FIG. 5.8: Deflected Shapes for AXO5J in inches.

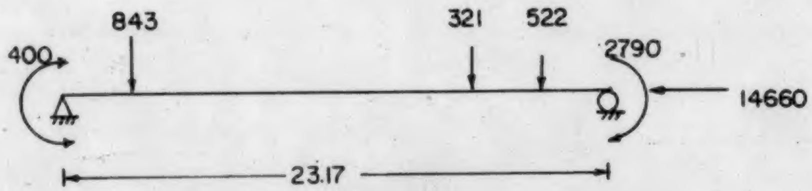
400
843
321
522
2790
14660
23.17

(a) AX01 : F

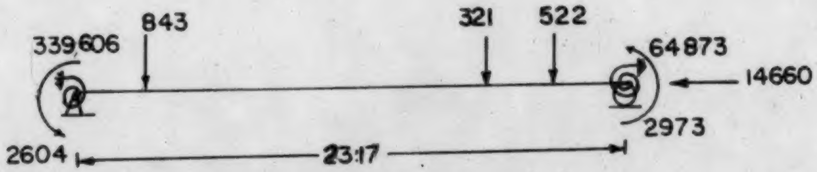
339,606
843
321
522
64873
14660
2973
2604
23.17

(b) AX01 : S

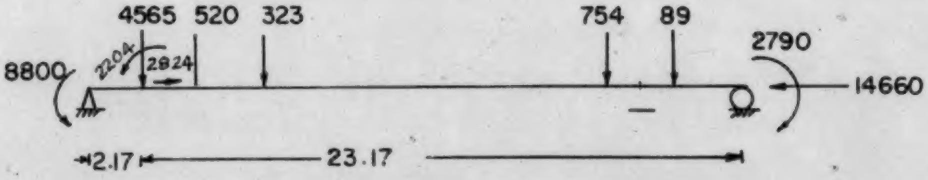
4565
520
323
754
89
2790
8800
2204
2824
14660
2.17
23.17

(c) AX01J : F

Note: Units are inches and pounds.

Fig. 5.9. Loading and Boundary Conditions for AX0.1 - Models.

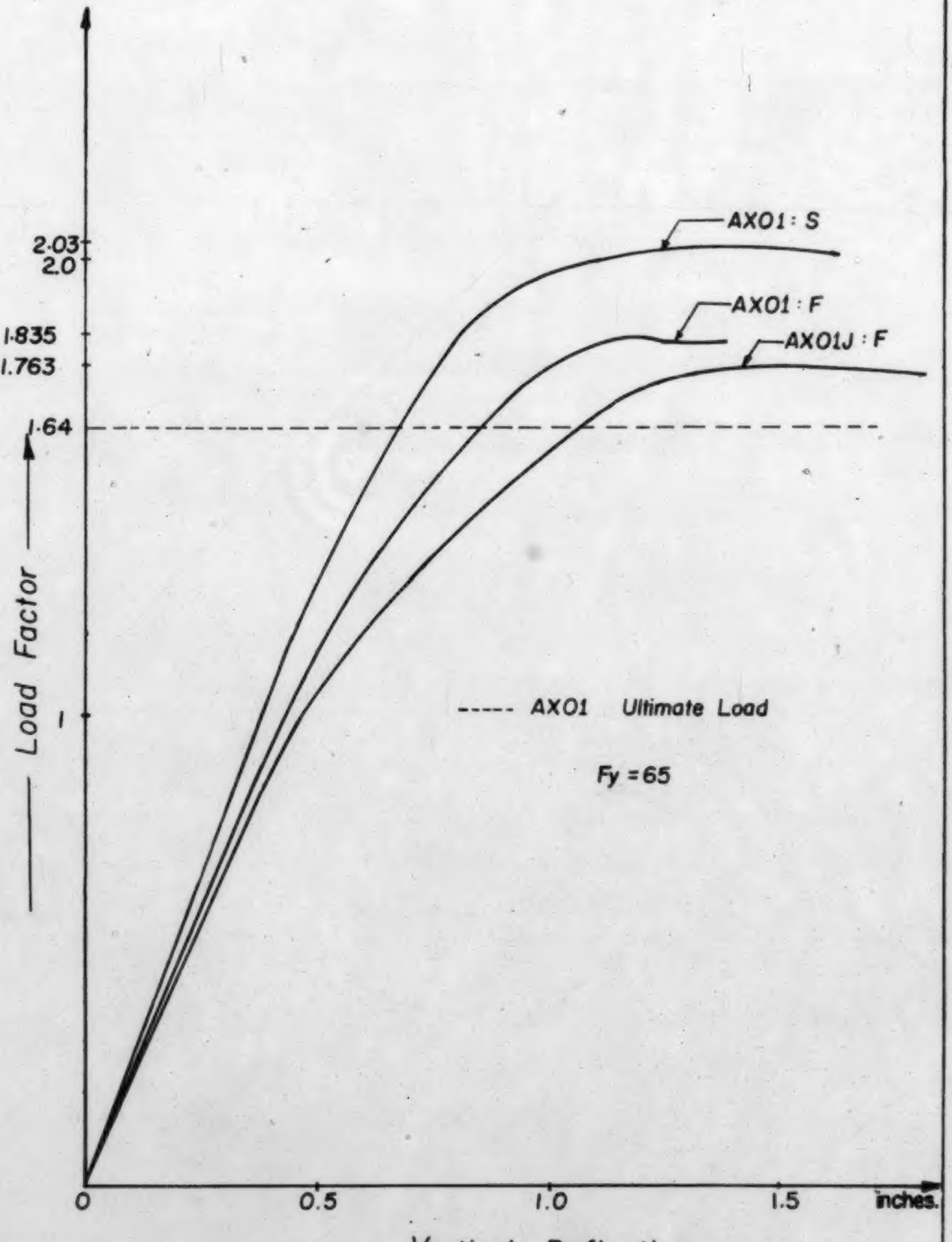

FIG. 5.10. Load-Deflection Curves for AXO1 Models

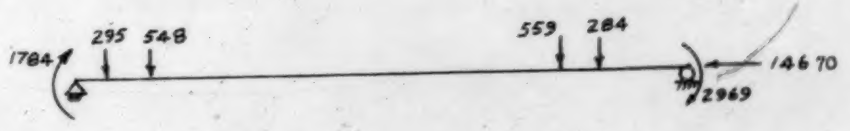
1784
295
548
559
284
14670
2969

(a) AX02 : F

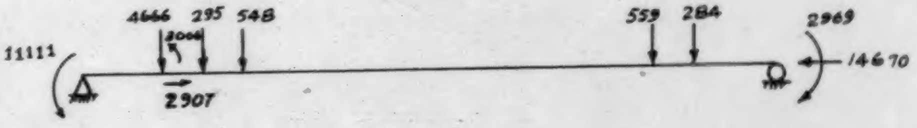
11111
4666
2006
295
548
2907
559
284
2969
14670

(b) AX02J : F

Note: Units are inches and pounds.

Fig. 5.11. Loading and Boundary Conditions for AX02 Models

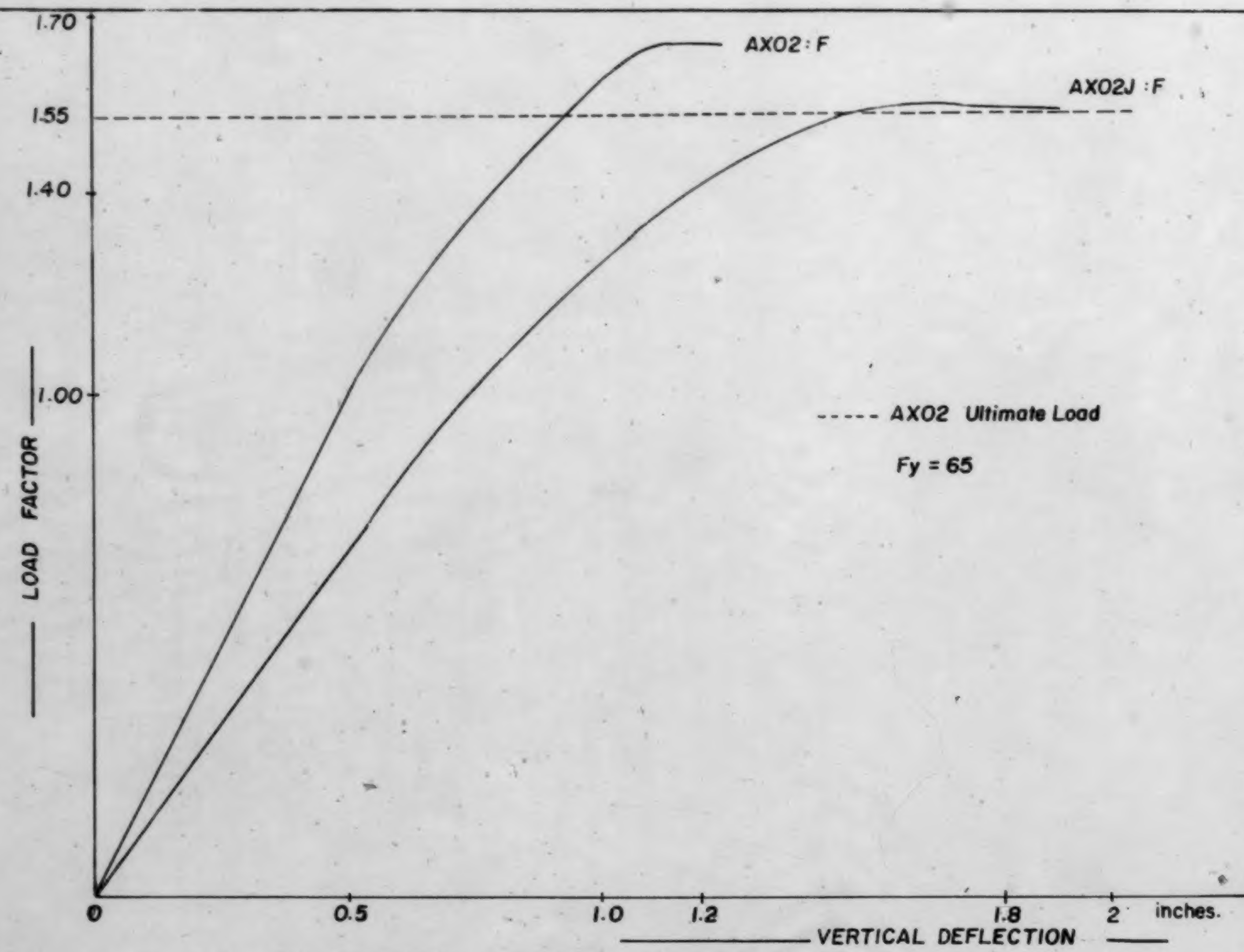

Fig. 5.12 LOAD-DEFLECTION CURVES FOR AX02 MODELS

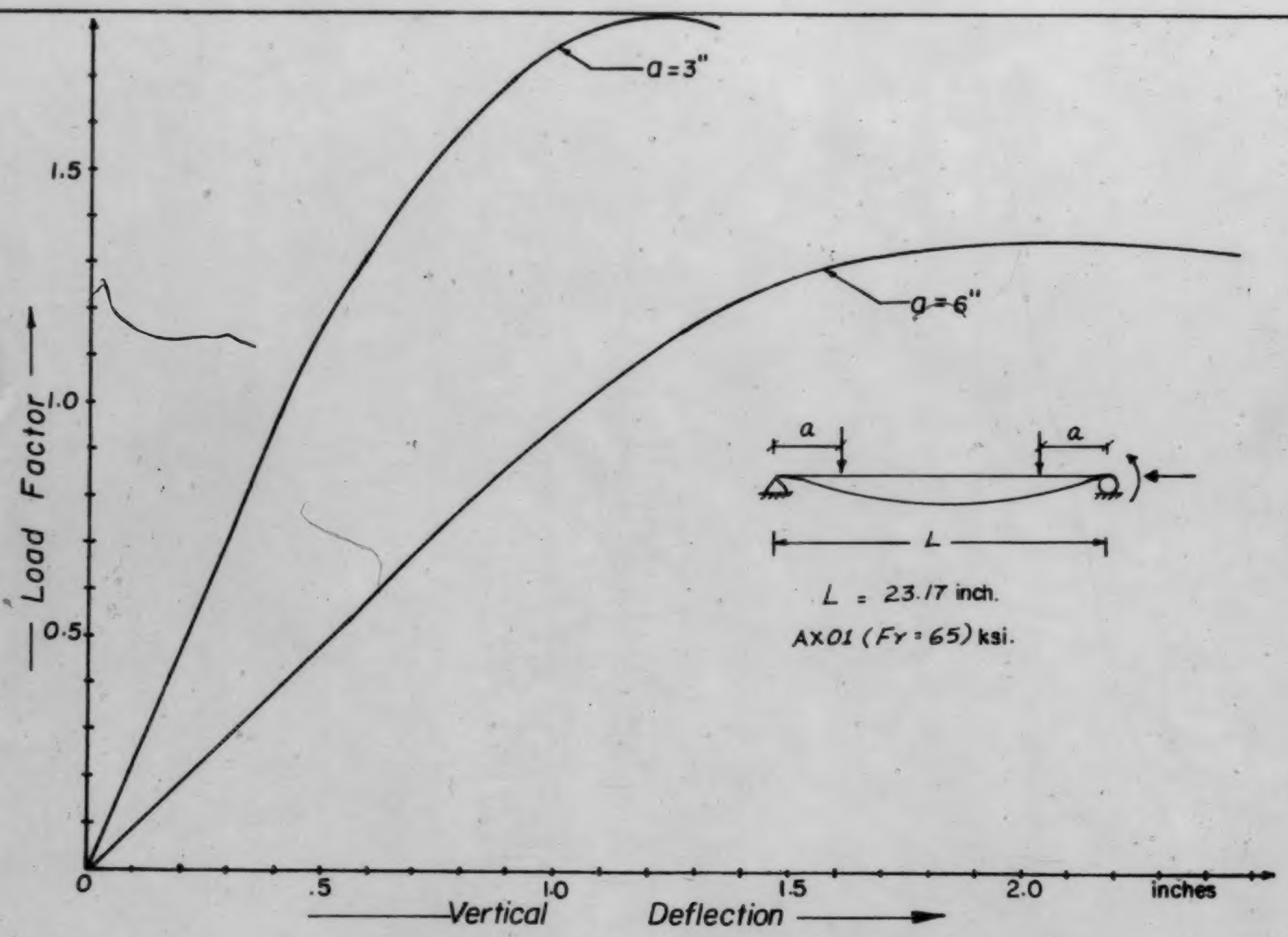

FIG. 5.13. Effect of Load Positioning in Member Behavior.

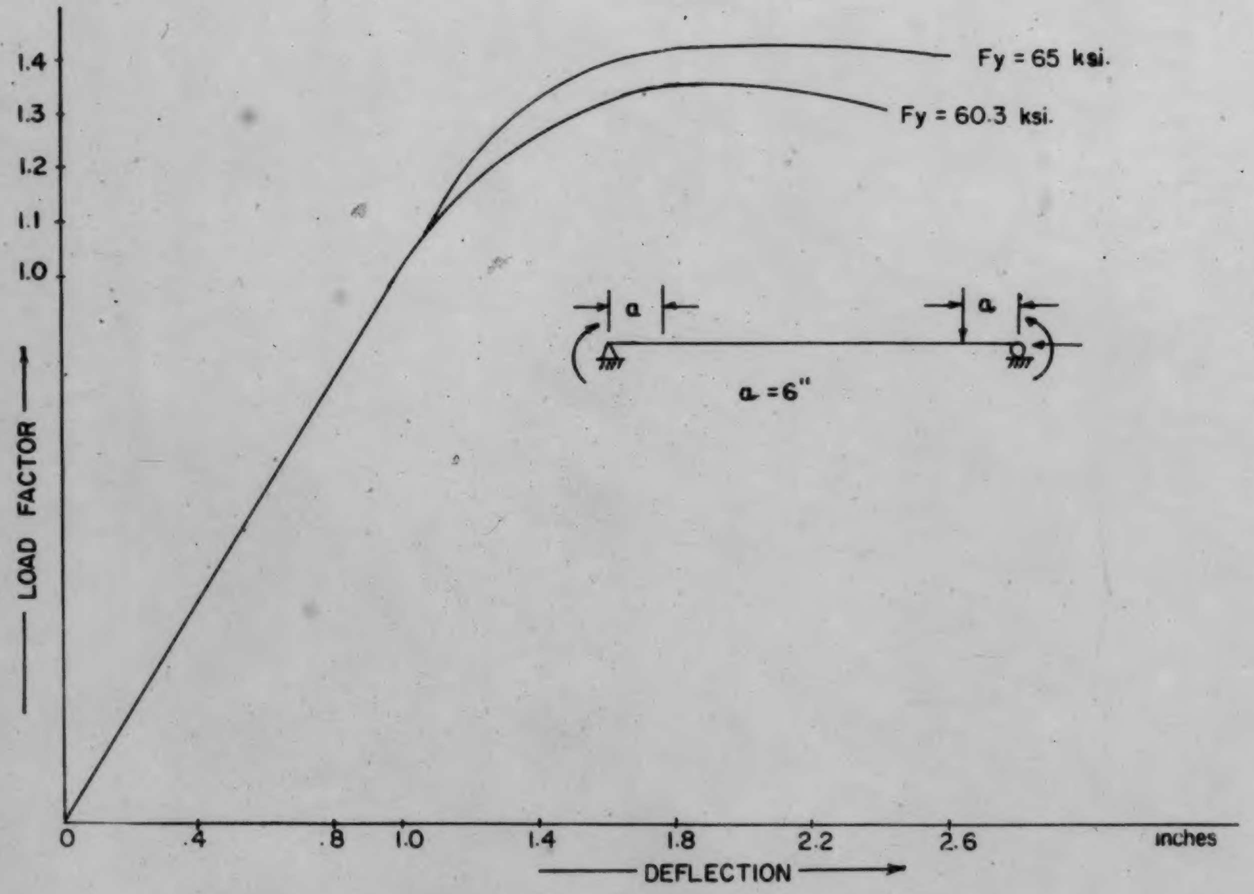

Fig. 5.14. EFFECT OF YIELD STRESS ON MEMBER BEHAVIOUR

APPENDIX A

ASSUMED DISTRIBUTION OF RESIDUAL STRESSES

The residual stress distribution for a typical wide flange section is as shown in Figure A.1. The value of σ_{rt}, in terms of σ_{rc}, is given as

$$\sigma_{rt} = \{\frac{bt}{bt + w(d-2t)}\} \sigma_{rc} \tag{A-1}$$

where b and d are the width and depth of the section and t and w are the thickness of flange and web respectively. The distribution of residual stresses on an unsymmetric I-section equivalent to a hat shaped section (Type C, manufactured by Great West Steel) has been assumed as shown in Figure A.2. This figure indicates the residual stress in terms of three controlling values. (σ_{rc_1}, σ_{rc} and σ_{rt}). However, the two equations of equilibrium which these residual stresses must satisfy are constraint equations which reduce the number of independent values to one. In this Appendix the values of σ_{rt} and σ_{rc_1} are evaluated as functions of σ_{rc}.

Equilibrium of forces (that is, $\Sigma M = 0$ and $\Sigma F=0$), are considered, assuming the forces act at the middle of the fibre, and taking the moment about the middle fibre of wide flange. Considering the stress diagram and section properties of the unsymmetric section shown in Figure A.2 and Figure 1.3, and writting the equilibrium equations, one obtains, for the $\Sigma F = 0$,

$$-\sigma_{rc_1}(a_1b_1) - \frac{\sigma_{rc_1}}{2}\left(\frac{a_2\sigma_{rc_1}}{\sigma_{rc_1}+\sigma_{rt}}\right) b_2 + \frac{\sigma_{rt}}{2}\left(\frac{a_2(\sigma_{rt})}{\sigma_{rc_1}+\sigma_{rt}}\right) b_2$$

$$+\left(\frac{a_3b_3\sigma_{rt}}{\sigma_{rc}+\sigma_{rt}}\right)\frac{\sigma_{rt}}{2} - \left(\frac{a_3b_3\,\sigma_{rc}}{\sigma_{rc}+\sigma_{rt}}\right)\frac{\sigma_{rc}}{2} = 0 \qquad \text{(A-2)}$$

where (b_1, b_2, b_3) and (a_1, a_2, a_3) are widths and depths of the narrow flange; web and wide flange respectively. σ_{rc_1} is the maximum compressive stress at the top of the web and is considered to be uniform in the narrow flange. σ_{rt} is the tensile stress at the bottom of the web and the middle of the wide flange and σ_{rc} is the maximum compressive stress at the tip of the wide flange. Compression and tension are indicated as negative and positive, respectively.

Simplyfying Equation A-2, it can be written as

$$-\sigma_{rc_1}(a_1b_1) + \frac{a_2b_2}{2}(\sigma_{rt} - \sigma_{rc_1}) + \frac{a_3b_3}{2}(\sigma_{rt} - \sigma_{rc}) = 0 \qquad \text{(A-3)}$$

Considering now the equilibrium of moments, the following equation is obtained.

$$a_1b_1(\sigma_{rc_1})(a_2 + \frac{a_1+a_3}{2}) + \frac{\sigma_{rc_1}}{2}\left(\frac{a_2b_2\sigma_{rc_1}}{\sigma_{rc_1}+\sigma_{rt}}\right)\Big(\frac{a_2\sigma_{rt}}{\sigma_{rc_1}+\sigma_{rt}} + \frac{a_3}{2}$$

$$+\frac{2}{3}a_2\,\frac{\sigma_{rc_1}}{(\sigma_{rc_1}+\sigma_{rt})}\Big)$$

$$-\frac{\sigma_{rt}}{2}\,\frac{a_2b_2\sigma_{rt}}{\sigma_{rc}+\sigma_{rt}}\left(\frac{a_3}{2} + \frac{a_2\sigma_{rt}}{3(\sigma_{rc_1}+\sigma_{rt})}\right) = 0 \qquad \text{(A-4)}$$

or

$$\frac{a_2 b_2}{2(\sigma_{rc_1} + \sigma_{rt})}[\sigma_{rc_1}^2 \left(\frac{a_2 \sigma_{rt}}{\sigma_{rc_1} + \sigma_{rt}} + \frac{a_3}{2} + \frac{2}{3} \frac{a_2 \sigma_{rc_1}}{\sigma_{rc_1} + \sigma_{rt}}\right) - \sigma_{rt}^2 \left(\frac{a_3}{2} + \frac{1}{3} \frac{a_2 \sigma_{rt}}{\sigma_{rc_1} + \sigma_{rt}}\right)]$$

$$+ a_1 b_1 \sigma_{rc_1} (a_2 + \frac{a_1 + a_3}{2}) = 0$$

or

$$a_1 b_1 \sigma_{rc_1} (a_2 + \frac{a_1 + a_3}{2}) + \frac{a_2 b_2}{2(\sigma_{rc_1} + \sigma_{rt})} [\frac{a_3}{2}(\sigma_{rc_1}^2 - \sigma_{rt}^2) + \frac{2}{3} \frac{a_2 \sigma_{rc_1}^2}{\sigma_{rc_1} + \sigma_{rt}} (\sigma_{rc_1} + \sigma_{rt})$$

$$+ \frac{1}{3} \frac{a_2 (\sigma_{rt})(\sigma_{rc_1}^2)}{\sigma_{rc_1} + \sigma_{rt}} \quad - \frac{1}{3} \frac{a_2 \sigma_{rt}^3}{\sigma_{rc_1} + \sigma_{rt}}]$$

or

$$a_1 b_1 \sigma_{rc_1} (a_2 + \frac{a_1 + a_3}{2}) + \frac{a_2 b_2}{2} [\frac{a_3}{2}(\sigma_{rc_1} - \sigma_{rt}) + \frac{2}{3} \frac{a_2 \sigma_{rc_1}^2}{\sigma_{rc_1} + \sigma_{rt}} + \frac{a_2}{3} \sigma_{rt}$$

$$\left(\frac{\sigma_{rc_1} - \sigma_{rt}}{\sigma_{rc_1} + \sigma_{rt}} \right)]$$

or

$$a_1 b_1 \sigma_{rc_1} (a_2 + \frac{a_1 + a_3}{2}) + \frac{a_2 b_2}{2} [\frac{a_3}{2}(\sigma_{rc_1} - \sigma_{rt}) + \frac{a_2}{3}(2\sigma_{rc_1} - \sigma_{rt})] \tag{A-5}$$

Equation A-5 can also be written as

$$\sigma_{rc_1}[a_1b_1(a_2+\frac{a_1+a_3}{2}+\frac{a_2b_2a_3}{4})+\frac{a_2^2b_2}{3}]=\sigma_{rt}[\frac{a_2b_2a_3}{4}+\frac{a_2^2b_2}{6}] \tag{A-6}$$

Putting the value of σ_{rc_1} in terms of σ_{rt}, from Equation (A-6), into Equation (A-3)

$$\sigma_{rt}[(a_2b_2+a_3b_3)-\frac{(2a_1b_1+a_2b_2)(\frac{a_3}{4}+\frac{a_2}{6})}{\frac{a_1b_1}{a_2b_2}(a_2+\frac{a_1+a_3}{2})+\frac{a_3}{4}+\frac{a_2}{3}}]=a_3b_3\sigma_{rc} \tag{A-7}$$

Substituting

$$D=(a_2b_2+a_3b_3)[\frac{a_1b_1}{2a_2b_2}(2a_2+a_1+a_3)+\frac{a_3}{4}+\frac{a_2}{3}]-(2a_1b_1+a_2b_2)(\frac{a_3}{4}+\frac{a_2}{6})$$

yields

$$\sigma_{rt}=\frac{a_3b_3\sigma_{rc}}{D}[\frac{6a_1b_1}{a_2b_2}(2a_2+a_1+a_3)+3a_3+4a_2] \tag{A-8}$$

Putting the value of σ_{rt}, from Equation(A-8),into Equation (A-6), and simplifying, it becomes

$$\sigma_{rc_1}=\frac{(3a_3+2a_2)a_3b_3\sigma_{rc}}{D} \tag{A-9}$$

The values of σ_{rc_1} and σ_{rt} are expressed in the program in terms of σ_{rc} by Equations (A-8) and (A-9).

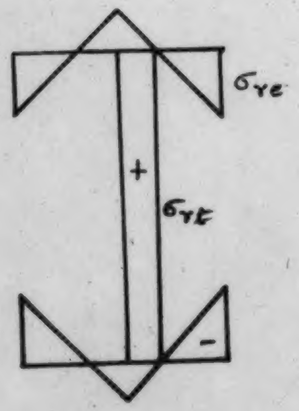
σ_{rc}
+
σ_{rt}
−

Fig. A.1. Residual Stress Distribution on Symmetrical Section.

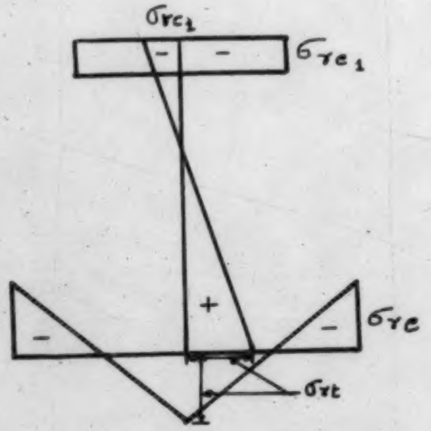
σ_{rc_2}
−
−
σ_{rc_1}
+
−
−
σ_{rc}
σ_{rt}

Fig. A.2. Assumed Residual Stress Distribution on An Unsymmetrical Section.

APPENDIX B

DETERMINATION OF CRITICAL STRAIN LOCATIONS

The purpose of this appendix is to determine the points in the web of a simulated hat section, where changes in the modulus of elasticity occur.

The equation of any linear variation of strain through the web may be written as

$$\varepsilon = m\,x + b \qquad \text{(B-1)}$$

where (x,ε) are co-ordinates of any point on the line, m is slope of the line, and b is the intercept on the ε axis. Assuming linear distribution of residual strain, as shown in Figure B.1, and substituting the co-ordinates of A and B into Equation B-1, the constants m and c can be obtained for the line A-B. Sign conventions are also shown in Figure B·1 and Figure B.2.

Evaluating Equation B-1 at A yields

$$-\varepsilon_{rc_1} = m(x_g - a_1) + b \qquad \text{(B-2a)}$$

and evaluating Equation B-1 at B yields

$$\varepsilon_{rt} = m[-(a_1 + a_2) + x_g] + b \qquad \text{(B-2b)}$$

Substracting Equation B-2a from Equation B-2b gives

$$\varepsilon_{rt} + \varepsilon_{rc_1} = m[x_g - (a_1 + a_2) - xg + a_1]$$

$$= - m\, a_2 \qquad \text{(B-3)}$$

Hence

$$m = - \frac{\varepsilon_{rt} + \varepsilon_{rc_1}}{a_2} \qquad \text{(B-4)}$$

Substituting the value of m from Equation B-4 into Equation B-2, the value of b can be obtained as shown:

$$\varepsilon_{rt} = \frac{\varepsilon_{rt} + \varepsilon_{rc_1}}{a_2} (a_1 + a_2 - x_g) + b \qquad \text{(B-5)}$$

By algebraic manipulation

$$b = \frac{\varepsilon_{rc_1}[xg - (a_1 + a_2)] + \varepsilon_{rt}(x_g - a_1)}{a_2} \qquad \text{(B-6)}$$

The above values of m and b define the residual strains in the web. The critical strain points where changes in elasticity occur are shown in Figure B.2 and, if the strain from superimposed loads may be expressed as f + cx,are located from the following expressions.

$$f + c\,x + m\,x + b = \begin{cases} \varepsilon_{y2} & \text{at } y_1 \\ \varepsilon_{y1} & \text{at } y_2 \\ -\varepsilon_{y1} & \text{at } y_3 \\ -\varepsilon_{y2} & \text{at } y_4 \end{cases} \qquad \text{(B-7)}$$

Solving Equation B-7 for each case, the strain locations are obtained as

$$y_1 = + \frac{f + b - \varepsilon_{y2}}{c + m} \qquad \text{(B-8)}$$

$$y_2 = + \frac{f + b - \varepsilon_{y1}}{c + m} \qquad \text{(B-9)}$$

$$y_3 = - \frac{f + b + \varepsilon_{y1}}{c + m} \qquad \text{(B-10)}$$

$$y_4 = - \frac{f + b + \varepsilon_{y2}}{c + m} \qquad \text{(B-11)}$$

$$y_5 = x_g - a_1 \qquad \text{(B-12)}$$

The strain locations y_1 to y_4 define the begining of positive and negative strain hardening from the centroid of the section. The distance from the centroid to the top of the web is denoted by y_5.

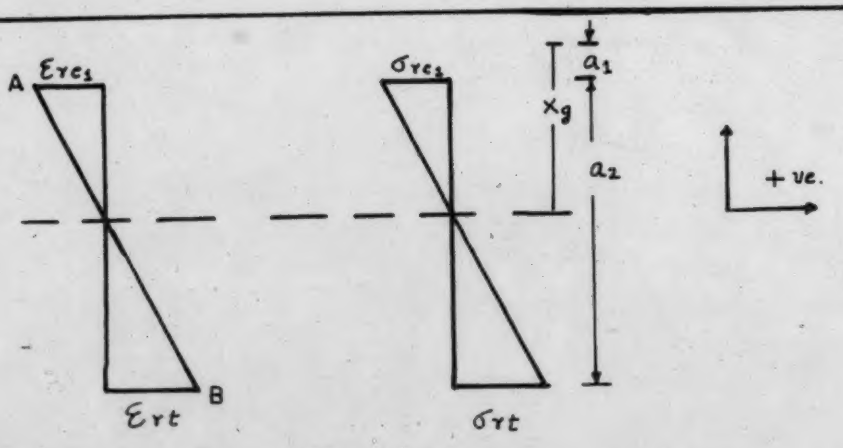
A
ε_{rc_1}
B
ε_{rt}
σ_{rc_1}
σ_{rt}
a_1
x_g
a_2
+ ve.

FIG. B.1. Residual Stress and Strain Distribution in the Web.

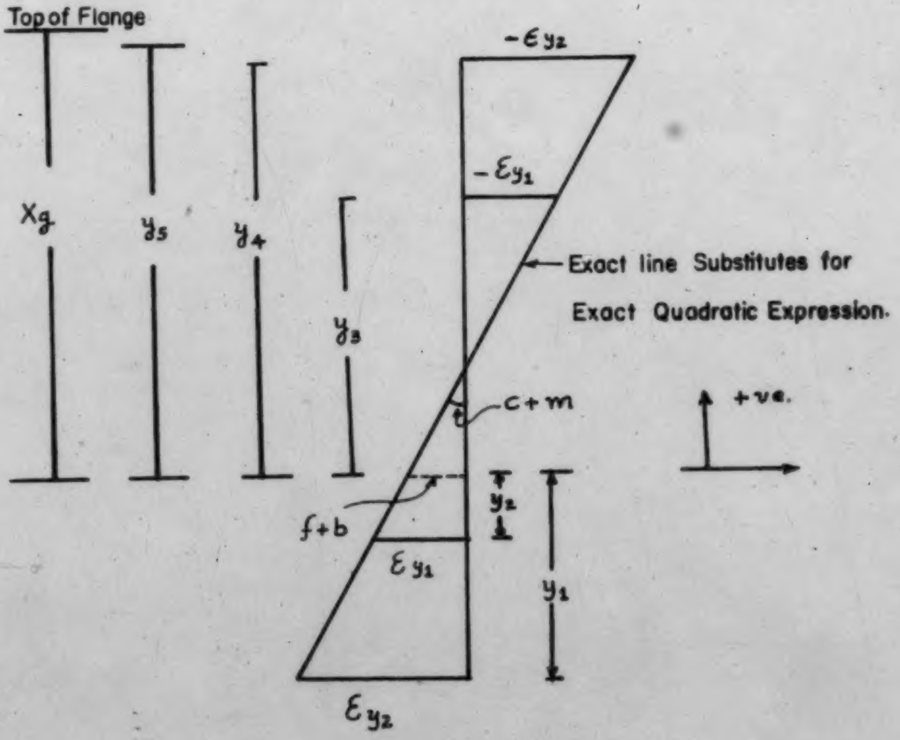
Top of Flange
x_g
y_5
y_4
y_3
$-\varepsilon_{y_2}$
$-\varepsilon_{y_1}$
Exact line Substitutes for Exact Quadratic Expression.
c+m
+ve.
f+b
y_2
ε_{y_1}
y_1
ε_{y_2}

FIG. B.2. Critical Strain locations from Centroid in Web.

APPENDIX C

HAND COMPUTATION OF INTERACTION CURVE ($\frac{\ell}{r} = o$)

In order to determine the fully plastic stress resultants for the given equivalent unsymmetrical I-section shown in Figure 1.3, it is first divided into small strips as shown in Figure C.1(a). The centre of gravity and the equal area axis of this section are at 0.453 and .251 inches from the extreme fibre of the wide flange. The stress diagram for the fully plastified section is also illustrated in Figure C.1(b).The area of each of the strips is calculated and the moment of area of all these strips is evaluated about point O (Figure C.1(b)),and given in Table C-1. The location of the discontinuity in the yield stress (point A of Figure C.1(b) is assumed to move to the edge of each strip in succession and positive and negative plastic areas, the net area and the net moment of area are calculated as shown in Table C-2. The moment of area about the center of gravity is then obtained by adding the net moment of area about point O and the product of the area times 0.4536 inches (i.e. - the distance of the center of gravity from the bottom of wide flange). These computations are shown in Table C-3. The top of the fifth strip is the equal area axis and at this section, it is observed that the net area is equal to zero and the net moment of area therefore represents the fully plastic moment in pure bending. Areas at the other penetrations are divided by this net area to obtain $\frac{P}{Py}$ values and corresponding values of $\frac{M}{M_p}$ are obtained by dividing the total moment of area at every section by this net moment of area. Detailed calculations to obtain these values are shown in Table C-3.

Table C-1 Calculation of Static Moments

Section	Area A	$\bar{y}$	$A\bar{y}$
1	.07303	.01675	.00122
2	.07303	.05025	.00367
3	.07303	.08375	.00612
4	.07303	.11725	.00856
5	.02679	.1925	.00516
6	.02859	.31341	.00896
7	.02859	.43823	.01253
8	.02859	.56308	.01610
9	.02859	.68791	.01967
10	.02859	.81274	.02324
11	.02859	.93757	.02681
12	.03685	1.01675	.03747
13	.03685	1.05025	.0387
14	.03685	1.08375	.03994
15	.03685	1.11725	.04117

Table C-2 Calculation of Net Static Moments

Penetration	Positive Area A^+	Negative Area A^-	Net Area A^N	$A\bar{y}^+$	$A\bar{y}^-$	$A\bar{y}^N$
0	0	.6378	-.6378	0	.2893	-.2893
1	.07303	.5648	-.4917	.00122	.28808	-.28686
2	.14606	.4917	-.3457	.00489	.28441	-.27952
3	.21909	.4187	-.1996	.01101	.27829	-.26728
4	.29212	.3457	-.0536	.01957	.26973	-.25016
5	.3189	.3189	0	.02473	.26457	-.23984
6	.3475	.2903	.0572	.03369	.25561	-.22192
7	.3751	.2617	.1144	.04622	.24308	-.19686
8	.4047	.2331	.1716	.06232	.22699	-.16467
9	.4333	.2045	.2288	.08198	.20732	-.12533
10	.4619	.1759	.2860	.10522	.18408	-.07886
11	.4905	.1473	.3432	.13203	.15728	-.02525
12	.5273	.1105	.4168	.16949	.119808	+.04969
13	.5642	.0736	.4906	.2082	.0811	+.12709
14	.60101	.0368	.5642	.24813	.04117	+.20696
15	.6378	0	.6378	.2893	0	.2893

Table C-3 Calculation of Points for Interaction Curves

Penetration	A net	$A\bar{y}$ net	$(A\bar{y}$ net$)+$ 0.4536(A net)	$\frac{P}{P_y}$	$\frac{M}{M_p}$
0	-.6378	-.2893	0	-1	0
1	-.4917	-.28686	-.0638	-.771	.26
2	-.3457	-.27952	-.12270	-.542	.51
3	-.1996	-.26728	-.1767	-.31295	.74
4	-.0536	-.25016	-.2258	-.084	.94
5	0	-.23984	-.2399	0	1
6	.0572	-.22192	-.2478	.09	1.026
7	.1144	-.19686	-.2487	.18	1.03
8	.1716	-.16467	0.2425	.27	1.01
9	.2288	-.12533	-.2291	.36	.95
10	.286	-.07886	-.2086	.45	.87
11	.3432	-.02525	-.1809	.54	.75
12	.4168	+.04969	-.1394	.65	.58
13	.4906	+.12709	-.0954	.77	.398
14	.5642	+.20696	-.04896	.88	.204
15	.6378	+.2893	0	1	0

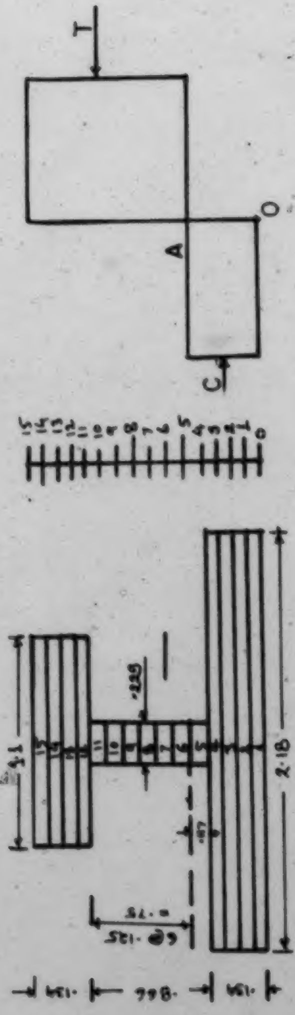
T
O
A
C
15
14
13
12
11
10
9
8
7
6
5
4
3
2
1
0
2.1
.235
.187
2.18
6@.125
= .75
.134
.866
.134

FIG. C.1. Subdivision of Equivalent Section for Fully Plastic Computations.

APPENDIX D

PROGRAM NLHAT

D-1 Preparation of Input Data for Program NLHAT

Program Limitations

Number of elements ≤ 20

Number of nodes ≤ 20

Input:

(1) ALFA (1 card) (Format F10.0)

ALFA is a value used in numerical differentiation of the equilibrium equations (normally specified as -.05).

(2) (NEL, MAX, NI, IPRINT) (1 card) (Format 4I8)

NEL : Number of elements

MAX : Maximum number of iterations in the Newton-Raphson procedure

NI : Number of subdivisions for the application of Simpson's rule (1≤NI ≤ 24) A good choice is NI=5, unless the elements are too long.

IPRINT: Indicator for intermediate printing. The Jacobian matrix is specified at each step when IPRINT = 1

(3) (XL, A1, A2, A3, B1, B2, B3) (1 card) (Format 7F10.0)

XL : Beam Length

A1, A2, A3, B1, B2, B3 : cross sectional dimensions as shown in Figure 1.3.

(4) (ET1, ET2, ET3, EY1, EY2, SRC) (1 card) (Format 6F10.0)

ET1, ET2, ET3 : Three moduli of elasticity involved in the trilinear constitutive equations.

EY1, EY2 : The strains corresponding to changes in modulus of elasticity

SRC : The compressive initial residual stress whose distribution is shown in Figure A.2

(5) INUMSP, EPS) (1 card) (Format I4, F16.0)

NUMSP : Number of springs

EPS : Specified accuracy for convergence criterion

In case the number of springs is not zero then for each spring a separate card is included in sequential order.

(6) (NPS(I), NDEG(I), ESP(I)) (one card for each spring)(Format 2I4, F16.0)

NPS : Nodal point number at which a spring is attached

NDEG : Local number of the degree of freedom (1,2,3, or 4 for u, w, u' or w', respectively)

ESP : Spring stiffness associated with the degree of freedom

(7) IB(1), IB(2), IB(4*NEL+4)) (Format 10I8)

IB(1) : 0 for an unconstrained degree of freedom
1 for a constrained degree of freedom

If IB(I) = 1 then BND(I) is the value of the displacement for constrained (I^{th}) degree of freedom

(8) (BND(1), BND(2),...BND(4*NEL+4)) (Format 8F10.0)

BND : The displacement specified for the degree of freedom

(9) X(1), X(2),...X(NEL+1) (Format 8F10.0)

X(I) : X force (transverse) at the I th node

(10) Z(1), Z(2)...Z(NEL+1) (Format 8F10.0)

Z(I) : Axial force at the I th node

(11) XM(1), XM(2), XM(NEL+1) (Format 8F10.0)

XM(I) : Moment at the I th node

(12) NF, NF1 (Format 2I8)

0 Initial trial vector on cards
NF = 1 Initial trial vector in file 15
2 Initial trial vector in file 16

0 last trial vector will be written on file 15, file 16
NF1 = will be left unchanged
1 last trial vector will be written on file 15 but
converged solution will be written on file 16, erasing
previous vector

(13) U(1),...U(4*NEL+4) (Format 8F10.0)

These are the values of the initial trial vector and cards containing this are included in the data preparation if NF is specified as zero.

D-2 Program Listing

A listing of the program follows:

```
C MAIN PROGRAM FOR NONLINEAR ANALYSIS OF UNSYMMETRIC I-BEAM
      IMPLICIT REAL*8(A-H,O-Z)
      DIMENSION U(100),DU(100),MI(25)
      COMMON/PUAD/Z(21),X(21),XM(21)
      COMMON/IBND/IB(100)
      COMMON/BNDCON/BND(100)
      COMMON/CNSTEC/ET1,ET2,ET3,EY1,EY2
      COMMON/SECT/XG,A1,A2,A3,B1,B2,B3
      COMMON/RESID/SRC1,SRT,SRC
      COMMON/FINITE/H
      COMMON/NCHK/IPRINT
      COMMON/SPRING/ESP(40),NPS(40),NDEG(40)
      COMMON/DERIV/ALFA
      READ(5,1000)    ALFA
      WRITE(6,1234)   ALFA
      READ(5,2000)    NEL,MAX,NI,IPRINT
      WRITE(6,1111)   NEL,MAX,NI,IPRINT
 1111 FORMAT(1H0,4I10)
      READ(5,1000)    XL,A1,A2,A3,B1,B2,B3
      WRITE(6,1234)   XL,A1,A2,A3,B1,B2,B3
 1234 FORMAT(1H0,8E11.3)
      READ(5,1000)  ET1,ET2,ET3,EY1,EY2,SRC
      WRITE(6,1234) ET1,ET2,ET3,EY1,EY2,SRC
      D=((A2*B2+A3*B3)*((2.*A2+A1+A3)*(6.*A1*B1/(A2*B2))+3.*A3+4.*A2)-(
     1                                  2.*A1*B1+A2*B2)*(3.*A3+2.*A2))
      SRC1=(A3*B3*(3.*A3+2.*A2)/D)*SRC
      SRT=(A3*B3*((6.*A1*B1/(A2*B2))*(2.*A2+A1+A3)+3.*A3+4.*A2))*SRC/D
      WRITE(6,1234)    SRC1,SRT
      XG=0.5*A1+(A2*B2*0.5*(A2+A1)+A3*B3*(A2+0.5*(A3+A1)))/(A1*B1+A2*B2+
     -A3*B3)
      WRITE(6,1235)  XG
 1235 FORMAT(1H0,10X,'XG=',E15.5)
      READ(5,1200) NUMSP,EPS
      DO 55 I=1,40
      NPS(I)=0.
      NDEG(I)=0.
   55 ESP(I)=0.
      IF(NUMSP.GT.0) READ(5,1201) (NPS(I),NDEG(I),ESP(I),I=1,NUMSP)
 1200 FORMAT(I4,F16.0)
 1201 FORMAT(2I4,F16.0)
      NPOT=NEL+1
      N=4*NPOT
      H=XL/NEL
      READ(5,2000)     (IB(I),I=1,N)
      WRITE(6,1111)    (IB(I),I=1,N)
      READ(5,1000)     (BND(I),I=1,N)
      WRITE(6,1234)    (BND(I),I=1,N)
      READ(5,1000)     (X(I),I=1,NPOT)
      WRITE(6,1234)    (X(I),I=1,NPOT)
      READ(5,1000)    (Z(I),I=1,NPOT)
      WRITE(6,1234)  (Z(I),I=1,NPOT)
      READ(5,1000)    (XM(I),I=1,NPOT)
      WRITE(6,1234)   (XM(I),I=1,NPOT)
      READ(5,2000)   NF,NF1
      IF(NF.GT.0)   GO TO 234
      READ(5,1000)     (U(I),I=1,N)
      GO TO 237
  234 I15=1
      NNR=14+NF
      DO 235   I=1,NPOT
      III=4*(I-1)
      READ(NNR'I15)   (U(III+KR),KR=1,4)
  235 I15=I15+1
  237 CONTINUE
      WRITE(6,1234)     (U(I),I=1,N)
      CALL NEWRAP(N,U,DU,NPOT,EPS,MAX,MI,NI)
      WRITE(6,3000)    (U(I),I=1,N)
 3000 FORMAT(1H0,10X,'RESULTS',//,10X,'U',19X,'W',19X,'UP',18X,'WP',//,
     1        (4E20.7))
      IF(NF1.EQ.0)   GO TO 77
      I16=1
      DO 335   I=1,NPOT
      III=4*(I-1)
      WRITE(16'I16)    (U(III+KR),KR=1,4)
  335 I16=I16+1
   77 CONTINUE
      WRITE(6,5000)
 5000 FORMAT(1H0,////,6X,'ELEMENT NO.',10X,'BENDING MOMENT',5X,
     1  'MOD. AXIAL FORCE',8X,'AXIAL FORCE',5X,
     2  'YTF1+-',5X,'YTF2+-',5X,'YTF3-+',5X,'YTF4-+'/
     3  'YW1+-',5X,'YW2+-',5X,'YW3-+',5X,'YW4-+',5X,
     4  'YBF1+-',5X,'YBF2+-',5X,'YBF3-+',5X,'YBF4-+',//)
      DO 88  I=1,NEL
      CALL NMP(I,NI,U,N,1)
   88 CONTINUE
      IF(NUMSP.EQ.0) GO TO 19
      DO 100 I=1,NUMSP
      NN=NPS(I)
      N2=4*NN
      J=NDEG(I)
      GO TO (96,97,98),J
   96 EX=X(NN)-ESP(I)*U(N2-3)
      GO TO 99
   97 EX=Z(NN)-ESP(I)*U(N2-2)
      GO TO 99
   98 EX=XM(NN)-ESP(I)*DATAN2(U(N2-1),(1.+U(N2)))
   99 WRITE(6,5500)  NN,J,EX
  100 CONTINUE
 5500 FORMAT(1H0,////,10X,'NET FORCE AT NODE',I4,'DEGREE OF FREEDOM',I4,
     1  'EXTERNAL FORCE',E12.5)
   19 DO 20    I=1,NPOT
   20 U(4*I-2)=U(4*I-2)+H*(I-1)
      WRITE(6,4000)     (U(4*I-3),U(4*I-2),I=1,NPOT)
 4000 FORMAT(1H0,////,10X,'COORDINATES',//,10X,'X',19X,'Z',//,(2E20.7))
 1000 FORMAT(8F10.0)
 2000 FORMAT(10I8)
      CALL EXIT
      END
      SUBROUTINE NMP(I,NI,U,N,IND)
      IMPLICIT REAL*8(A-H,O-Z)
C   IND=0 - NO PRINT          =1 - PRINT ONLY            =OTHER - PRINT ALSO
      DIMENSION U(N)
      DIMENSION WI(50)
      DIMENSION YTF(5),YW(5),YBF(5)
      COMMON/FINITE/H
      COMMON/XNM/PN(4),PPN(4,4),PM(4),PPM(4,4)
      COMMON/SECT/XG,A1,A2,A3,B1,B2,B3
      F1P(Z)=6.*Z*(Z-1.0)/H
      F2P(Z)=3.*Z*Z-4.*Z+1.
      F3P(Z)=-F1P(Z)
      F4P(Z)=3.*Z*Z-2.*Z
      F1PP(Z)=(12.*Z-6.)/(H*H)
      F2PP(Z)=(6.*Z-4.)/H
      F3PP(Z)=-F1PP(Z)
      F4PP(Z)=(6.*Z-2.)/H
      DO 10   IZ=1,4
      PN(IZ)=0.
      PM(IZ)=0.
      DO 10    JZ=1,4
      PPN(IZ,JZ)=0.
      PPM(IZ,JZ)=0.
   10 CONTINUE
      UL=U(4*I-3)
      UPL=U(4*I-1)
      UR=U(4*I+1)
      UPR=U(4*I+3)
      WL=U(4*I-2)
      WPL=U(4*I)
      WR=U(4*I+2)
      WPR=U(4*I+4)
C FOR SIMPSON'S RULE
      NI2=2*NI+1
      IF(NI2.GE.3.AND.NI2.LT.50)    GO TO 13
      WRITE(6,1111) NI
 1111 FORMAT(1H0,'ERROR -    NI=',I2)
      CALL EXIT
   13 WI(1)=1./6.
      DO 15  IW=1,NI
      WI(2*IW)=4./6.
   15 WI(2*IW+1)=2./6.
```

```
      WI(NI2)=1./6.
      DO 400   J=1,NI2
      Z=DFLOAT(J-1)/DFLOAT(NI2-1)
      UP=UL*F1P(Z)+UPL*F2P(Z)+UR*F3P(Z)+UPR*F4P(Z)
      UPP=UL*F1PP(Z)+UPL*F2PP(Z)+UR*F3PP(Z)+UPR*F4PP(Z)
      WP=WL*F1P(Z)+WPL*F2P(Z)+WR*F3P(Z)+WPR*F4P(Z)
      WPP=WL*F1PP(Z)+WPL*F2PP(Z)+WR*F3PP(Z)+WPR*F4PP(Z)
      E=WP+0.5*(WP*WP+UP*UP)
      C=UPP*(1.+WP)-UP*WPP
      C=C/((2.*E+1.)*DSQRT(2.*E+1.))
      CALL FORMOM(E,C,XN,XM,YTF,YW,YBF)
      IF(IND.EQ.0)   GO TO 300
      XXM=XM*(2.*E+1.)
      XXN=DSQRT(2.*E+1.)*XN+2.*(2.*E+1.)*C*XM
      WRITE(6,2000)    I,J,XXM,XN,XXN,(YTF(IYTF),IYTF=1,4),
     1(YW(IYW),IYW=1,4),(YBF(IYBF),IYBF=1,4)
 2000 FORMAT(1H ,2I5,10X,3E18.7,4E11.3/8E11.3)
      IF(IND.EQ.1)  GO TO 400
  300 PN(1)=PN(1)+WI(J)*XN*F1P(Z)/NI
      PN(2)=PN(2)+WI(J)*XN*F2P(Z)/NI
      PN(4)=PN(4)+WI(J)*XN*F4P(Z)/NI
      PM(1)=PM(1)+WI(J)*XM*F1PP(Z)/NI
      PM(2)=PM(2)+WI(J)*XM*F2PP(Z)/NI
      PM(4)=PM(4)+WI(J)*XM*F4PP(Z)/NI
      PPN(1,1)=PPN(1,1)+WI(J)*XN*F1P(Z)*F1P(Z)/NI
      PPN(1,2)=PPN(1,2)+WI(J)*XN*F1P(Z)*F2P(Z)/NI
      PPN(1,4)=PPN(1,4)+WI(J)*XN*F1P(Z)*F4P(Z)/NI
      PPN(2,2)=PPN(2,2)+WI(J)*XN*F2P(Z)*F2P(Z)/NI
      PPN(2,4)=PPN(2,4)+WI(J)*XN*F2P(Z)*F4P(Z)/NI
      PPN(4,4)=PPN(4,4)+WI(J)*XN*F4P(Z)*F4P(Z)/NI
      PPM(1,1)=PPM(1,1)+WI(J)*XM*F1PP(Z)*F1P(Z)/NI
      PPM(1,2)=PPM(1,2)+WI(J)*XM*F1PP(Z)*F2P(Z)/NI
      PPM(1,4)=PPM(1,4)+WI(J)*XM*F1PP(Z)*F4P(Z)/NI
      PPM(2,1)=PPM(2,1)+WI(J)*XM*F2PP(Z)*F1P(Z)/NI
      PPM(2,2)=PPM(2,2)+WI(J)*XM*F2PP(Z)*F2P(Z)/NI
      PPM(2,4)=PPM(2,4)+WI(J)*XM*F2PP(Z)*F4P(Z)/NI
      PPM(4,1)=PPM(4,1)+WI(J)*XM*F4PP(Z)*F1P(Z)/NI
      PPM(4,2)=PPM(4,2)+WI(J)*XM*F4PP(Z)*F2P(Z)/NI
      PPM(4,4)=PPM(4,4)+WI(J)*XM*F4PP(Z)*F4P(Z)/NI
  400 CONTINUE
      IF(IND.EQ.1)   RETURN
      PN(3)=-PN(1)
      PM(3)=-PM(1)
      PPN(1,3)=-PPN(1,1)
      PPN(2,3)=-PPN(1,2)
      PPN(3,3)=PPN(1,1)
      PPN(3,4)=-PPN(1,4)
      PPM(1,3)=-PPM(1,1)
      PPM(2,3)=-PPM(2,1)
      PPM(3,1)=-PPM(1,1)
      PPM(3,2)=-PPM(1,2)
      PPM(3,3)=PPM(1,1)
      PPM(3,4)=-PPM(1,4)
      PPM(4,3)=-PPM(4,1)
      PPN(2,1)=PPN(1,2)
      PPN(3,1)=PPN(1,3)
      PPN(3,2)=PPN(2,3)
      PPN(4,1)=PPN(1,4)
      PPN(4,2)=PPN(2,4)
      PPN(4,3)=PPN(3,4)
      RETURN
      END
      SUBROUTINE FORMOM(E,C,SN,SM,YTF,YW,YBF)
      IMPLICIT REAL*8(A-H,O-Z)
      COMMON/RESID/SRC1,SRT,SRC
      COMMON/SECT/XG,A1,A2,A3,B1,B2,B3
      COMMON/CNSTEQ/ET1,ET2,ET3,EY1,EY2
      DIMENSION YTF(5),YW(5),YBF(5),STR(5)
      SN=0.
      SM=0.
      DO 5 I=1,5
      YTF(I)=0.
      YW(I)=0.
    5 YBF(I)=0.
      ERC=SRC/ET1
      ERC1=SRC1/ET1
      ERT=SRT/ET1
      STR(2)=ET1*EY1
      STR(1)=STR(2)+ET2*(EY2-EY1)
      STR(3)=-STR(2)
      STR(4)=-STR(1)
      GO TO 200
C       THIS IS A SOLUTION OF HAT SHAPED SECTION WITH CONSTANT C RESI
C        STR AT TOP
   10 WRITE(6,1100)
 1100 FORMAT(1H0,10X,'ERROR -RESIDUAL STRESSES MUST BE INPUT POSITIVE')
      CALL EXIT
C TOP FLANGE
   20 SLOPE1=2.*(ERT1+ERC)/B1
      X=XG-A1/2.
      EB=E-2.*C*X*(1.-.5*C*X)*(E+0.5)
      YTF(1)=(EB+ERT1-EY2)/SLOPE1
      YTF(2)=(EB+ERT1-EY1)/SLOPE1
      YTF(3)=(EB+ERT1+EY1)/SLOPE1
      YTF(4)=(EB+ERT1+EY2)/SLOPE1
      YTF(5)=B1/2.
      STR(5)=STR(4)+ET3*(EB-ERC+EY2)
      SB=STR(1)+ET3*(EB+ERT1-EY2)
      SUM=0.
      A0=0.
      DO 50 I=1,5
      IF(YTF(I))  45,45,25
   25 IF(YTF(I)-(B1/2.)) 40,30,30
   30 SB=SO+(STR(I)-SO)*(B1/2.-AO)/(YTF(I)-AO)
      SUM=SUM+0.5*(SO+SB)*(B1/2.-AO)
      GO TO 100
   40 SUM=SUM+0.5*(SO+STR(I))*(YTF(I)-AO)
      AO=YTF(I)
      SO=STR(I)
      GO TO 50
   45 SO=STR(I)-(STR(I+1)-STR(I))*YTF(I)/(YTF(I+1)-YTF(I))
   50 CONTINUE
  100 SN=SN+2.*SUM*A1
      SM=SM-2.*SUM*A1*X
      GO TO 250
  200 X=XG-A1/2.
      EB=E-2.*C*X*(1.-0.5*C*X)*(E+0.5)-ERC1
      IF(EB+EY2)  210,210,212
  210 STF=STR(4)+ET3*(EB+EY2)
      GO TO 239
  212 IF(EB+EY1)  214,214,216
  214 STF=STR(3)+ET2*(EB+EY1)
      GO TO 239
  216 IF(EB-EY1)  218,218,220
  218 STF=ET1*EB
      GO TO 239
  220 IF(EB-EY2)  222,222,224
  222 STF=STR(2)+ET2*(EB-EY1)
      GO TO 239
  224 STF=STR(1)+ET3*(EB-EY2)
  239 SN=SN+B1*A1*STF
      SM=SM-B1*A1*STF*X
  250 CONTINUE
C BOTTOM FLANGE
      IF(ERT)  10,201,21
   21 SLOPE2=2.*(ERT+ERC)/B3
      X=-(A1+A2+A3/2.-XG)
      EB=E-2.*C*X*(1.-0.5*C*X)*(E+0.5)
      YBF(1)=(EB+ERT-EY2)/SLOPE2
      YBF(2)=(EB+ERT-EY1)/SLOPE2
      YBF(3)=(EB+ERT+EY1)/SLOPE2
      YBF(4)=(EB+ERT+EY2)/SLOPE2
      YBF(5)=B3/2.
      STR(5)=STR(4)+ET3*(EB-ERC+EY2)
      SO=STR(1)+ET3*(EB+ERT-EY2)
      SUM=0.
      AO=0.
      DO 51  I=1,5
      IF(YBF(I))  46,46,26
   26 IF(YBF(I)-(B3/2.))  41,31,31
```

```
 31 SB=S0+(STR(I)-S0)*(B3/2.-A0)/(YBF(I)-A0)
    SUM=SUM+0.5*(S0+SB)*(B3/2.-A0)
    GO TO 101
 41 SUM=SUM+0.5*(S0+STR(I))*(YBF(I)-A0)
    A0=YBF(I)
    S0=STR(I)
    GO TO 51
 46 S0=STR(I)-(STR(I+1)-STR(I))*YBF(I)/(YBF(I+1)-YBF(I))
 51 CONTINUE
101 SN=SN+2.*SUM*A3
    SM=SM-2.*SUM*A3*X
    GO TO 251
201 X=-(A1+A2+A3/2.-XG)
    EB=E-2.*C*X*(1.-0.5*C*X)*(E+0.5)
    IF(EB+EY2)  211,211,213
211 STF=STR(4)+ET3*(EB+EY2)
    GO TO 238
213 IF(EB+EY1)  215,215,217
215 STF=STR(3)+ET2*(EB+EY1)
    GO TO 238
217 IF(EB-EY1)  219,219,221
219 STF=ET1*EB
    GO TO 238
221 IF(EB-EY2)  223,223,225
223 STF=STR(2)+ET2*(EB-EY1)
    GO TO 238
225 STF=STR(1)+ET3*(EB-EY2)
238 SN=SN+B3*A3*STF
    SM=SM-B3*A3*STF*X
251 CONTINUE
C  WEB
    SIGN=1.0
    A=+(ERT+ERC1)/A2
    B=(ERC1*(XG-(A1+A2))+ERT*(XG-A1))/A2
    IF(C+A) 300,500,305
300 SIGN=-1.0
    DO 310  K=1,4
310 STR(K)=-STR(K)
305 YW(1)=(E+B-SIGN*EY2)/(C+A)
    YW(2)=(E+B-SIGN*EY1)/(C+A)
    YW(3)=(E+B+SIGN*EY1)/(C+A)
    YW(4)=(E+B+SIGN*EY2)/(C+A)
    YW(5)=(XG-A1)
    STR(5)=STR(4)+ET3*(E+B-(C+A)*YW(5)+SIGN*EY2)
    S0=STR(1)+ET3*(E+B+(C+A)*YW(5)-SIGN*EY2)
    A0=XG-(A1+A2)
    DO 350 I=1,5
    IF(YW(I)-A0)  345,345,325
325 IF(YW(I)-YW(5))  340,330,330
330 SB=S0+(STR(I)-S0)*(YW(5)-A0)/(YW(I)-A0)
```

```
      SN=SN+0.5*(SO+SB)*(YW(5)-AO)*B2
      SM=SM-(YW(5)-AO)*B2*(SO*0.5*(YW(5)+AO)+(SB-SO)*0.5*(AO+2.*
     -(YW(5)-AO)/3.))
      GO TO 400
  340 SN=SN+0.5*(SO+STR(I))*(YW(I)-AO)*B2
      SM=SM-(YW(I)-AO)*B2*(SO*0.5*(YW(I)+AO)+(STR(I)-SO)*0.5*(AO+
     *2.*(YW(I)-AO)/3.))
      AO=YW(I)
      SO=STR(I)
      GO TO 350
  345 SO=STR(I)-(STR(I+1)-STR(I))*(YW(I)-AO)/(YW(I+1)-YW(I))
  350 CONTINUE
  400 RETURN
  500 IF(E+B+EY2)  510,510,512
  510 STF=STR(4)+ET3*(E+B+EY2)
      GO TO 539
  512 IF(E+B+EY1)  514,514,516
  514 STF=STR(3)+ET2*(E+B+EY1)
      GO TO 539
  516 IF(E+B-EY1)  518,518,520
  518 STF=ET1*(E+B)
      GO TO 539
  520 IF(E+B-EY2)  522,522,524
  522 STF=STR(2)+ET2*(E+B-EY1)
      GO TO 539
  524 STF=STR(1)+ET3*(E+B-EY2)
  539 SN=SN+STF*B2*A2
      RETURN
      END
      SUBROUTINE DNMP(I,U,N,NI)
      IMPLICIT REAL*8(A-H,O-Z)
      DIMENSION U(N)
      COMMON/FINITE/H
      COMMON/XNM/PN(4),PPN(4,4),PM(4),PPM(4,4)
      COMMON/DXNM/DPN(4,8),DPPN(4,4,8),DPM(4,8),DPPM(4,4,8)
      COMMON/CNSTEQ/ET1,ET2,ET3,EY1,EY2
      COMMON/DERIV/ALFA
      DIMENSION APN(4),APPN(4,4),APM(4),APPM(4,4)
      DIMENSION BPN(4),BPPN(4,4),BPM(4),BPPM(4,4)
      EY=EY1
      DO 50   K=1,4
      APN(K)=PN(K)
      APM(K)=PM(K)
      DO 50  L=1,4
      APPN(K,L)=PPN(K,L)
      APPM(K,L)=PPM(K,L)
   50 CONTINUE
      DO 100   J=1,8
      DELTA=ALFA*EY*H
      IF((J-((J-1)/4)*4).GT.2)  DELTA=ALFA*EY
      JJ=4*(I-1)+J
      A=U(JJ)
C ALFA.LT.0 ACTS AS INDICATOR TO USE A FIRST-ORDER DERIVATIVE
      IF(ALFA)  500,600,700
  600 WRITE(6,1000)
 1000 FORMAT(1H0,'ERROR. ALFA=0.')
      CALL EXIT
  500  DEL=-DELTA
      U(JJ)=A-DEL
      CALL NMP(I,NI,U,N,0)
      U(JJ)=A
      DO 550  K=1,4
      DPN(K,J)=(APN(K)-PN(K))/DEL
      DPM(K,J)=(APM(K)-PM(K))/DEL
      DO 550  L=1,4
      DPPN(K,L,J)=(APPN(K,L)-PPN(K,L))/DEL
      DPPM(K,L,J)=(APPM(K,L)-PPM(K,L))/DEL
  550 CONTINUE
      GO TO 100
  700 U(JJ)=A-DELTA
      CALL  NMP(I,NI,U,N,0)
      DO 150  IC=1,4
      BPN(IC)=PN(IC)
      BPM(IC)=PM(IC)
      DO 150  JC=1,4
      BPPN(IC,JC)=PPN(IC,JC)
      BPPM(IC,JC)=PPM(IC,JC)
  150 CONTINUE
      U(JJ)=A+DELTA
      CALL NMP(I,NI,U,N,0)
      U(JJ)=A
      DO 200   K=1,4
      DPN(K,J)=(PN(K)-BPN(K))/(2.*DELTA)
      DPM(K,J)=(PM(K)-BPM(K))/(2.*DELTA)
      DO 200  L=1,4
      DPPN(K,L,J)=(PPN(K,L)-BPPN(K,L))/(2.*DELTA)
      DPPM(K,L,J)=(PPM(K,L)-BPPM(K,L))/(2.*DELTA)
  200 CONTINUE
  100 CONTINUE
      DO 300   K=1,4
      PN(K)=APN(K)
      PM(K)=APM(K)
      DO 300   L=1,4
      PPN(K,L)=APPN(K,L)
      PPM(K,L)=APPM(K,L)
  300 CONTINUE
      RETURN
      END
      SUBROUTINE ABCG(N,U,NI)
      IMPLICIT REAL*8(A-H,O-Z)
      DIMENSION U(N)
      DIMENSION C(4,4),B(4,4),A(4,4),G(4)
      DIMENSION APN(4),APM(4),APPN(4,4),APPM(4,4)
      DIMENSION ADPN(4,8),ADPM(4,8),ADPPN(4,4,8),ADPPM(4,4,8)
      COMMON/XNM/PN(4),PPN(4,4),PM(4),PPM(4,4)
      COMMON/DXNM/DPN(4,8),DPPN(4,4,8),DPM(4,8),DPPM(4,4,8)
      COMMON/FINITE/H
      COMMON/NCHK/IPRINT
      COMMON/POAD/Z(21),X(21),XM(21)
      COMMON/IBND/IB(100)
      COMMON/BNDCON/BND(100)
      COMMON/SPRING/ESP(40),NPS(40),NDEG(40)
      I11=1
      I12=1
      NP=N/4
      KOUNT2=1
      KOUNT=1
      DO 500  I=1,NP
      FI=DATAN2(U(4*I-1),(1.+U(4*I)))
      CF=DCOS(FI)
      SF=DSIN(FI)
      G(1)=-X(I)
      G(2)=-Z(I)
      G(3)=-XM(I)*(1.+U(4*I))
      G(4)=XM(I)*U(4*I-1)
      IF(I.EQ.NP)   GO TO 100
      CALL NMP(I,NI,C,N,U)
      CALL DNMP(I,U,N,NI)
      G(1)=G(1)+H*PM(1)
      G(2)=G(2)+H*PN(1)
      G(3)=G(3)+H*PM(2)
      G(4)=G(4)+H*PN(2)
      IF(I.EQ.1)        GO TO 110
  100 G(1)=G(1)+H*APM(3)
      G(2)=G(2)+H*APN(3)
      G(3)=G(3)+H*APM(4)
      G(4)=G(4)+H*APN(4)
  110 CONTINUE
      DO 200  K=1,2
      DO 200  L=1,4
      II=4*I+2*L
      IF(I.EQ.NP)   GO TO 120
      G(2*K-1)=G(2*K-1)+H*(PPN(K,L)*U(II-5)+(PPM(K,L)-PPM(L,K))*U(II-4))
      G(2*K)=G(2*K)+H*(PPN(K,L)*U(II-4)+(PPM(L,K)-PPM(K,L))*U(II-5))
      IF(I.EQ.1)  GO TO 200
  120 G(2*K-1)=G(2*K-1)+H*(APPN(K+2,L)*U(II-9)+(APPM(K+2,L)-APPM(L,K+2))
     1                                              *U(II-8))
      G(2*K)=G(2*K)+H*(APPN(K+2,L)*U(II-8)+(APPM(L,K+2)-APPM(K+2,L))*
     1                                  U(II-9))
  200 CONTINUE
```

```
190 IF(I.NE.NPS(KOUNT)) GO TO 202
    LL = NDEG(KOUNT)
    GO TO (221,222,223),LL
221 G(1)=G(1)+ESP(KOUNT)*U(4*I-3)
    GO TO 224
222 G(2)=G(2)+ESP(KOUNT)*U(4*I-2)
    GO TO 224
223 G(3)=G(3)+ESP(KOUNT)*FI*(1.+U(4*I))
    G(4)=G(4)-ESP(KOUNT)*FI*U(4*I-1)
224 KOUNT=KOUNT+1
    GO TO 190
202 CONTINUE
    DO 210   K=1,4
    L=4-K
    G(K)=G(K)*(1.-IB(4*I-L))+(U(4*I-L)-BND(4*I-L))*IB(4*I-L)
210 CONTINUE
    DO 300  K=1,2
    DO 300 L=1,4
    IND=L/2-(L-1)/2
    LL=(L+1)/2
    IF(I.EQ.1)  GO TO 310
    C(2*K-1,L)=H*(ADPM(K+2,L)+APPN(K+2,LL)*(1-IND)+(APPM(K+2,LL)-
   1                  APPM(LL,K+2))*IND)
    C(2*K,L)=H*(ADPN(K+2,L)+APPN(K+2,LL)*IND+(APPM(LL,K+2)-APPM(K+2,
   1    LL))*(1-IND))
310 B(2*K-1,L)=0.
    B(2*K,L)=0.
    IF(I.EQ.NP)    GO TO 320
    B(2*K-1,L)=H*(DPM(K,L)+PPN(K,LL)*(1-IND)+(PPM(K,LL)-PPM(LL,K))*
   1                                                          IND)
    B(2*K,L)=H*(DPN(K,L)+PPN(K,LL)*IND+(PPM(LL,K)-PPM(K,LL))*(1-IND))
    IF(I.EQ.1)   GO TO 330
320 B(2*K-1,L)=B(2*K-1,L)+H*(ADPM(K+2,L+4)+APPN(K+2,LL+2)*(1-IND)+
   1 (APPM(K+2,LL+2)-APPM(LL+2,K+2))*IND)
    B(2*K,L)=B(2*K,L)+H*(ADPN(K+2,L+4)+APPN(K+2,LL+2)*IND+
   1 (APPM(LL+2,K+2)-APPM(K+2,LL+2))*(1-IND))
330 IF(I.EQ.NP)  GO TO 340
    A(2*K-1,L)=H*(DPM(K,L+4)+PPN(K,LL+2)*(1-IND)+(PPM(K,LL+2)-
   1                PPM(LL+2,K))*IND)
    A(2*K,L)=H*(DPN(K,L+4)+PPN(K,LL+2)*IND+(PPN(LL+2,K)-
   1                 PPM(K,LL+2))*(1-IND))
340 CONTINUE
    DO 300  M=1,4
    II=4*I+2*M
    IF(I.EQ.1)     GO TO 350
    C(2*K-1,L)=C(2*K-1,L)+H*(ADPPN(K+2,M,L)*U(II-9)+
   1      (ADPPM(K+2,M,L)-ADPPM(M,K+2,L))*U(II-8))
    C(2*K,L)=C(2*K,L)+H*(ADPPN(K+2,M,L)*U(II-8)+
   1    (ADPPM(M,K+2,L)-ADPPM(K+2,M,L))*U(II-9))
350 IF(I.EQ.NP)  GO TO 360
```

```
      B(2*K-1,L)=B(2*K-1,L)+H*(DPPN(K,M,L)*U(II-5)+
     1     (DPPM(K,M,L)-DPPM(M,K,L))*U(II-4))
      B(2*K,L)=B(2*K,L)+H*(DPPN(K,M,L)*U(II-4)+
     1         (DPPM(M,K,L)-DPPM(K,M,L))*U(II-5))
      IF(I.EQ.1)    GO TO 370
  360 B(2*K-1,L)=B(2*K-1,L)+H*(ADPPN(K+2,M,L+4)*U(II-9)+
     1    (ADPPM(K+2,M,L+4)-ADPPM(M,K+2,L+4))*U(II-8))
      B(2*K,L)=B(2*K,L)+H*(ADPPN(K+2,M,L+4)*U(II-8)+
     1     (ADPPM(M,K+2,L+4)-ADPPM(K+2,M,L+4))*U(II-9))
  370 CONTINUE
      A(2*K-1,L)=A(2*K-1,L)+H*(DPPN(K,M,L+4)*U(II-5)+
     1    (DPPM(K,M,L+4)-DPPM(M,K,L+4))*U(II-4))
      A(2*K,L)=A(2*K,L)+H*(DPPN(K,M,L+4)*U(II-4)+
     1    (DPPM(M,K,L+4)-DPPM(K,M,L+4))*U(II-5))
  300 CONTINUE
      B(3,4)=B(3,4)-XM(I)
      B(4,3)=B(4,3)+XM(I)
      DO 400  L=1,4
      IL=4*I+L-4
      DO 400    M=1,4
      IF(I.EQ.NP)    GO TO 410
      A(L,M)=A(L,M)*(1-IB(IL))
  410 B(L,M)=B(L,M)*(1-IB(IL))
      IF(M.EQ.L)  B(L,M)=B(L,M)+IB(IL)
      IF(I.EQ.1)    GO TO 400
      C(L,M)=C(L,M)*(1-IB(IL))
  400 CONTINUE
  422 IF(I.NE.NPS(KOUNT2)) GO TO 421
      KK = NDEG(KOUNT2)
      GO TO (420,423,424),KK
  420 B(1,1)=B(1,1)+ESP(KOUNT2)
      GO TO 429
  423 B(2,2)=B(2,2)+ESP(KOUNT2)
      GO TO 429
  424 B(3,3)=B(3,3)+ESP(KOUNT2)*CF*CF
      B(4,4)=B(4,4)+ESP(KOUNT2)*SF*SF
      B(3,4)=B(3,4)+ESP(KOUNT2)*(-SF*CF+FI)
      B(4,3)=B(4,3)+ESP(KOUNT2)*(-SF*CF-FI)
  429 KOUNT2=KOUNT2+1
      GO TO 422
  421 CONTINUE
      IF(I.EQ.1)    GO TO 450
      WRITE(12'I12)   ((C(IP,JP),JP=1,4),IP=1,4)
      I12=I12+1
      IF(IPRINT.EQ.1)  WRITE(6,1313)  ((C(IP,JP),JP=1,4),IP=1,4)
  450 WRITE(12'I12)    ((B(IP,JP),JP=1,4),IP=1,4)
      I12=I12+1
      IF(IPRINT.EQ.1)    WRITE(6,1313)  ((B(IP,JP),JP=1,4),IP=1,4)
      IF(I.EQ.NP)    GO TO 460
      WRITE(12'I12)  ((A(IP,JP),JP=1,4),IP=1,4)
      I12=I12+1
      IF(IPRINT.EQ.1)   WRITE(6,1313)    ((A(IP,JP),JP=1,4),IP=1,4)
  460 DO 461  IP=1,4
  461 G(IP)=-G(IP)
      WRITE(11'I11)     (G(IP),IP=1,4)
      I11=I11+1
      WRITE(6,1313)    (G(IP),IP=1,4)
 1313 FORMAT(1H ,4E20.7)
      DO 480    K=1,4
      APN(K)=PN(K)
      APM(K)=PM(K)
      DO 490    L=1,4
      APPN(K,L)=PPN(K,L)
      APPM(K,L)=PPM(K,L)
      DO 490  M=1,6
      ADPPN(K,L,M)=DPPN(K,L,M)
      ADPPM(K,L,M)=DPPM(K,L,M)
  490 CONTINUE
      DO 480    M=1,8
      ADPN(K,M)=DPN(K,M)
      ADPM(K,M)=DPM(K,M)
  480 CONTINUE
  500 CONTINUE
      RETURN
      END
      SUBROUTINE NEWRAP(N,U,DU,NPCT,EPS,MAX,MI,NI)
      IMPLICIT REAL*8 (A-H,O-Z)
      DIMENSION U(N),MI(NPOT),PP(16),GP(4),XP(4),AUX(16),LAUX(4),
     1   MAUX(4),AP(16),BP(16),CP(16),DU(N)
      DO 10    I=1,NPCT
   10 MI(I)=4
      NRHS=1
      DO 100   J=1,MAX
      CALL ABCG(N,U,NI)
      CALL POTRS(NPOT,MI,AP,BP,CP,PP,GP,XP,NRHS,AUX,LAUX,MAUX)
      CALL ERRPCT(NPCT)
      I22=1
      DO 19    I=1,NPCT
      III=4*(I-1)
      READ(14'I22)    (DU(III+KR),KR=1,4)
   19 I22=I22+1
      DO 20 I=1,N
   20 U(I)=U(I)+DU(I)
      S1=0.
      S2=0.
      DO 30   I=1,N
      S1=S1+DU(I)*DU(I)
   30 S2=S2+U(I)*U(I)
      E=DSQRT(S1/S2)
      WRITE(6,2222)    (U(III),III=1,N),E
```

```
2222 FORMAT(1H ,8E11.3)
     I15=1
     DO 31  I=1,NPUT
     III=4*(I-1)
     WRITE(15'I15)  (U(III+KR),KR=1,4)
  31 I15=I15+1
     IF(E.LT.EPS)   GO TO 200
 100 CONTINUE
     WRITE(6,1000)  MAX,E,(U(I),I=1,N)
1000 FORMAT(1H0,'CONVERGENCE NOT ACHIEVED AFTER',I4,1X,'CYCLES',/,5X,
    1  'PRESENT RELATIVE ERROR IS',E10.3,/,5X,'PRESENT RESULT IS',/,
    2   (4E20.7))
     CALL EXIT
 200 RETURN
     END
     SUBROUTINE ERRPCT(NPUT)
     IMPLICIT REAL*8(A-H,O-Z)
     DIMENSION ABC(16),XP(4),X(4),XN(4),AUX(4)
     I12=1
     DO 100 I=1,NPUT
     DO 10 J=1,4
     XP(J)=0.
  10 XN(J)=0.
     IF(I.EQ.1)  GO TO 20
     I14=I-1
     READ(14'I14) (XP(K),K=1,4)
     READ(12'I12)  (ABC(K),K=1,16)
     I12=I12+1
     CALL XMX(ABC,XP,XP,4,4,1,AUX)
  20 READ(14'I)  (X(K),K=1,4)
     READ(12'I12)  (ABC(K),K=1,16)
     I12=I12+1
     CALL XMX(ABC,X,X,4,4,1,AUX)
     IF(I.EQ.NPUT)  GO TO 50
     I14=I+1
     READ(14'I14) (XN(K),K=1,4)
     READ(12'I12)  (ABC(K),K=1,16)
     I12=I12+1
     CALL XMX(ABC,XN,XN,4,4,1,AUX)
  50 READ(11'I) (AUX(K),K=1,4)
     DO 60 K=1,4
     X(K)=XP(K)+X(K)+XN(K)
  60 AUX(K)=AUX(K)-X(K)
 100 WRITE(6,1000)  (X(K),K=1,4),(AUX(K),K=1,4)
1000 FORMAT(1H ,10X,4E12.4,10X,4E12.4)
     RETURN
     END
     SUBROUTINE INV(A,N,D,L,M)
     IMPLICIT REAL*8 (A-H,O-Z)
C  THIS IS THE 1130-SSP MINV SUBROUTINE
```

```
      DIMENSION A(1),L(1),M(1)
C   SEARCH FOR LARGEST ELEMENT
      D=1.
      NK=-N
      DO 80  K=1,N
      NK=NK+N
      L(K)=K
      M(K)=K
      KK=NK+K
      BIGA=A(KK)
      DO 20  J=K,N
      IZ=N*(J-1)
      DO 20  I=K,N
      IJ=IZ+1
   10 IF(DABS(BIGA)-DABS(A(IJ))) 15,20,20
   15 BIGA=A(IJ)
      L(K)=I
      M(K)=J
   20 CONTINUE
C   INTERCHANGE ROWS
      J=L(K)
      IF(J-K)   35,35,25
   25 KI=K-N
      DO 30    I=1,N
      KI=KI+N
      HOLD=-A(KI)
      JI=KI-K+J
      A(KI)=A(JI)
   30 A(JI)=HOLD
C INTERCHANGE COLUMNS
   35 I=M(K)
      IF(I-K)  45,45,38
   38 JP=N*(I-1)
      DO 40    J=1,N
      JK=NK+J
      JI=JP+J
      HOLD=-A(JK)
      A(JK)=A(JI)
   40 A(JI)=HOLD
C   DIVIDE COLUMN BY MINUS PIVOT (VALUE OF PIVOT ELEMENT IS
C          CONTAINED IN BIGA)
   45 IF(DABS(BIGA)-1.D-20)  46,46,48
   46 D=0.0
      WRITE(6,1000)
 1000 FORMAT(1H0,'DETERMINANT = 0.')
      CALL EXIT
   48 DO 55  I=1,N
      IF(I-K)  50,55,50
   50 IK=NK+I
      A(IK)=A(IK)/(-BIGA)
   55 CONTINUE
C   REDUCE MATRIX
      DO 65  I=1,N
      IK=NK+I
      HOLD=A(IK)
      IJ=I-N
      DO 65  J=1,N
      IJ=IJ+N
      IF(I-K)    60,65,60
   60 IF(J-K)  62,65,62
   62 KJ=IJ-I+K
      A(IJ)=HOLD*A(KJ)+A(IJ)
   65 CONTINUE
C   DIVIDE ROW BY PIVOT
      KJ=K-N
      DO 75  J=1,N
      KJ=KJ+N
      IF(J-K)    70,75,70
   70 A(KJ)=A(KJ)/BIGA
   75 CONTINUE
C   PRODUCT OF PIVOTS
      D=D*BIGA
C   REPLACE PIVOT BY RECIPROCAL
      A(KK)=1./BIGA
   80 CONTINUE
C   FINAL ROW AND COLUMN INTERCHANGE
      K=N
  100 K=K-1
      IF(K)  150,150,105
  105 I=L(K)
      IF(I-K)  120,120,108
  108 JQ=N*(K-1)
      JR=N*(I-1)
      DO 110    J=1,N
      JK=JQ+J
      HOLD=A(JK)
      JI=JR+J
      A(JK)=-A(JI)
  110 A(JI)=HOLD
  120 J=M(K)
      IF(J-K)  100,100,125
  125 KI=K-N
      DO 130  I=1,N
      KI=KI+N
      HOLD=A(KI)
      JI=KI-K+J
      A(KI)=-A(JI)
  130 A(JI)=HOLD
      GO TO 100
  150 RETURN
```

```
END
SUBROUTINE  PUTRS(NEQ,MI,AP,BP,CP,PP,GP,XP,NRHS,AUX,LAUX,MAUX)
IMPLICIT REAL*8 (A-H,O-Z)
DIMENSION LAUX(1),MAUX(1)
DIMENSION MI(1),AP(1),BP(1),CP(1),PP(1),GP(1),XP(1),AUX(1)
I11=1
I12=1
I21=1
I22=1
N=MI(I21)
NP1=MI(I21+1)
NN=N*N
NNP1=N*NP1
NNRHS=N*NRHS
READ(12'I12)  (BP(K),K=1,NN)
I12=I12+1
READ(12'I12)  (AP(K),K=1,NNP1)
I12=I12+1
READ(11'I11)  (GP(K),K=1,NNRHS)
I11=I11+1
CALL INV(BP,N,DET,LAUX,MAUX)
CALL XMX(BP,AP,PP,N,N,NP1,AUX)
CALL XMX(BP,GP,XP,N,N,NRHS,AUX)
WRITE(13'I21)  (PP(K),K=1,NNP1)
I21=I21+1
WRITE(14'I22)  (XP(K),K=1,NNRHS)
I22=I22+1
IF(NEQ.EQ.2) GO TO 101
NEQ1=NEQ-1
DO 100 I=2,NEQ1
NM1=MI(I-1)
N=MI(I)
NP1=MI(I+1)
NNM1=N*NM1
NN=N*N
NNP1=N*NP1
NNRHS=N*NRHS
READ(12'I12)  (CP(K),K=1,NNM1)
I12=I12+1
READ(12'I12)  (BP(K),K=1,NN)
I12=I12+1
READ(12'I12)  (AP(K),K=1,NNP1)
I12=I12+1
READ(11'I11)  (GP(K),K=1,NNRHS)
I11=I11+1
CALL XSXMX(BP,CP,PP,BP,N,NM1,N,AUX)
CALL INV(BP,N,DET,LAUX,MAUX)
CALL XMX(BP,AP,PP,N,N,NP1,AUX)
CALL XSXMX(GP,CP,XP,GP,N,NM1,NRHS,AUX)
CALL XMX(BP,GP,XP,N,N,NRHS,AUX)
```

L

```
      WRITE(13'I21)  (PP(K),K=1,NNP1)
      I21=I21+1
      WRITE(14'I22)  (XP(K),K=1,NNRHS)
      I22=I22+1
  100 CONTINUE
  101 NM1=MI(NEQ-1)
      N=MI(NEQ)
      NNM1=N*NM1
      NN=N*N
      NNRHS=N*NRHS
      READ(12'I12)  (CP(K),K=1,NNM1)
      I12=I12+1
      READ(12'I12)  (BP(K),K=1,NN)
      I12=I12+1
      READ(11'I11)  (GP(K),K=1,NNRHS)
      I11=I11+1
      CALL  XSXMX(BP,CP,PP,BP,N,NM1,N,AUX)
      CALL  INV(BP,N,DET,LAUX,MAUX)
      CALL  XSXMX(GP,CP,XP,GP,N,NM1,NRHS,AUX)
      CALL  XMX(BP,GP,XP,N,N,NRHS,AUX)
      WRITE(14'I22)  (XP(K),K=1,NNRHS)
      DO 200  I=2,NEQ
      I21=NEQ-I+1
      I22=I21
      N=MI(I21+1)
      NM1=MI(I21)
      NNM1=N*NM1
      NNRHS=NM1*NRHS
      READ(13'I21)  (PP(K),K=1,NNM1)
      READ(14'I22)  (GP(K),K=1,NNRHS)
      CALL  XSXMX(GP,PP,XP,XP,NM1,N,NRHS,AUX)
      WRITE(14'I22)  (XP(K),K=1,NNRHS)
  200 CONTINUE
      RETURN
      END
      SUBROUTINE XSXMX(A,B,C,D,L,M,N,AUX)
      IMPLICIT REAL*8 (A-H,O-Z)
      DIMENSION A(1),B(1),C(1),D(1),AUX(1)
C  MATRICES ARE GIVEN BY ROWS
      LN=L*N
      DO 100  I=1,LN
      NR=(I-1)/N+1
      NC=I-(NR-1)*N
      AUX(I)=0.
      DO 100 K=1,M
      N1=M*(NR-1)+K
      N2=NC+(K-1)*N
      AUX(I)=AUX(I)+B(N1)*C(N2)
  100 CONTINUE
      DO 200  I=1,LN
      D(I)=A(I)-AUX(I)
  200 CONTINUE
      RETURN
      END
      SUBROUTINE XMX(A,B,C,L,M,N,AUX)
      IMPLICIT REAL*8 (A-H,O-Z)
      DIMENSION A(1),B(1),C(1),AUX(1)
C MATRICES ARE GIVEN BY ROWS
      LN=L*N
      DO 100 I=1,LN
      NR=(I-1)/N+1
      NC=I-(NR-1)*N
      AUX(I)=0.
      DO 100  K=1,M
      N1=M*(NR-1)+K
      N2=NC+(K-1)*N
      AUX(I)=AUX(I)+A(N1)*B(N2)
  100 CONTINUE
      DO 200  I=1,LN
      C(I)=AUX(I)
  200 CONTINUE
      RETURN
      END
```

APPENDIX E

CALCULATION OF NET CHORD ROTATIONS

The top chord compression member of joists AX05 and AX01 have been investigated under various boundary conditions. Net chord rotations at both ends of the top chord compression member need to be calculated for the specification of displacement and spring boundary conditions. For displacement boundary conditions the net chord rotation is applied at both ends, while for spring boundary conditions the spring stiffness is calculated on the basis of the calculated net chord rotation. Calculation of the net chord rotations and spring stiffnesses are illustrated below.

E-1 Calculation of Net Chord Rotation in Joist AX05

The length of the top chord member $\ell = 22.96"$

From Figure 5.5(b) and Table 5.1:

(a) Vertical deflection at the right support (u_6) = .5756908

(b) Vertical deflection at the left support (u_5) = .4625646

(c) Relative deflection = .1131262

(d) Rotation of chord due to this relative deflection = $\frac{.1131262}{22.96}$

$= .004927$

(e) Absolute rotation of the left support (θ_5) = -.0109852

(f) Absolute rotation of the right support (θ_6)= -.0021092

(g) Net rotation from the chord at the left support (θ'_5)

$= -.0109852 + .004927 = -.0060582$

(h) Net rotation from the chord at the right support (θ'_6)

= -.0021092 + .004927 = .0028178

E-2 Calculation of Net Chord Rotation and Spring Stiffness in Joist AX01

Length of the top chord member (ℓ) = 23.17 inch

From Figure 5.4(b) and Table 5.1:

(a) Relative deflection = .5159207 - .4091547 = .106766

(b) Chord rotation due to relative deflection = $\frac{.106766}{23.17}$ = .0046

(c) Net rotation from the chord at the left support

= -.0110928 + .0046 = -.0064928

(d) Net rotation from the chord at the right support

= -.0017483 + .0046 = .0028517

Once these net rotations are obtained,the spring stiffnesses are obtained as shown below.

(e) Spring stiffness at left support (K_5)

$$= \frac{\text{Moment at joint 5 for member 34}}{\text{Net rotation at the left support}}$$

(f) Spring stiffness at right support (K_6)

$$= \frac{\text{Moment at joint 6 for member 35}}{\text{Net rotation at the right support}}$$

From Table 5.2,

$$K_5 = \frac{2205}{.0064928} = 339606 \quad \text{in-lb/radian}$$

$$K_6 = \frac{185}{.0028517} = 64873 \quad \text{in-lb/radian}$$